Towards Realizing 5G

Efficient Medium Access and Beamwidth Adaptation in 60GHz Communications

Chandra, Kishor

DOI
10.4233/uuid:015b9f35-1330-4bfb-9ce9-4a4939b7e79b

Publication date
2017

Document Version
Final published version

Citation (APA)
Chandra, K. (2017). *Towards Realizing 5G: Efficient Medium Access and Beamwidth Adaptation in 60GHz Communications*. [Dissertation (TU Delft), Delft University of Technology].
https://doi.org/10.4233/uuid:015b9f35-1330-4bfb-9ce9-4a4939b7e79b

Important note
To cite this publication, please use the final published version (if applicable).
Please check the document version above.

Towards Realizing 5G: Efficient Medium Access and Beamwidth Adaptation in 60 GHz Communications

Towards Realizing 5G: Efficient Medium Access and Beamwidth Adaptation in 60 GHz Communications

Proefschrift

ter verkrijging van de graad van doctor
aan de Technische Universiteit Delft,
op gezag van de Rector Magnificus prof. ir. K.C.A.M. Luyben,
voorzitter van het College voor Promoties,
in het openbaar te verdedigen op maandag 27 februari 2017 om 15:00 uur

door

Kishor CHANDRA

Master of Technology, Electronics and Communications Engineering,
Indian Institute of Technology (IIT) Guwahati, India
geboren te Bazwar, Chamoli, India.

This dissertation has been approved by the

promotor: Prof. dr. ir. I.G.M.M. Niemegeers
copromotor: Dr. R. Venkatesha Prasad

Composition of the doctoral committee:

Rector Magnificus	chairman
Prof. dr. ir. I.G.M.M. Niemegeers	Delft University of Technology
Dr. R. Venkatesha Prasad	Delft University of Technology

Independent Members:

Prof. E. Hossain	University of Manitoba
Prof. J. Hoebeke	Ghent University
Prof. dr. ir. S. M. Heemstra	Eindhoven University of Technology
Prof. dr. A. G. Yarovoy	Delft University of Technology
Prof. dr. L. C. N. de Vreede	Delft University of Technology

Author email: kishor@ieee.org

ISBN 978-94-6186-788-9

An electronic version is available at http://repository.tudelft.nl/.

This work was carried out in the TU Delft Graduate School.

This work was funded by SOWICI, a project sponsored by the NWO.

Printed in the Netherlands by Ipskamp Drukkers.
Thesis cover conceptualized by Vijay S. Rao.

Far better to do your duty, tread your path, live your life imperfectly than to follow another's perfectly.

Shri Krishna in Bhagavad Gita

Summary

The unprecedented growth of mobile devices and high data rate applications have resulted in an enormous surge in the wireless data traffic. The existing wireless communication systems operating in the sub-6 GHz frequency band have already reached their capacity limits. This has led to research on the next generation of wireless communications, also known as 5G. Due to the availability of large unused bandwidth in the millimetre wave (mmWave) frequency band (30—300 GHz), new air interfaces in this band have emerged as promising candidates for multi-Gbps wireless access in 5G communications. Although the first ever demonstration of wireless signal reception was in the year 1889 by Sir J. C. Bose consisting of 60 GHz signals, mmWave radios have mainly remained confined to the military. This was mainly due to the exorbitant cost of equipment and the not so conducive propagation properties. The recent developments in silicon-based complementary metal–oxide–semiconductor (CMOS) processes allow inexpensive implementation of mmWave systems for consumer applications. The possibility of low-cost implementation coupled with the demand for multi-Gbps wireless access, has accelerated the investigations into mmWave based wireless local area networks (WLANs) and mobile communications.

The high free-space path loss in the mmWave band mandates the use of directional antennas to provide the required signal power at the receiver. This brings many challenges at the medium access control (MAC) and network layers. mmWave communication standards such as IEEE 802.11ad and IEEE 802.15.3c – targeting short-range high data rate communications in the 60 GHz frequency band – have specified the use of directional antennas. The aim of this dissertation is to investigate the MAC and network layer challenges of 60 GHz directional communications in the context of multi-Gbps connectivity for 5G networks. We propose a modelling framework for the performance evaluation of the IEEE 802.11ad MAC protocol that considers the presence of both contention and non-contention channel access modes. Further, we consider the parameters unique to mmWave communications such as transmit and receive beamwidths and the spatio-angular distribution of communicating devices and propose a beamwidth allocation scheme that minimizes the packet collision probability in contention based channel access and maximizes the channel utilization. While using directional antennas, a common assumption is that a narrow-beamwidth link provides more capacity compared to a wide beamwidth link. This is because a decrease in beamwidth results in an increase in the antenna gain. However, narrow beamwidth links are highly susceptible to beam alignment errors. Further, selection of the best transmit and receive directions requires the transmission of training packets resulting in beam setup overhead. The beam alignment and setup overheads depend on the transmit and receive beamwidths, resulting in

trade-offs between antenna gains and the corresponding beam alignment and link setup overheads. We investigate the impact of these overheads on the capacity of directional mmWave links to determine the optimum beamwidths. We also propose an efficient beam searching mechanism, employing an approach called decrease-and-conquer, resulting in a significant reduction in the link setup time. Further, to solve the problem of frequent link misalignment caused by the movement of users, we propose to use motion sensors (accelerometer, gyroscope and magnetometer) that are present in consumer devices, such as smartphones, to detect and circumvent beam misalignment. We show that motion sensor data can be used to predict the next location and orientation of the user. This information is used to reconfigure the directional antennas in advance and hence avoid frequent link disruptions.

Multiple access points (APs) are required to facilitate seamless multi-Gbps connectivity in indoor environments since mmWave signals are subject to very high attenuation across walls. This triggers frequent handovers in case of mobile users. Moreover, beam blockage can happen because of humans obstructing the beam, and because of the orientation of the devices with respect to APs, prompting recurrent beam searching. These issues require methods for efficient network management to ensure seamless multi-Gbps connectivity in the mmWave bands. Therefore, we propose a hybrid network architecture consisting of both 2.4/5 GHz and 60 GHz links that exploits the excellent coverage provided by the 2.4/5 GHz signals for control and the enormous capacity potential of the mmWave band for data transmissions. This results in a faster device discovery, leading to a speedy network association and reduced latency in the medium access. Further, we also investigate the radio-over-fiber (RoF) based network architecture which promises excellent central management of 60 GHz APs. The RoF based network architecture is particularly attractive for mmWave communication systems as multiple APs would be operating in a small area where dynamic capacity allocation and seamless handover can be provided by the RoF-based central coordinator. We investigate the performance of the IEEE 802.11ad MAC protocol for a 60 GHz RoF network architecture and discuss the crucial constraints on MAC parameters due to the extra delay introduced by the fiber. The proposed solutions in this dissertation, which were investigated for the 60 GHz band, concerning the MAC and network layers, we argue, will provide efficient multi-Gbps wireless access in the mmWave bands in general.

Contents

1

Introduction

In recent years, a massive increase in mobile data traffic has been witnessed due to the rapid proliferation of wireless communication devices and the emergence of a variety of new applications. This has triggered research on the next generation of mobile broadband systems, i.e., the fifth generation (5G). The 5G Infrastructure Public Private Partnership (5G PPP) [1] has set as its target a 1000 fold increase in the current network capacity to fulfil the traffic demand in the coming decade. The Next Generation Mobile Networks (NGMN) Alliance has also identified several scenarios for 5G communications to support the high data rate application such as mass data download from a kiosk, 8K ultra high definition wireless video transfer, augmented and virtual reality applications, video on demand systems in crowded public spaces and in-vehicle environments requiring data rates ranging from tens of Mbps to multi-Gbps [2]. Further, the mobile offloading and wireless fronthauling and backhauling would require enormous data rates. For example, extremely high quality (8K) video conferencing and gaming would require a per-user data rate of 300 Mbps in the downlink (DL) and 50 Mbps in the uplink (UL). Considering the mobile broadband access in a highly dense urban environment with 2500 connections/km^2, the resulting DL and UL traffic density is around 750 Gbps/km^2 and 125 Gbps/km^2, respectively [1]. On the other hand, current 4G system technology, i.e., Long Term Evolution (LTE), can only provide a peak data rate of 100 Mbps per user with a DL traffic density 0.77 Gbps/km^2 [3]. It is evident that a huge gap exists between the future data traffic projections and the capacity of current mobile communication systems.

Traditionally, reducing the cell size has been the main driver behind the network capacity growth from 2G to 4G cellular systems. However, the network densification resulting due to the closely-spaced small cells in the sub-6 GHz frequency bands is interference-limited. Although several techniques of coordinated transmission have been proposed to avoid the interference in small cells, the capacity is still limited by the inter-cell interference in dense small cell environments. Currently, WiFi (IEEE 802.11b/g/n/ac) operating over 2.4/5 GHz

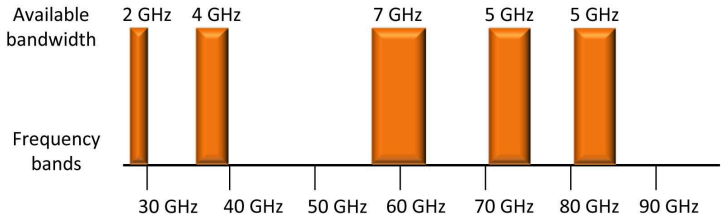

Figure 1.1: Available bandwidths in millimeter wave bands below 90 GHz [4].

dominates the indoor wireless space. Since its inception, WiFi technology has gone through several amendments to meet the data rate requirements. Despite very sophisticated physical (PHY) and medium access control (MAC) layer techniques such as multiple user multiple input multiple output (MU-MIMO), higher order modulation and coding, channel bonding and frame aggregation, it is hard to improve the 2.4/5 GHz WiFi data rates any further. For example, the IEEE 802.11ac uses channel bonding and multi-user MIMO schemes but it can only provide a peak data rate of around 1 Gbps because of the limited available bandwidth in the 5 GHz frequency band.

To achieve the targeted 1000x increase in the network capacity, many disruptive approaches are being pursued for 5G communications. These includes dense small cell deployment, massive MIMO, millimeter wave (mmWave) radio access and the cloud radio access network (CRAN) architecture, etc. Due to the presence of multiple radio access technologies ranging from the microwave frequencies (LTE, LTE-advanced, WiFi, etc.) to mmWave frequencies, the 5G air-interface will be highly integrative. Because of the availability of large bandwidth, radio access in the mmWave band (30 GHz to 300 GHz) has emerged as a key candidate for the multi-Gbps wireless connectivity in the 5G communications [4]. The large frequency chunks are available in 27.5–29.5 GHz, 38.6–40 GHz, 57–66 GHz, 71–86 GHz and 81–86 GHz bands comprising of both the licensed and unlicensed spectrum (see Fig. 1.1). These frequency bands are being investigated for wireless personal area networks (WPANs), wireless local area networks (WLANs), mobile broadband access and small cell fronthaul and backhaul connectivity in 5G networks. The unlicensed frequency band in 60 GHz band (57–66 GHz) has received most attention for short range high data rate communication resulting in standards such as IEEE 802.15.3c [5] and ECMA-387 [6] for WPAN applications and IEEE 802.11ad [7] for WLAN applications. IEEE 802.11ad is an extension of IEEE 802.11b/g/n/ac in the 60 GHz band and provides backward compatibility with the IEEE 802.11b/g/n/ac in 2.4/5 GHz band with a provision of tri-band operations in the 2.4/5 GHz and 60 GHz bands.

The initial standardization efforts in the mmWave bands have mainly focused on WLAN/WPAN operation in the 60 GHz frequency band. However, a few recent measurement studies have supported the feasibility of mmWave-based mobile communication [8, 9]. A further amendment to the 60 GHz WLAN standard

IEEE 802.11ad is underway through the recently setup IEEE 802.11ay working group targeting a peak data rate of 20 Gbps using MU-MIMO and channel bonding in unlicensed mmWave bands above 45 GHz. Apart from the WLAN applications, IEEE 802.11ay targets new usage scenarios and applications including broadband access in crowded public spaces, wireless connectivity in data centers, and fronthaul and backhaul communications in mmWave bands. It also maintains back compatibility with IEEE 802.11ad. Although no standardization activity has been initiated for mobile communications in mmWave bands, there are several 5G-PPP projects under the Horizon 2020 Framework Program of the European Commission, such as mmMagic [10], FLEX5GWARE [11] and METIS [12] that are investigating mobile communications at mmWave frequencies.

1.1. mmWave Propagation characteristics

mmWave based small cells can provide much needed capacity gain due to the availability of large bandwidth. However, the mmWave signal propagation is significantly different from the sub-6 GHz signal propagation leading to several unique propagation characteristics. Firstly, the free-space path loss is very high at mmWave frequencies. For example, the free-space path loss at 60 GHz is at least 20 dB worse than that at 5 GHz. Secondly, the high oxygen absorption (10 –15 dB/km) is an issue in the 60 GHz mmWave band, though only prominent in outdoor environments at a distance of more than 100 m [13]. However, mmWave frequencies in the 27.5–29.5 GHz and 38.6–40 GHz bands are not much affected by oxygen absorption. To compensate for the high free-space path loss at mmWave band, directional antennas using narrow beamwidth pencil beams are proposed [14]. Fortunately, due to the small wavelengths in the mmWave frequency bands, a large number of antenna elements can be closely packed to form the compact and highly directional antenna arrays to compensate the high path loss experienced at mmWave frequencies.

Another important propagation characteristic of 60 GHz signals is their limited ability to diffract around obstacles due to the short wavelengths. Apart from this, mmWave signals cannot penetrate through solid materials such as walls and metals. These properties make mmWave links highly susceptible to blockage from obstacles [15]. Fig. 1.2 shows the impact of different types of obstacles *viz*, human, wooden plank and a metal plate if placed between the 60 GHz transmitter-receiver (Tx-Rx) pair. We can observe that the human and metal severely affect the quadrature phase shift keying (QPSK) constellations making them almost indistinguishable leading to ambiguities in symbol decoding. To circumvent the link blockage, dynamically steerable antennas to find the alternate path using reflections or support of relay devices is required [14, 8, 16].

Apart from the multi-Gbps wireless transmission capability, the unique propagation characteristics of mmWave signals brings many advantages with respect to the sub-6 GHz communication systems. Since mmWave signals exhibit a poor penetration across the walls, it is possible to place AP/BSs at short distances without any significant inter-AP/BS interference. Further, the narrow beamwidth transmission and reception enables simultaneous scheduling of com-

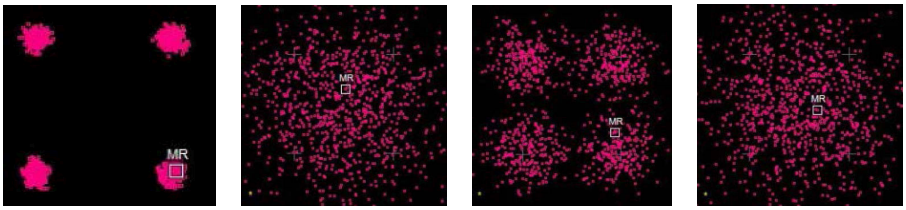

(a) (b) (c) (d)

Figure 1.2: Impact of blockage on 60 GHz link for QPSK modulation: (a) no blockage, (b) human blackage, (c) wood blockage, (d) metal blockage.

munication links that are very close to each other resulting in excellent spatial reuse. The inability to penetrate walls and the use of highly directional transmission is also beneficial from the security perspective. Nevertheless, all these potential benefits can be reaped only if some important challenges in mmWave communication are addressed.

1.2. Challenges of mmWave communications

The use of high-gain directional antennas helps to compensate the high path loss in mmWave bands. To provide a seamless network connectivity, multiple access points (APs) or base stations (BS) are required at short distances (20–200 m). Irrespective of the distance, areas separated by obstacles and walls need separate AP/BSs. The use of directional antennas and closely spaced APs bring many challenges for mmwave based WLANs and cellular communications. Let us discuss these challenges here.

1.2.1. Complexity in medium access

The unique propagation characteristics of mmWave signals have a strong impact on the design of the medium access mechanism [17]. To mitigate the effects of increased attenuation at mmWave frequencies, directional antennas are employed to confine the signal energy in a desired direction. A directional antenna exhibits reciprocity in transmission and reception. Therefore, when a directional transmitter is transmitting in a particular direction, the directional receiver antenna must be aligned in the direction of the transmitter. This is particularly challenging when random access based channel access protocols are used. The random access based protocols play an important role in existing cellular and WLAN systems. For example, IEEE 802.11 primarily uses a CSMA/CA channel access protocol which has become one of the most successful medium access protocols because of its simplicity and adaptability without the need for synchronization. Similarly, cellular systems such as LTE use a random access channel (RACH) for initial access and handover. Since sub-6 GHz communication systems such as LTE and WiFi (802.11b/g/n/ac) employ omnidirectional transmission and reception, random access based channel contention can be easily facilitated. However,

in mmWave directional transmission and reception, it is important to ensure the alignment of transmitter and receiver antennas. To solve this problem, hybrid MAC protocols have been proposed in the presently available mmWave standards IEEE 802.11ad and IEEE 802.15.3c. These hybrid MAC protocols employ both time division multiple access (TDMA) and the CSMA/CA based medium access mechanisms. For example, the IEEE 802.11ad MAC protocol consists of contention based access periods (CBAPs) and fixed access period called service periods (SPs). In CBAPs, channel access is provided using the CSMA/CA protocol while TDMA is used during SPs.

Since all the devices cannot simultaneously listen –to and hear –from the Access point (AP) due to the inherent directionality of APs and devices, the area around an AP is divided into angular sectors to ensure the complete coverage. Devices in a sector can compete for the channel using CSMA/CA only during the allocated time period for that particular sector. Thus the simple CSMA/CA protocol is transformed into a time-shared CSMA/CA among STAs located in different sectors. There have been several investigations [18, 19, 20, 21] on the throughput, delay and fairness performance analysis of IEEE 802.11 CSMA/CA protocol operating in the 2.4/5 GHz frequency bands where omni-directional antennas are used. However, these models are not directly applicable in case of the CSMA/CA protocol in mmWave bands due to the provision for hybrid medium access and the use of directional antennas. Therefore, a novel modeling framework for mmWave MAC protocols is needed that can take into account the unique characteristics of mmWave signal propagation and directional antennas.

1.2.2. Efficient beam searching

To establish narrow beamwidth directional links, MAC layer beamforming mechanisms are specified in mmWave communications standards [7, 5]. MAC layer beamforming is chosen over PHY layer beamforming for two reasons: (i) to avoid the high energy consumption of the signal processing algorithms involving complex computations; and (ii) to overcome the dependence of the beamforming procedure on the antenna structures. For each beam direction, pre-defined antenna weight vectors (amplitude and phase configurations) are defined which is also called the beam codebook [22]. The codebook based beamforming employs beam searching protocols that match the transmit and receive antenna orientations to find the best beam directions. The IEEE 802.15.3c and 802.11ad have proposed beamforming procedures employing codebook based beam searching protocols at the MAC layer. These beamforming protocols rely on an exhaustive-search resulting in a very high beam searching overhead [23, 24, 25, 26, 27]. The beam search space scales with the sum of the Tx and Rx beam resolutions. Therefore, a considerable fraction of the allocated time slot is wasted in searching the best direction. In dynamic channel conditions, frequent beam searching would be required which will significantly hamper the transmission capacity. Therefore, efficient MAC layer beamforming protocols are required that can find the appropriate beam directions with minimum overhead.

1.2.3. Ensuring beam alignment

Antenna gains and beamwidths are inversely proportional to each other. This leads to a common assumption that a narrow beamwidth antenna would always perform better than a wide beamwidth antenna. Though narrow beamwidth antennas can provide excellent received signal quality in mmWave communications, a slight beam misalignment can cause link outage. The susceptibility to link misalignment increases with the decrease in beamwidth [28, 29]. If the beamwidth is very small (1°-5°), even a small misalignment can result in highly unstable links with frequent outages. Once the misalignment exceeds the permissible limits, the directional link setup process is re-initiated requiring the exchange of beam searching packets to re-establish the link. Therefore, the trade-offs arising from the high gain of narrow beamwidth links and the corresponding beam searching overhead and the susceptibility to beam misalignment should be investigated. The narrowest possible beamwidth does not always result in the best link throughput. Therefore it is important to find the beamwidths that ensure the optimum link performance.

1.2.4. Network architecture

The mandatory use of directional antennas and the occurrence of frequent blockages bring many challenges from the perspective of network architecture such as faster device discovery, seamless connectivity and smooth handovers. Due to the limited ability of mmWave signals to penetrate walls, the inter-BS or AP distance would be in the range 20–200 m in mmWave based WLANs or cellular networks. Further, the link blockage due to the dynamic channel conditions would frequently require the selection of an alternate path, such as a reflected path from walls or ceilings or the use of relay devices to compensate for the obstructed path. Providing guaranteed connectivity in a dynamic environment would not only require new approaches for intelligent path or relay selection, but it also requires support for fallback to sub-6 GHz frequency bands given the excellent coverage these provide compared to the mmWave bands. This requires novel interworking among different radio-interfaces in multiple radio access environment.

Further, the use of directional antennas in mmWave cellular and WLANs makes the initial network discovery (BS or AP discovery) a challenging task. In existing communication systems, initial BS/AP discovery is performed with omni-directional antennas. However, due to the necessary use of directional antennas at mmWave frequencies, faster BS or AP discovery mechanisms are required. It would not be possible to establish the initial link using omni-directional transmission and reception. Further, in mobile scenarios, frequent BS or AP handovers would be needed because of the small coverage areas of AP or BSs. Thus network management would require novel approaches to solve these challenges.

1.3. Contributions and the thesis outline

In this thesis we primarily focus on the MAC and network layer challenges. For evaluation purposes, we have considered IEEE 802.11ad MAC and PHY specifica-

tions. From the MAC layer perspective, we have provided a thorough analysis of the IEEE 802.11ad MAC and beam-searching protocols. Since mmWave communication systems are bound to use directional antennas, facilitating channel access becomes a challenging task when devices are located in different sectors. Considering this aspect, we have proposed an analytical model for the performance evaluation of the IEEE 802.11ad MAC protocol that considers the unique features of mmWave communications, such as transmit and receive beamwidths and spatio-angular distributions of devices with respect to BS or AP. Since mmWave systems are going to use hybrid MAC protocols as proposed in IEEE 802.11ad, our performance evaluation framework considers both the contention as well as the contention-free access. Further, we investigate the impact of MAC layer overhead such as antenna misalignment and beam searching overhead that are unique to mmWave communications as compared to the sub-6 GHz communications. The trade-off analysis is extremely helpful in determining the answer of the important question, i.e., *–what are the optimum transmit and receive beamwidths of a mmWave link?* We have also explored the application of motion sensors, i.e., accelerometer, gyroscope and magnetometer to alleviate the problem of frequent beam misalignment by estimating the next beam direction based on the prediction of the next location and orientation of a mobile device.

From the network layer perspective, we investigate the challenges of providing a seamless user experience. The main challenges arise because of–the localized coverage provided by the directional antennas, and –the intermittent outages induced by the frequent blockage. We consider the opportunity to take advantage of the excellent coverage provided by the 2.4/5 GHz signals to complement the enormous capacity of the 60 GHz signals. For this we propose CogCell, a hybrid network architecture consisting of a 2.4/5 GHz control plane and a 60 GHz data plane. The CogCell architecture attempts to exploit the best of both the worlds. i.e., the excellent coverage provided by the capacity limited sub-6 GHz band and the enormous capacity potential of the coverage limited 60 GHz mmWave band nicely complement each other. Further, we also investigate a radio-over-fiber (RoF) based network architecture which promises excellent central management of the 60 GHz AP or BSs. The RoF based network architecture is particularly attractive for mmWave communication systems as multiple of AP or BSs would be operating in a small area where dynamic capacity allocation and seamless handover can be provided by an RoF based central coordinator. Let us now present each of our contributions.

Efficient channel utilization – Chapter 2. We propose a new analytical model for the IEEE 802.11ad MAC protocol and derive important performance metrics. We employ a three dimensional Markov chain that considers all the features of the IEEE 802.11ad medium access mechanism including the non-contention mode of channel access and different numbers of Quasi-Omni (QO) level sectors facilitating contention based access in a round-robin fashion. We investigate the impact of sector beamwidths and the duration of the contention period on the network throughput and packet delay. Our results indicate that a suitable choice of the number of sectors and the contention period can consider-

ably improve the channel utilization and MAC delay performance. Further, we propose an algorithm to determine the beamwidth of each QO sector. The proposed algorithm takes into account the spatial distribution of nodes to allocate the beamwidth of each QO sector in an adaptive fashion in order to maximize the channel utilization. Since the proposed algorithm minimizes the collisions, it also minimizes the average time required to transmit total packets in a QO sector.

Trade-offs in narrow beamwidth mmWave links – Chapter 3. Although the narrow beamwidth antennas can provide excellent signal quality at the receiver, alignment errors and beam searching overhead increase with the decrease in beamwidth. Nevertheless, narrow beamwidth antennas are necessary for mmWave communications. We present a novel capacity modeling framework for mmWave links to investigate the trade-offs in highly directional mmWave links considering beamwidth, beam searching overhead and beam misalignment. We show that the narrowest possible beamwidth may not always result in the best link throughput. We demonstrate that there is an optimum beamwidth after which, if the beamwidth is decreased further, the effects of beam setup time and random antenna misalignments take precedence and deteriorate the actual link throughput. We also use commercial off-the-shelf IEEE 802.11ad hardware to conduct simple experiments to assess the impact of beam searching and misalignment on 60 GHz directional links. Further, we propose a misalignment-aware beamwidth adaptation mechanism to stabilize the performance of 60 GHz links resulting in a significant improvement in the link capacity.

Fast mmWave link setup mechanism – Chapter 4. We investigate the beam searching overhead of the IEEE 802.11ad protocol and propose a multilevel beam searching mechanism. The proposed mechanism, based on a decrease-and-conquer approach, results in a massive reduction in the number of beam searching packets required to establish the directional mmWave links. For very narrow beamwidths (2°-5°), the proposed algorithm results in a huge reduction in the number of beam searching packets as compared to the standard IEEE 802.11ad beam searching mechanism. This would be very beneficial in case of mobile users where frequent beamforming is required. The proposed algorithm is equally effective in two dimensional (2-D) as well as three dimensional (3-D) beamforming systems and it does not alter the structure of the IEEE 802.11ad training packets, hence it can be easily integrated in the IEEE 802.11ad standard.

Sensor-assisted beam switching – Chapter 6. Motion sensors such as accelerometers, gyroscopes and magnetometers are excellent means to estimate the rotational and translational movements. We use these sensors to identify and circumvent the beam misalignments. By finding the extent of misaligned beams, corrective actions are carried out to reconfigure the antenna beam directions. We collect real data from motion sensors and used it to steer the beams in the desired direction. The results from our study show that the sensors are capable

of detecting the cause of errors as translational or rotational movements. Furthermore, it is also shown that the sensor data can be used to predict the next location of the user. This can be used to reconfigure the directional antenna in advance to switch the antenna beam directions and hence avoid frequent link disruptions. This decreases the frequency of re-beamforming and thus lowers the beam searching overhead.

CogCell: A split data and control plane network architecture – Chapter 5. We propose a 60 GHz picocellular network architecture, called CogCell, leveraging the ubiquitous WiFi. We propose to use 60 GHz for the data plane and 2.4/5 GHz for the control plane. We envision a 60 GHz mmWave picocell architecture to support high-speed indoor and hotspot communications. We envisage the 5G indoor/hotspot network as a combination of-, and interplay between, 2.4/5 GHz having robust coverage and 60 GHz links offering high data rate. The hybrid network architecture also considers an opportunistic fall-back to 2.4/5 GHz in case of poor connectivity in the 60 GHz domain. The CogCell architecture promises easier network management, a robust user experience and better spectrum utilization by switching between 2.4/5 GHz and 60 GHz bands for control and data transmissions.

μC-RAN: A 60 GHz radio-over-fiber based network architecture – Chapter 7. The cloud radio access network (CRAN) has emerged as the most promising architectural alternative to enable efficient baseband processing and dynamic resource allocation in 5G communications. This is in particular an attractive choice for mmWave radio access due to the multiplicity of closely spaced BS or APs. We proposed a radio-over-fiber network architecture called micro-CRAN (μC-RAN) that leverages the flexibility of the high bandwidth 60 GHz wireless access and the centralized baseband processing capabilities offered by RoF systems. The RoF based centralized network architecture also promises adaptive resource allocation and easier network management due to the presence of a central controller. We discuss in detail the requirements and research challenges such as beamforming and medium access mechanisms for various system modules of the μC-RAN based network architecture. We also investigate the applicability of the IEEE 802.11ad MAC protocol for the proposed μC-RAN architecture.

The chapters 2, 3, 4, 5, 6 and 7 are based on the following publications.

Journals, Magazines and Book Chapters

- K. Chandra, R. V. Prasad and I. Niemegeers, "Performance Analysis of IEEE 802.11ad MAC Protocol," *Accepted for Publication in IEEE Communications Letters*.
- K. Chandra, R. V. Prasad, Q. Bien, Niemegeers, and I. Niemieegers„ "Cogcell: Cognitive Interplay between 60 GHz Picocells and 2.4/5 GHz Hotspots in the 5G Era," *IEEE Communications Magazine, Special issue on Emerging Applications, Services and Engineering for Cognitive Cellular Systems (EASE4CCS)*, July 2015.

- Z. Cao, H. P. van den Boom, E. Tangdiongga, K. Chandra, and A. Koonen, "Long-Reach Hybrid Fiber-Wireless System with Remote Up-conversion and Local Exchange," *IEEE Photonics Technology Letters*, vol. 25, no. 8, 2013.
- K. Chandra and R. V. Prasad, [Book Chapter] "Directional MAC Protocols for 60 GHz Millimeter Wave WLAN," in *Wireless Network Performance Enhancement via Directional Antennas: Models, Protocols, and Systems*. CRC Press, 2015,
- K. Chandra, R. V. Prasad and I. Niemegeers, "A *Decrease-and-Conquer* based Beam Searching Protocol for mmWave Communications," *Submitted to IEEE Wireless Communications Letters*.
- K. Chandra, R. V. Prasad and I. Niemegeers, "Trade-offs in Narrow Beamwidth mmWave Links," *Submitted to IEEE Transactions on Wireless Communications*.

Conference Papers

- K. Chandra, Z. Cao, T. Bruintjes, R. V. Prasad, G. Karagiannis, E. Tangdiongga, H. van den Boom, and A. Kokkeler, "mCRAN: A Radio Access Network Architecture for 5G Indoor Communications," in *In IEEE ICC 2015 - Workshop on Fiber-Wireless Integrated Technologies, Systems and Networks (ICC'15 - Workshops 09)*., 2015.
- K. Chandra, R. V. Prasad, and I. Niemegeers, "An Architectural Framework for 5G Indoor Communications," in *2015 International Wireless Communications and Mobile Computing Conference (IWCMC)*. IEEE, 2015.
- A. W. Doff, K. Chandra, and R. V. Prasad, "Sensor-Assisted Movement Identification and Prediction for Beamformed 60 GHz Links," in *2015 12th Annual IEEE Consumer Communications and Networking Conference (CCNC)*. IEEE, 2015.
- K. Chandra, A. Doff, Z. Cao, R. V. Prasad, and I. Niemegeers, "60 GHz MAC Standardization: Progress and Way Forward," in *2015 12th Annual IEEE Consumer Communications and Networking Conference (CCNC)*. IEEE, 2015.
- K. Chandra, R. V. Prasad, I. Niemegeers, and A. R. Biswas, "Adaptive Beamwidth Selection for Contention based Access Periods in Millimeter Wave WLANs," in *2014 IEEE 11th Consumer Communications and Networking Conference (CCNC)*. IEEE, 2014.
- K. Chandra, R. V. Prasad, B. Van Quang, I. Niemegeers, and A. R. Biswas, "Analysis of Fi-Wi Indoor Network Architecture based on IEEE 802.15.3c," in *2014 IEEE 11th Consumer Communications and Networking Conference (CCNC)*. IEEE, 2014.

2

Efficient Medium Access Control in Millimeter Wave WLANs

IEEE 802.11ad specifies a hybrid medium access control (MAC) protocol consisting of contention as well as non-contention based channel access mechanisms. In this chapter, we propose a new analytical model for performance analysis of the IEEE 802.11ad medium access control (MAC) protocol and derive important performance metrics. The proposed model employing a three dimensional (3-D) Markov chain considers all the features of the IEEE 802.11ad medium access mechanism including the non-contention mode of channel access and different number of sectors due to the use of directional antennas. Our results indicate that a suitable choice of the number of sectors and the contention period can considerably improve the channel utilization and MAC delay performance. Further we propose an adaptive beamwidth selection mechanism that considers distribution of devices to determine the sector beamwidths and results in a significant improvement in the channel utilization and the delay performance of the IEEE 802.11ad MAC protocol.

2.1. Introduction

As explained in Chapter 1, the wave propagation in the 60 GHz frequency band is significantly different from the 2.4 GHz and 5 GHz frequency bands. Firstly, 60 GHz wireless propagation is subject to a very high free-space path loss. Considering a path (path loss exponent = 2), the path loss at 60 GHz is at least 20 dB worse than that of 5 GHz. Secondly, 60 GHz signals' limited ability to diffract around the obstacles, makes them less suitable for non-line of sight communication [15]. High oxygen absorption (10 to 15 dB/km) is another issue at 60 GHz, although it is only prominent in outdoor environments at a distance of more than

100 m [13].

The high attenuation due to path loss and absorption can be mitigated by using directional antennas [30]. Fortunately, because of the small wavelengths (order of millimeter) in the 60 GHz frequency band, a high number of antenna elements can be closely packed to form compact and highly directional antenna arrays. To overcome the frequent disruption by obstacles, intelligent beam switching [31], alternate path selection [32] and the use of relays [33] are proposed.

The proposed solutions to tackle the challenges listed above have a strong impact on the design of the medium access mechanism for mmWave networks [17]. Considering these characteristics, IEEE 802.15.3c [5] for Wireless Personal Area Networks (WPANs) and IEEE 802.11ad [7] for Wireless Local Area Networks (WLANs) have proposed hybrid Medium Access Control (MAC) protocols for 60 GHz frequency band. These hybrid MAC protocols consist of carrier sense multiple access with collision avoidance (CSMA/CA) and time division multiple access (TDMA) for channel access. Since IEEE 802.11ad provides compatibility with the popular IEEE 802.11 series (at 2.4/5 GHz), it has become the preferred choice over IEEE 802.15.3c and the other 60 GHz standards.

Although IEEE 802.11ad is back compatible with the existing IEEE 802.11 standard, comparing with the IEEE 802.11b/g/n/ac Distributed Coordination Function (DCF), the IEEE 802.11ad DCF has significantly distinct features attributed to the use of directional antennas. These are listed as below.

- All the STAs cannot simultaneously listen to and hear from the Access point (AP) due to the inherent directionality of APs and STAs. To ensure complete coverage, the area around an AP is divided into several levels of beamwidth with different granularity. For example, in IEEE 802.11ad, these levels are called the Quasi-Omni (QO), sector and beam levels. Fig. 2.1 depicts these different antenna beamwidth levels. QO patterns have the widest beam followed by sector-level having a finer beamwidth, and beam-levels have a very narrow beamwidth. Usually, QO patterns are used during contention based access periods (CBAP), while fine beams (sector and beam levels) are used during TDMA based channel access. During the contention period, STAs in a particular QO level can compete for the channel only during the allocated time period for that particular QO level.
- The CSMA/CA operation is suspended when TDMA based channel access is instantiated.
- When the CSMA/CA operation is suspended, backoff counters of all the involved STAs are frozen and in the next round, STAs resume the backoff process with the frozen values of backoff counters.

Owing to these features of the IEEE 802.11ad MAC protocol, new performance analysis models are needed that can accommodate these. The available analytical methods used for IEEE 802.11b/g/n/ac [18, 19, 20, 21] considering omnidirectional transmission at 2.4/5 GHz cannot be directly applied to evaluate the performance of the IEEE 802.11ad MAC protocol as directional communications

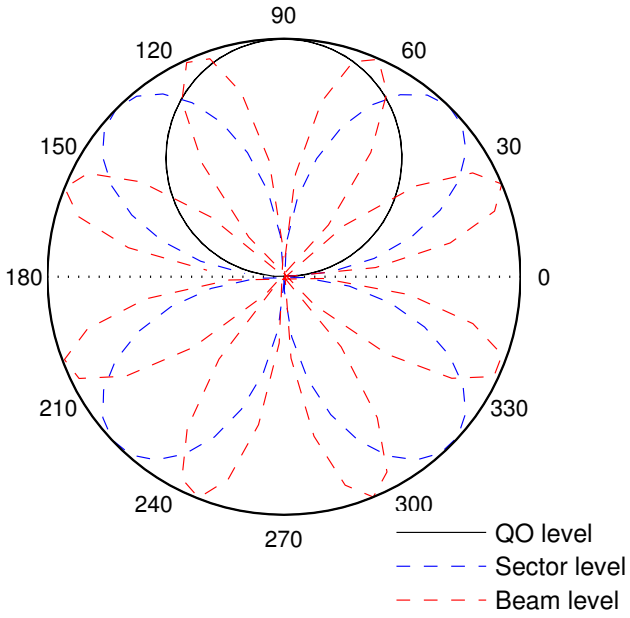

Figure 2.1: Different antenna beamwidth patterns defined in IEEE 802.11ad.

brings additional functionalities. Furthermore, the available literature on the performance analysis of the IEEE 802.11ad MAC protocol does not considers all the parameters [34, 35, 36, 37]. Moreover, there is no work on the assessment of the impact of QO beamwidths on the channel utilization of the IEEE 802.11ad DCF; either impact of the QO beamwidth is ignored or fixed QO beamwidths are considered [36, 38, 39].

In this chapter, we propose a 3-D Markov chain based model for the analytical modeling of the IEEE 802.11ad MAC protocol. The proposed model takes into account the detail features of the MAC protocol and provides new insights on the MAC performance attributed to the use of directional antennas and hybrid access mechanism. Our contributions are:

(i) The derivation of an accurate analytical expression for the channel utilization of the IEEE 802.11ad DCF.

(ii) The derivation of the average MAC delay experienced by a packet taking into account the presence of the contention-free periods.

(iii) The investigation of the effects of the number of QO sectors on the CBAP channel utilization.

(iv) The investigation of the impact of CBAP duration on channel utilization and average MAC delay experienced by a packet.

(v) The proposal of an adaptive beamwidth allocation algorithm for the formation of QO levels which takes into account the spatial distribution of nodes and the link budget to decide the beamwidth of an AP in the CBAP period. We show that the proposed algorithm results in a significant improvement in channel utilization and MAC delay performance. Although we have only considered the IEEE 802.11ad MAC protocol for the proposed adaptive beamwidth algorithm, it is also general enough to be applicable to the IEEE 802.15.3c MAC or any other MAC protocol which employs directional antennas and uses a CSMA/CA MAC protocol on a time sharing basis in different spatial directions around APs.

2.2. Related work

The seminal work by Bianchi [18] on the modeling of the IEEE 802.11 CSMA/CA protocol using Markov chains has been widely used. There are several modified versions of Bianchi's model considering various factors such as a finite retransmission limit[19], busy channel conditions [20] and differentiated quality-of-service [21], etc. However, these models consider CSMA/CA over an infinite duration where all the STAs simultaneously participate in the channel contention process. On the other hand, in IEEE 802.11ad, CSMA/CA is truncated to a finite time duration in each beacon interval (BI) and STAs under different QO levels separately contend for the channel time.

There are a few papers in the literature that deals with the performance analysis of IEEE 802.11ad based WLANs [34, 35, 36, 37]. In [34], detailed physical layer performance analysis is presented considering different modulation and coding schemes (MCS). However, the MAC layer analysis is limited to a single link and it only considers the overhead introduced by MAC headers and acknowledgment schemes, thus the impact of the channel access scheme is ignored. The performance of Orthogonal Frequency Division Multiplexing (OFDM) PHY of IEEE 802.11ad for different MCS is evaluated in [35]. To the best of our knowledge, only [36] and [37] have attempted to model the IEEE 802.11ad MAC protocol. Chen *et al.* [36] have incorporated cooperative relaying with the IEEE 802.11ad MAC protocol. A relay selection mechanism is proposed to enhance the data rate, however, equal beamwidth QO levels are assumed and CSMA/CA suspension is not considered. The authors ignored the hybrid nature of the IEEE 802.11ad medium access and did not take into account the presence of the non-contention mode channel access. Although, Hemanth *et al.* [37] have considered non-contention part of the IEEE 802.ad MAC protocol, the interpretation of the IEEE 802.11ad DCF is incomplete. It is assumed that after the end of every contention period, STAs refresh the backoff counters when the next contention period starts. This is however not the case with the IEEE 802.11ad protocol, since STAs resume their backoff counters across multiple CSMA/CA periods.

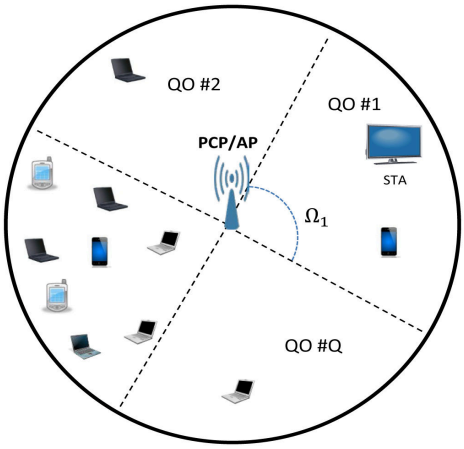

Figure 2.2: IEEE 802.11ad system model.

2.3. System model and IEEE 802.11ad MAC protocol

Let us describe the main functionalities of the IEEE 802.11ad access mechanism that will be part of our system model. A full description can be found in [7]. The IEEE 802.11ad defines a personal basic service set (PBSS) which is the operating area of the network formed by 60 GHz wireless stations (STAs). One of the STAs in a PBSS acts as the PBSS control point/access point (PCP/AP) to coordinate the channel access among the STAs. STAs operating at 60 GHz are called DMG-STAs (Directional Multi Gigabit STAs)[1]. Fig. 2.2 shows an IEEE 802.11ad PBSS where PCP is in the center of the circle and the STAs are distributed around the area covered by the PCP. The typical radius of a PBSS is about 10 to 20 m.

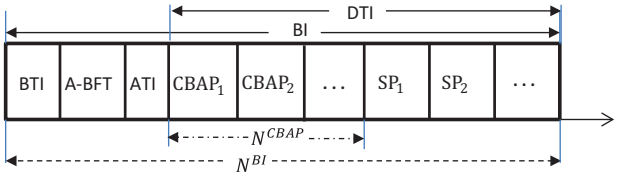

BI: Beacon Interval
BTI: Beacon Transmission Interval
A-BFT: Association Beamforming Training
SP: Service Period
DTI: Data Transmission Interval
CBAP: Contention Based Access Period

Figure 2.3: IEEE 802.11ad BI structure.

Timing in IEEE 802.11ad is based on beacon intervals (BIs) set by the PCP/AP. The time between two beacon intervals is divided into different ac-

[1]For simplicity, all the STAs are DMG-STAs and are referred as STAs.

cess periods having different medium access rules. Fig. 2.3 illustrates the IEEE 802.11ad BI which consists of:

(i) Beacon Transmission Interval (BTI) where beacons are transmitted in all the QO directions in a round-robin fashion.

(ii) Association Beamforming Training (A-BFT) where member STAs train their beams with the PCP/AP.

(iii) Announcement Time Interval (ATI), which is used for the exchange of the management information between the PCP/AP and the member STAs.

(iv) Data Transfer Interval (DTI), during which data transfer happens.

The DTI consists of contention-based access periods (CBAPs) and service periods (SPs). CBAPs employ the CSMA/CA for channel access by STAs, while SPs are reserved using a service period request (SPR) command after the PCP/AP polls the STAs during the ATI period.

Here, we focus on the uplink channel access during the CBAP period. It is assumed that each STA associated with the PCP/AP has trained its beams during the A-BFT period using the sector level sweep (SLS) procedure. Once the SLS phase is completed, the best transmit beams between PCP/AP and other STAs are assumed to be known. The Channel contention during the CBAP in different QO levels is allowed on a time sharing basis. The STAs under each QO level contend for the channel using CSMA/CA mechanism during the allotted CBAP period for that QO level.

As shown in Fig. 2.2, only those STAs that are within the current PCP/AP QO level will contend for the channel during the current CBAP duration. Since the PCP/AP is aware of the STAs that would contend for the channel time in the current QO level, it would listen to the STAs in that particular QO direction. Hence, the problem of deafness arising due to misalignment of transmit and receive antennas is eliminated. Considering the provision of the request to send (RTS) - clear to send (CTS) mechanism, the problem of hidden terminals can be neglected.

Let there be a total of n STAs in a PBSS and Q QO levels with the k^{th} QO level having a beamwidth of Ω_k and number of STAs n_k such that $\sum_{k=1}^{k=Q} \Omega_k = 2\pi$, and $\sum_{k=1}^{k=Q} n_k = n$, where, $1 \leq k \leq Q$. Let τ_k be the transmission probability of each device in k^{th} QO level, which is assumed to be constant over all the time slots, and p_k be the probability of collision experienced by a packet given that it is transmitted on the channel in the k^{th} QO level. p_k is also known as the *conditional collision probability* and is assumed to be constant and independent of the number of retransmission attempts in a QO level. For simplicity, henceforth, we will represent τ_k and p_k by τ and p, respectively (though each QO level can have different values for τ and p if they have different number of STAs). In saturation condition (i.e., each STA always has a packet to send), the relation of τ and p is given by, In saturation condition (i.e., each STA always has a packet

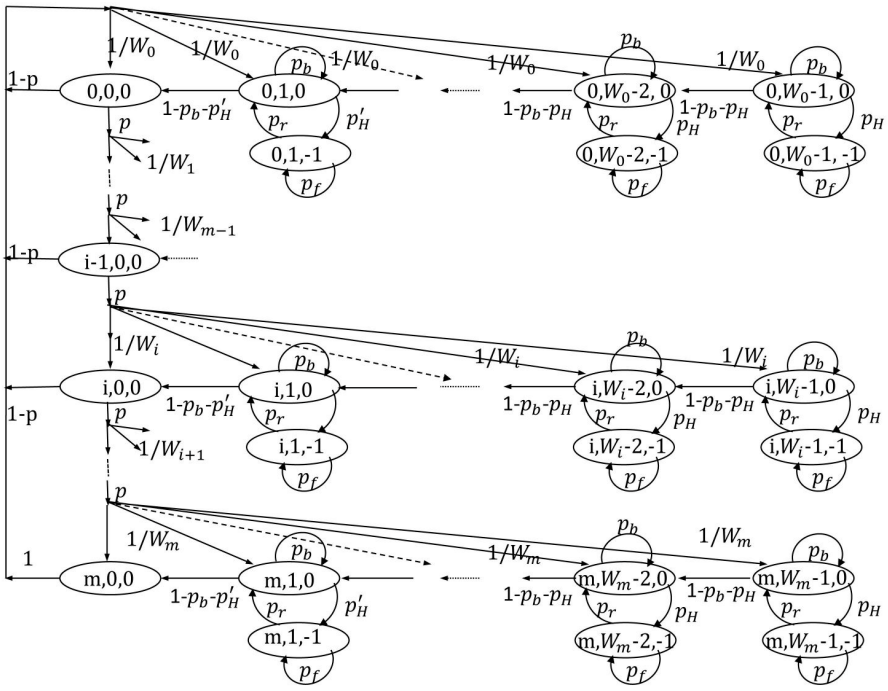

Figure 2.4: Markov chain model for packet transmission states.

to send), the relation of τ and p is given by [18],

$$p = 1 - (1 - \tau)^{n_k - 1}. \tag{2.1}$$

IEEE 802.11ad CSMA/CA employs the random binary exponential back-off mechanism. If the channel is idle, the backoff counter is decreased by one. When the backoff counter of an STA reaches zero, it transmits the RTS frame. If the RTS frame is successfully received by the PCP/AP, after the short inter-frame space (SIFS) duration, it responds with a directional multi-gigabit CTS (DMG CTS) frame. After the successful reception of a DMG CTS frame by the STA, the communication link between the STA and PCP/AP is established. Since other STAs in the given QO level can hear the DMG CTS frame, their backoff counters are suspended. After data transmission is completed, the PCP/AP sends an acknowledgment (ACK) frame and the STA generates a fresh backoff counter for the next frame to be sent. If the RTS frame collides, the STA moves to the next backoff stage until the maximum retransmission limit expires. Let the maximum retransmission limit be defined by m and W_0 be the minimum window size, then the window size at the i^{th} retransmission stage is W_i=$2^i W_0$. After the maximum retry limit m, the packet is dropped.

2.4. Three dimensional Markov chain model for packet transmissions

We introduce the 3-D Markov chain shown in Fig. 2.4 in which each packet transmission state is represented by a triplet $(s(t), b(t), h(t))$. Here, $s(t)$ and $b(t)$ represent the stochastic process of the backoff stage i, $i \in [0, H]$ and the residual backoff time j, $j \in [0, W_i - 1]$, respectively. To differentiate between the contention and non-contention part of BI, we define $h(t)$, $h(t) \in [-1, 0]$ which represents whether a packet is part of an ongoing CBAP ($h(t) = 0$), or CBAP is over and its in a suspended period outside CBAP ($h(t) = -1$).

$$h(t) = \begin{cases} 0, & \text{if the packet is part of an ongoing CBAP} \\ -1, & \text{otherwise} \end{cases} \tag{2.2}$$

2.4.1. Transition probabilities of the Markov chain

Let N^{bi} be the duration of a beacon interval and N^{cbap} is the total CBAP period. The CBAP fraction, ρ_{cbap}, is defined as $\frac{N^{cbap}}{N^{bi}}$. Let the CBAP period allocated to the k^{th} sector be equal to N_k^{cbap} such that $\sum_{k=1}^{k=Q} N_k^{cbap} = N^{cbap}$, and N^{frame} is the time required to successfully transmit a data frame. All the time durations here are expressed in the unit of slot time σ. The probabilities p_H and p'_H represent the probabilities of transitions from contention to non-contention period when the backoff counter value is $j = 1$ and $j \in [2, W_i - 1]$, respectively. The one step Markov chain transition probabilities from contention to non-contention states can be expressed as,

$$P\{i, j, -1 | i, j, 0\} = \begin{cases} p_H, & j \in [2, W_i - 1], i \in [0, m] \\ p'_H, & j = 1, i \in [0, m] \end{cases} \tag{2.3}$$

Two different probabilities account for the fact that according to the IEEE 802.11ad MAC protocol, when $j \in [2, W_i - 1]$, STAs jump to the non-contention state if the CBAP time counter reaches zero. However, if $j = 1$, and the channel becomes idle, the STAs have to avert the packet transmission and jump to the non-contention state even if the allocated CBAP duration is not finished but the CBAP counter has reached a value that is less than the total time required to transmit a packet. The values of p_H and p'_H depend on the BI parameters, and for STAs in the k^{th} sector can be expressed as $p_H = \frac{1}{N_k^{cbap}}$ and $p'_H = \frac{N^{frame}}{N_k^{cbap}}$, respectively.

Let p_r and p_f be the transition probabilities of non-contention states to contention states and staying in non-contention state, respectively. Then, the one-step Markov chain transition probabilities can be written as,

$$P\{i, j, 0 | i, j, -1\} = p_r,\ j \in [1, W_i - 1], i \in [0, m], \tag{2.4a}$$

$$P\{i, j, -1 | i, j, -1\} = p_f,\ j \in [1, W_i - 1], i \in [0, m], \tag{2.4b}$$

where, $p_r = \frac{N_k^{cbap}}{N^{bi}}$ and $p_f = 1 - p_r$.
Let p_b be the state transition probability of the channel being busy during the contention period, then, from the Markov chain, the state transition during a busy contention period is defined by,

$$P\{i, j, 0|i, j, 0\} = p_b,\ j \in [1, W_i - 1], i \in [0, m], \tag{2.5}$$

An STA will observe a busy channel when at least one STA among the remaining $n_k - 1$ STAs occupies the channel. Hence p_b, i.e., the probability of not decreasing the backoff counter during the CBAP period, is calculated as, $p_b = 1-(1-\tau)^{n_k-1}$. The remaining one-step transition probabilities from the Markov chain can be expressed as follows,

$$P\{0, j, 0|i, 0, 0\} = (1 - p)/W_0, j \in (0, W_i - 1), i \in (0, H), \tag{2.6a}$$
$$P\{i, j, 0|i - 1, 0, 0\} = p/W_i, j \in (0, W_i - 1), i \in (0, H), \tag{2.6b}$$

$$P\{i, j - 1, 0|i, j, 0\} = \begin{cases} 1 - p_b - p_H, & j \in [2, W_i - 1], i \in [0, H], \\ 1 - p_b - p'_H, & j = 1, i \in [0, H], \end{cases} \tag{2.7}$$

here, (2.6a) and (2.6b) represent a state transitions because of a successful transmission and collision resulting in failed transmission, respectively. On the other hand, (2.7) refers to state transitions due to the backoff counter decrementing when the channel is observed idle for a slot-time .

2.4.2. Relations among steady state probabilities of the Markov chain

The steady state probability of being in the non-contention states $b_{i,j,-1}$ can be expressed as,

$$b_{i,j,-1} = p_f b_{i,j,-1} + p_H b_{i,j,0}, i \in [0, m], j \in [1, W_i - 1]$$

Where, p_H represents the transition probability from a contention state to a non-contention state while p_f represents the probability that a packet stays in the non-contention state after it reaches the non-contention state. By simplifying the above expression, we get,

$$(1 - p_f)b_{i,j,-1} = p_H b_{i,j,0}, i \in [0, m], j \in [1, W_i - 1].$$

Since $p_r = 1 - p_f$, above expression simplifies to,

$$p_r b_{i,j,-1} = p_H b_{i,j,0}, i \in [0, m], j \in [1, W_i - 1]. \tag{2.8}$$

Similarly, for $j = 0$,

$$p_r b_{i,0,-1} = p'_H b_{i,0,0}, i \in [0, m]. \tag{2.9}$$

Now we derive the relation between the steady state probabilities $b_{i,j,0}$ and $b_{i-1,0,0}$. Whenever a transmission suffers collision in the $i-1^{th}$ backoff stage, the packet jumps to one of the states $(i, j, 0)$, $j \in [0, W_i - 1]$. Let us start with the state $(i, W_i - 1, 0)$, i.e., the state with the maximum possible backoff counter value in the i^{th} backoff stage,

$$b_{i,W_i-1,0} = p_b b_{i,W_i-1,0} + \frac{p}{W_i} b_{i-1,0,0} + p_r b_{i,W_i-1,-1}, i \in [1, m]. \tag{2.10}$$

Substituting (2.8) into (2.10), we get,

$$(1 - p_b) b_{i,W_i-1,0} = \frac{p}{W_i} b_{i-1,0,0} + p_H b_{i-1,W_i-1,0}, i \in [1, m],$$

By simplifying the above expression, we obtain:

$$b_{i,W_i-1,0} = \frac{p}{(1 - p_b - p_H) W_i} b_{i-1,0,0}, i \in [1, m]. \tag{2.11}$$

Similarly for the state $(i, W_i - 2, 0)$,

$$b_{i,W_i-2,0} = p_b b_{i,W_i-2,0} + \frac{p}{W_i} b_{i-1,0,0} + p_r b_{i,W_i-2,-1} + (1 - p_b - p_H) b_{i,W_i-1,0}, i \in [1, m].$$

After the simplification, we get,

$$(1 - p_b - p_H) b_{i,W_i-2,0} = \frac{p}{W_i} b_{i-1,0,0} + (1 - p_b - p_H) b_{i,W_i-1,0}, i \in [1, m]. \tag{2.12}$$

By substituting the value of $(1 - p_b - p_H) b_{i,W_i-1,0}$ from (2.11) into (2.12), we get,

$$b_{i,W_i-2,0} = \frac{2p}{(1 - p_b - p_H) W_i} b_{i-1,0,0}, i \in [1, m]. \tag{2.13}$$

From (2.11) and (2.13), we deduce that,

$$b_{i,j,0} = \frac{p(W_i - j)}{(1 - p_b - p_H) W_i} b_{i-1,0,0}, i \in [1, m], j \in [2, W_i - 1]. \tag{2.14}$$

Similarly for, $j = 1$, $i \in [1, m]$,

$$b_{i,1,0} = \frac{p(W_i - 1)}{(1 - p_b - p'_H) W_i} b_{i-1,0,0}, i \in [1, m], j = 1. \tag{2.15}$$

Now we can derive the transition from the state $(i-1,0,0)$ to the state $(i,0,0)$, as follows:

$$b_{i,0,0} = \frac{p}{W_i} b_{i-1,0,0} + (1 - p_b - p'_H) b_{i,1,0}, i \in [1,m] \tag{2.16}$$

Substituting the result of (2.15) into (2.16), we get $b_{i,0,0} = p b_{i-1,0,0},\ i \in [1,m]$. This leads to the following generalized expression,

$$b_{i,0,0} = p^i b_{0,0,0}, i \in [1,m]. \tag{2.17}$$

The states in the zeroth backoff stage can be reached when: (i) a successful packet transmission occurs in any of the backoff stages $[0,m]$; and (ii) a packet collision occurs in the m^{th}) backoff stage. Hence, the steady state probability of being in the states $(0,j,0)$ can be expressed as,

$$b_{0,j,0} = \frac{1-p}{W_0} \sum_{i=0}^{H} b_{i,0,0} + p_b b_{0,j-1,0} + p_r b_{0,j-1,-1}, i = 0, j \in [0, W_0 - 1] \tag{2.18}$$

Employing the results of (2.10), (2.11), (2.16) and (2.18), we get the following state transition relations,

$$b_{0,j,0} = \frac{1-p}{1-p_b-p_H} \frac{W_0 - j}{W_0} \sum_{i=0}^{H} b_{i,0,0}, j \in [2, W_0 - 1], \tag{2.19}$$

For $j = 1$,

$$b_{0,1,0} = \frac{1-p}{1-p_b-p'_H} \frac{W_0 - 1}{W_0} \sum_{i=0}^{H} b_{i,0,0}. \tag{2.20}$$

The relations (2.14), (2.15), (2.17), (2.19) and (2.20) among the steady state probabilities would be used to find the collision probablity p and the transmission probability τ from the Markov chain of Fig. 2.4.

2.4.3. Deriving transmission and collision probabilities from the Markov chain

The sum of the steady state probabilities of all the packet transmission states in the Markov chain of Fig. 2.4 should be 1, hence,

$$\sum_{i=0}^{m} \sum_{j=0}^{W_i - 1} b_{i,j,0} + \sum_{i=0}^{m} \sum_{j=1}^{W_i - 1} b_{i,j,-1} = 1.$$

Here, the first term of the summation represents the steady state probabilities of the contention states, i.e., when the STAs in a QO level are allowed to contend for the channel using the DCF. On the other hand, the second term represents the steady state probabilities corresponding to the non-contention states, i.e.,

when the STAs in a QO level are not allowed to participate in the contention process.
Since the states of the Markov chain corresponding to the zeroth backoff stage ($i = 0$), have different dependencies as compared with the states of the other backoff stages, we further regroup the steady state probabilities as follows;

$$L.H.S = \sum_{j=0}^{W_0-1} b_{0,j,0} + \sum_{i=1}^{m}\sum_{j=0}^{W_i-1} b_{i,j,0} + \sum_{j=1}^{W_0-1} b_{0,j,-1} + \sum_{i=1}^{m}\sum_{j=1}^{W_i-1} b_{i,j,-1}.$$

Further expanding the above expression and regrouping, we obtain:

$$\begin{aligned} L.H.S &= b_{0,0,0} + b_{0,1,0} + \sum_{j=2}^{W_0-1} b_{0,j,0} + \sum_{i=1}^{m}\left(b_{i,0,0} + b_{i,1,0} + \sum_{j=2}^{W_i-1} b_{i,j,o}\right) + b_{0,1,-1} \\ &\quad + \sum_{j=2}^{W_i-1} b_{0,j,-1} + \sum_{i=1}^{m}\left(b_{i,1,-1} + \sum_{j=2}^{W_i-1} b_{i,j,-1}\right), \\ &= b_{0,0,0} + b_{0,1,0} + b_{0,1,-1} + \sum_{j=2}^{W_0-1}(b_{0,j,0} + b_{0,j,-1}) + \sum_{i=1}^{m}(b_{i,0,0} + b_{i,1,0} + b_{i,1,-1}) \\ &\quad + \sum_{i=1}^{m}\sum_{j=2}^{W_i-1}(b_{i,j,0} + b_{i,j,-1}). \end{aligned}$$

By using (i) the relation between $b_{i,j,0}$ and $b_{i,j,-1}$ given by (2.8), and (ii) the relation between $b_{i,1,0}$ and $b_{i-1,0,0}$ given by (2.15), we get:

$$\begin{aligned} L.H.S &= b_{0,0,0} + b_{0,1,0} + \frac{p'_H}{1-p_f} b_{0,1,0} + \left(1 + \frac{p_H}{1-p_f}\right)\sum_{j=2}^{W_0-1} b_{0,j,0} \\ &\quad + \sum_{i=1}^{m}\left(p^i b_{0,0,0} + \frac{W_i - 1}{W_i}\frac{p}{1-p_b-p'_H} b_{i-1,0,0} + \frac{p'_H}{1-p_f} b_{i,1,0}\right) \\ &\quad + \left(1 + \frac{p_H}{1-p_f}\right)\sum_{i=1}^{m}\sum_{j=2}^{W_i-1} b_{i,j,0}. \end{aligned}$$

Further, by using (i) the relation between $b_{i,j,0}$ and $b_{i-1,0,0}$ given by (2.14), (ii) the relation between $b_{0,j,0}$ and $b_{i,0,0}$ given by (2.19), (iii) the relation between $b_{0,1,0}$ and $b_{i,0,0}$ given by (2.20) and simplifying, we obtain:

$$L.H.S = b_{0,0,0} + \left(1 + \frac{p'_H}{1-p_f}\right) b_{0,1,0} + \left(1 + \frac{p_H}{1-p_f}\right)\sum_{j=2}^{W_0-1}\frac{W_0 - j}{W_0}\frac{1-p}{1-p_b-p_H}\sum_{i=0}^{m} b_{i,0,0}$$

$$+\sum_{i=1}^{m}\left(p^i+\left(1+\frac{p'_H}{1-p_f}\right)\frac{p}{1-p_b-p'_H}\left(1-\frac{1}{W_i}\right)p_{i-1}\right)b_{0,0,0}$$
$$+\left(1+\frac{p_H}{1-p_f}\right)\frac{p}{1-p_b-p_H}\sum_{i=1}^{m}\left(\frac{W_i}{2}-\frac{3}{2}+\frac{1}{W_i}\right)b_{i-1,0,0}.$$

Finally, using the relation between $b_{i,0,0}$ and $b_{0,0,0}$ given by (2.17), and simplifying the summations, we get:

$$\begin{aligned}
L.H.S &= \left(1+\left(1+\frac{p'_H}{1-p_f}\right)\frac{1}{1-p_b-p'_H}\frac{W_0-1}{W_0}(1-p^{m+1})\right)b_{0,0,0}\\
&+\left(\left(1+\frac{p_H}{1-p_f}\right)\frac{1}{1-p_b-p_H}\frac{(W_0-1)(W_0-2)}{2W_0}(1-p^{m+1})\right)b_{0,0,0}\\
&+\sum_{i=1}^{m}\left(p^i+\left(1+\frac{p'_H}{1-p_f}\right)\frac{p}{1-p_b-p'_H}\left(p^{i-1}-\frac{(p/2)^{i-1}}{2W_0}\right)\right)b_{0,0,0}\\
&+\left(1+\frac{p_H}{1-p_f}\right)\frac{p}{1-p_b-p_H}\sum_{i=1}^{m}\left(W_0(2p)^{i-1}-\frac{3}{2}p^{i-1}+\frac{(p/2)^{i-1}}{2W_0}\right)b_{0,0,0}\\
&=\left(1+\left(\eta'\frac{W_0-1}{W_0}+\eta\frac{(W_0-1)(W_0-2)}{2W_0}\right)(1-p^{m+1})+p\frac{1-p^m}{1-p}\right.\\
&+\eta' p\left(\frac{1-p^m}{1-p}-\frac{1-(p/2)^m}{(1-p/2)(2W_0)}\right)\\
&\left.+\eta p\left(W_0\frac{1-(2p)^m}{1-2p}-\frac{3}{2}\frac{1-p^m}{1-p}+\frac{1-(p/2)^m}{(1-p/2)(2W_0)}\right)\right)b_{0,0,0}\\
&=\left(1+\frac{W_0-1}{W_0}\left(\eta'+\eta\frac{W_0-2}{2}\right)(1-p^{m+1})+p\frac{1-p^m}{1-p}\left(1+\eta'-\frac{3}{2}\eta\right)\right.\\
&\left.+\frac{p}{2W_0}\frac{1-(\frac{p}{2})^m}{1-\frac{p}{2}}(\eta-\eta')+\eta pW_0\frac{1-(2p)^m}{1-2p}\right)b_{0,0,0}. \qquad (2.21)
\end{aligned}$$

Here, $\eta'=\left(1+\frac{p'_H}{1-p_f}\right)\frac{1}{1-p_b-p'_H}$ and $\eta=\left(1+\frac{p_H}{1-p_f}\right)\frac{1}{1-p_b-p_H}$.

During the i^{th} back-off stage, a packet is transmitted when it reaches the state $b_{i,0,0}$. This is also called the head-of-line state. From the Markov chain in Fig. 2.4, the transmission probability τ can be expressed as the sum of the steady state probabilities of being in the head-of-line states, hence,

$$\begin{aligned}
\tau &= \sum_{i=0}^{H} b_{i,0,0},\\
&= \frac{1-p^{m+1}}{1-p}b_{0,0,0}. \qquad (2.22)
\end{aligned}$$

Where $b_{0,0,0}$ is given by (2.21). Given this relation, (2.1) and (2.22) can be solved for p and τ for the given network parameters. Once p and τ are known, the channel utilization can be calculated as described in the next sub-section.

2.4.4. Channel utilization

During the contention process, the probability of a slot being idle, having a successful transmission or collision can be expressed as $P_{idle} = (1-\tau)^{n_k}$, $P_{suc} = n_k\tau(1-\tau)^{n_k-1}$, and $P_{col} = 1 - n_k\tau(1-\tau)^{n_k-1} - (1-\tau)^{n_k}$, respectively. Let U_k be the channel utilization in the k^{th} QO level, which is defined as the fraction of time that the channel is used to transmit the payload successfully. Let T_{idle} be the duration of an idle time slot, T_{suc} the duration of a successful transmission and T_{col} the duration of a failed transmission, then U_k is calculated as,

$$U_k = \frac{P_{succ}E[Payload]}{P_{idle}T_{idle} + P_{suc}T_{suc} + P_{col}T_{col}}. \tag{2.23}$$

Here, $E[Payload]$ is the average duration of a payload packet and $T_{idle} = \sigma$ is the duration of one slot. Here, $T_{suc} = T_{rts} + 2SIFS + T_{cts} + DIFS + T_{DATA} + T_{ACK}$ and $T_{col} = T_{rts} + SIFS + DIFS + RIFS$, where, T_{rts} is the duration of an RTS frame, T_{cts} is the duration of a DMG CTS frame, $DIFS$ is the Distributed Backoff Inter-Frame Space and $RIFS$ is the Retransmission Inter-Frame Space, i.e., the time-out duration. Considering all the QO levels, the average channel utilization during the CBAP period is given by,

$$U = \frac{1}{Q}\sum_{k=1}^{k=Q} U_k. \tag{2.24}$$

2.4.5. MAC delay analysis

We define the MAC delay $E[D]$ as the expected time between the arrival of a packet at the MAC layer and the instant it is successfully transmitted. The probability that a packet is discarded after m backoff stages is given by p^{m+1}. Hence the conditional probability $P(TX = i|success)$ representing the probability of successful transmission in the i^{th} backoff stage, is expressed as,

$$P(TX = i|success) = \frac{p^i(1-p)}{1-p^{m+1}}. \tag{2.25}$$

Note that the first transmission attempt corresponds to the $zero^{th}$ backoff stage. Let $E[D_i]$ represent the average delay encountered by a packet successfully transmitted in the i^{th} backoff stage, then $E[D]$, the average MAC delay is given as,

$$E[D] = \sum_{i=0}^{m} P(TX = i|success)E[D_i], \tag{2.26}$$

here, $E[D_i]$ consists of:
(i) the delay accumulated during i collisions,
(ii) the time taken by successful transmission in the i^{th} backoff stage, and
(iii) the backoff process delay corresponding to the $i+1$ backoff processes starting from zero to the i^{th} backoff stage. Hence,

$$E[D_i] = iT_{col} + T_{suc} + \sum_{z=0}^{z=i} E[BD_z]. \tag{2.27}$$

The backoff process delay $E[BD_i]$ is composed of the delay incurred due to the medium observed as busy because of other transmissions, the backoff counter decrement during idle channel conditions, and the delay caused by the system being in the non-contention part of BI. Let T_{tt} be the average time duration for the backoff counter to decrease by one step (from $(i, j, 0)$ to $(i, j-1, 0)$). Since the average number of backoff states in the i^{th} backoff stage is $\frac{W_i-1}{2}$, the backoff process delay $E[BD_i]$ is given as,

$$E[BD_z] = \frac{W_z - 1}{2} T_{tt}. \tag{2.28}$$

If the average one-step state transition period is represented by σ_{avg} and N_{tt} is the number of steps a packet stays in state $(i, j, 0)$ before jumping to state $(i, j-1, 0)$, then, T_{tt} can be calculated as following.

$$T_{tt} = \sum_{c=N_{tt}^{min}}^{c=N_{tt}^{max}} P(N_{tt} = c)[c\sigma_{avg}]. \tag{2.29}$$

$$\tag{2.30}$$

Next we find the bounds on minimum and maximum values of N_{tt} defined by N_{tt}^{min} and N_{tt}^{max}, respectively.

Proposition 1. *The number of one-step transition period N_{tt} in (2.29) is bounded by $N_{tt}^{min} = 1$ and $N_{tt}^{max} = \infty$*

Proof. Let us consider an STA having a packet in the backoff state $(i, j, 0)$. If the channel becomes idle after a busy period, the tagged STA waits for a minimum slot time length σ. If the channel is still observed idle after σ, than the tagged STA (and all other STAs as well) will decrease its backoff counter to $(i, j-1, 0)$. Hence a period of one slot-length is the minimum duration before the backoff counter decrement happens. This sets the lower limit on N_{tt} as $N_{tt}^{min} = 1$. On the other hand, if the backoff counter value of any other STA reaches zero, that STA starts transmission and the medium remains busy for the duration required for a successful transmission or collision. In this case, the tagged STA and all other STAs with non-zero backoff counter freeze their backoff counters. In the worst case (considering an infinite number of STA,) the medium would always remain busy as there will be STAs generating zero backoff counter values after every channel-busy period resulting in an upper limit on N_{tt} as $N_{tt}^{max} = \infty$. Hence,

$$\begin{aligned} T_{tt} &= \sum_{c=1}^{\infty} (1 - p_b - p_H)(p_b + p_H)^{c-1} c\sigma_{avg}, \\ &= (1 - p_b - p_H) \left(\sum_{c=1}^{\infty} c(p_b + p_H)^{c-1} \right) \sigma_{avg}. \end{aligned} \tag{2.31}$$

Using the mathematical summation formula $\sum_{c=1}^{\infty} cx^{c-1} = \frac{1}{(1-x)^2}$, (2.31) simplifies to,

$$T_{tt} = \frac{\sigma_{avg}}{1 - p_b - p_H}. \tag{2.32}$$

Let P^o_{idle}, P^o_{suc} and P^o_{col} represent the probabilities of the channel to be observed idle, to be busy with a successful transmission and to be busy with a collision, respectively, by a tagged STA during backoff process. Then, the average one-step state transition period σ_{avg} can be expressed as,

$$\sigma_{avg} = (1 - p_H)(P^o_{idle}T_{idle} + P^o_{suc}T_{suc} + P^o_{col}T_{col}) + p_H(T^{bi} - T^{cbap}). \tag{2.33}$$

Where $P^o_{idle} = (1-\tau)^{n_k-1}$, $P^o_{suc} = (n_k-1)\tau(1-\tau)^{n_k-2}$ and $P^o_{col} = 1-P^o_{idle}-P^o_{suc}$. By substituting (2.33), (2.32), (2.28), (2.27) and (2.25) into (2.26), the average MAC packet delay can be computed.

2.5. Numerical results

In this section, using MATLAB, we analyze the IEEE 802.11ad MAC performance as a function of various factors such as number of STAs, contention window sizes and AP beamwidth. The analytical expressions for the channel utilization and packet delay obtained in Sections 2.4.3, 2.4.4 and 2.4.5 are used. The analytical (A) results for the throughput and delay performance are validate using simulation (S) results obtained using a discrete event simulator built in MATLAB following the IEEE 802.11ad specifications. We assumed an ideal flat-top directional antenna with main lobe gain ($G = \frac{2\pi}{\omega}$) without any side lobes. We considered a uniform distribution of STAs such that each QO level accommodates an equal number of STAs. All the parameters used in the numerical evaluation are listed in Table 2.1. The IEEE 802.11ad Control PHY is used to transmit RTS, DMG CTS and ACK frames, while MCS4 (modulation and coding scheme 4) is used for data frame transmission. If not specified, the size of a data frame is 7995 Bytes, which is the maximum MSDU size specified in IEEE 802.11ad standard. The packet retransmission limit is set to 5. As explained earlier, we consider packet saturation at the MAC queue of each STA which implies that every STA has a head-of-line packet ready to join the contention process after the previous packet is transmitted. Fig. 2.5 shows the normalized throughput as a function of the number of STAs in one QO sector for varying contention window sizes. Here ρ_{cbap}, the fraction of BI used for CBAP is 0.40. We can see that for W_0=3, as number of STAs is increased, the throughput decreases faster compared with the higher values of CW_0. This is because for smaller W_0, the probability of collision is high. However, when there are less STAs (≤ 5), a smaller W_0 results in a better throughput as less amount of channel time would be wasted in the idle state.

Fig. 2.6 shows the impact of the number of QO levels on the CBAP throughput. It is evident from Fig. 2.6 that when the number of STAs is increased, having more QO levels is beneficial as the number of contending STAs at a given time would be divided by a factor equal to number of QO levels resulting in a

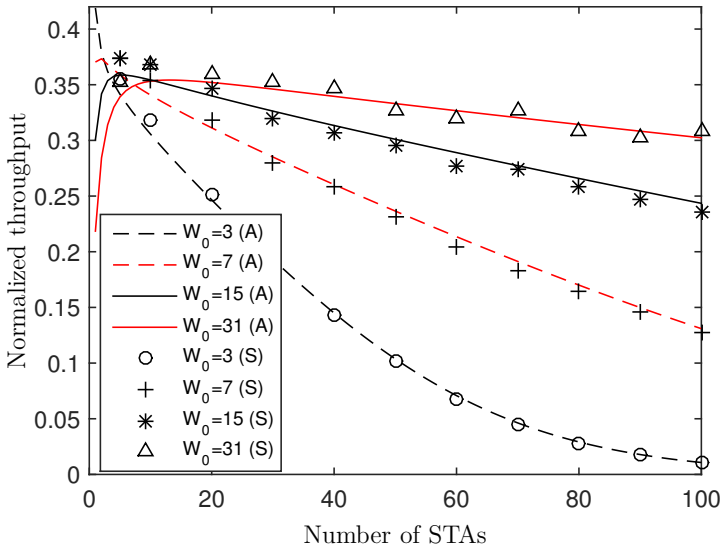

Figure 2.5: Throughput Vs number of STAs with varying contention window size, one sector, $m = 5$.

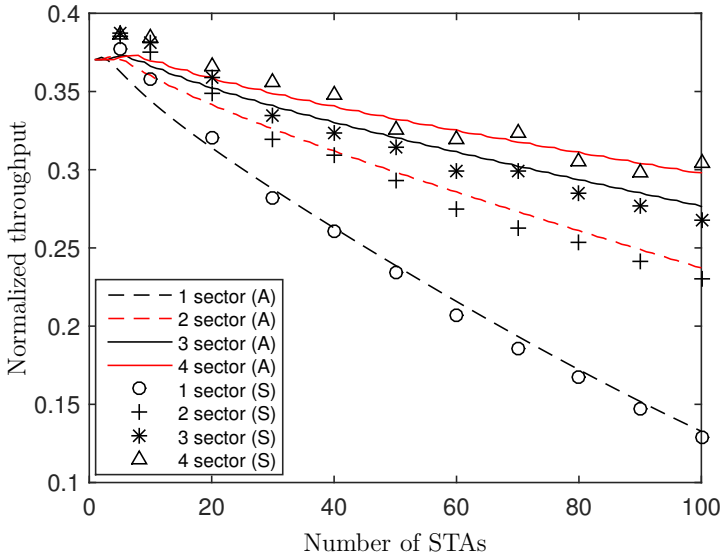

Figure 2.6: Throughput vs number of STAs for varying number of sectors, $W_0 = 15, m = 5$.

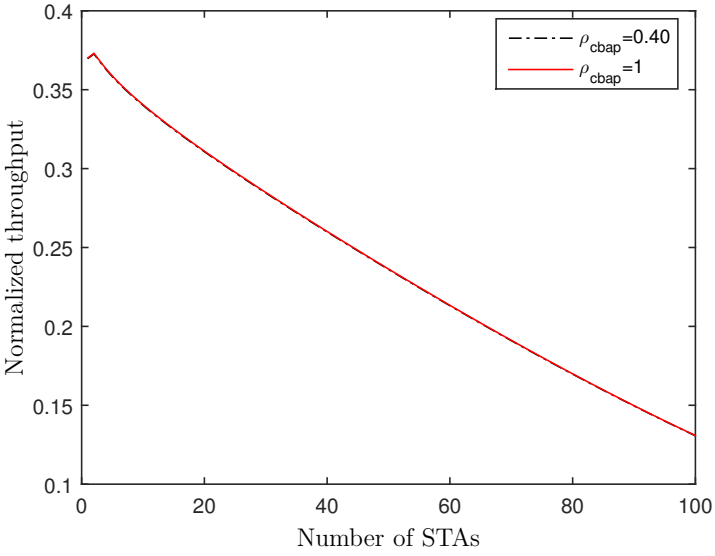

Figure 2.7: Throughput vs number of STAs for different values of CBAP fraction, one sector, $W_0 = 15, m = 5$.

smaller number of collisions and hence better channel utilization. On the other hand, if the total number of STAs is less, having more QO leads to an inefficient channel utilization. Hence, the QO beamwidth has a significant impact on the throughput performance and it should be carefully chosen so that an efficient channel utilization is ensured.

Fig. 2.7 shows the impact of ρ_{cbap} on the CBAP throughput with ρ_{cbap} equal to 0.40 and 1. It can be seen that the throughput values are almost equal. This is because the CBAP throughput calculation mainly depends on the total number of contending STAs at a particular time, the retransmission limits and the backoff window size. The amount of time when STAs are out of the CBAP period is not considered to calculate the throughput as during that time either STAs in other QO levels would contend for the channel or STAs would be utilizing the fixed access part of BI. On the other hand, ρ_{cbap} has a significant impact on the delay experienced by a packet as can be seen in Fig. 2.8.

Fig. 2.8 shows the average MAC delay for ρ_{cbap} equal to 0.40 and 1. We can see that for $\rho_{cbap} = 0.40$, the average packet delay is high as compared with the $\rho_{cbap} = 1$ because in the former case a packet will have to wait for $1 - \rho_{cbap}$ fraction of BI resulting in longer packet delays. From these results it is clear that ρ_{cbap}, i.e., the fraction of total BI time dedicated for CBAPs, should be carefully chosen. Fig. 2.9 shows the impact of packet size on the MAC delay. As expected, an increase in packet size results in an increase in MAC delay.

As discussed above, the QO beamwidth is an important parameter having a significant impact on the channel utilization of the CSMA/CA based medium

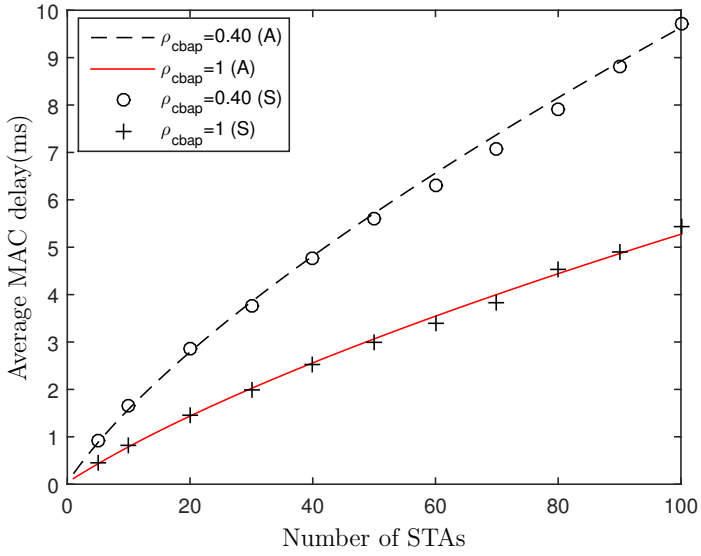

Figure 2.8: Delay vs number of STAs for different CBAP, $W_0 = 15, m = 5$.

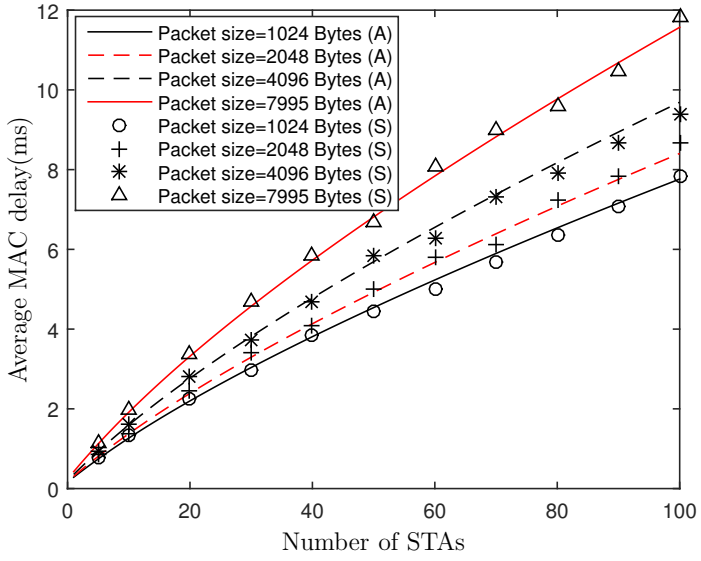

Figure 2.9: Delay vs Number of STAS for different values of packet size $W_0 = 15, m = 5$.

Table 2.1: CBAP Analysis Parameters.

RTS	20 Octets
DMG CTS	26 Octets
ACK	14 Octets
SIFS	2.5 μs
RIFS	9 μs
DIFS	13.5 μs
CCADetectTime	4 μs
Minimum window size W_0	15
Maximum Retry limit (m)	5
data size	1024 octets
Transmit power P_t	10 dBm
Fading loss X_σ	2 dB
Receiver sensitivity (MC4)	-64 dBm
Receiver sensitivity (MCS0)	-78 dBm
Link margin	3 dB
Path loss exponent α	2.5

access. Further, the CSMA/CA channel utilization decreases rapidly with an increase in the number of STAs. Maintaining an efficient utilization of the channel becomes very challenging when the number of contending STAs increases. For IEEE 802.11b/g/n, several solutions are proposed to improve the channel utilization such as controlling the minimum and maximum window size and retransmission limits, etc. However these schemes require that all the STAs adapt these parameters changes. Since contention based channel access in IEEE 802.11ad is provided in each QO level in a round robin fashion, it provides an extra degree of freedom (i.e., beamwidth) which can be used to control the number of simultaneously contending STAs by restricting the channel access in some spatial directions while not imposing restrictions in others. This is the motivation behind the adaptive beamwidth allocation proposed in the next section.

2.6. Adaptive beamwidth and timing allocation

IEEE 802.11ad does not provide any mechanism for selecting the beamwidth of individual QO levels. It only defines them as QO levels [40]. The average channel utilization during CBAP mainly depends on the conditional collision probability p. Consequently, using the equal beamwidth QO levels can lead to a very high collision probability in the densely populated regions or the under utilization of channel in the QO levels having a few STAs. To address this problem, we propose an algorithm for appropriate beamwidth selection for each QO level which tries to maximize the CSMA/CA channel utilization.

2.6.1. Beamwidth selection procedure

We neglect the beam switching time from one sector to another since switching the antenna beam from one direction to another takes very little time compared to the time wasted in a collision. [41] reports that an eight sector antenna array takes less than 100 ns to switch from one sector to another sector. Also, [5] suggests an interval of 0.5 μs for BIFS (Beam Switching Interframe Space) which is much less than the time spent in a collision.

Let us assume that the beamwidth Ω_k of the k^{th} QO level varies from Ω_{min} to Ω_{max}. The value of Ω_{min} is decided by the capability of the antenna array to narrow down its beamwidth to the least possible value, i.e., the highest possible beam resolution and Ω_{max} is limited by the intended maximum coverage distance of the PCP/AP. If we consider a perfect conical antenna model, the antenna gain $G(\Omega)$ for a beamwidth of Ω can be given by, $G(\Omega) = \frac{2\pi}{\Omega}$, where G is the gain of an omni-directional antenna. Thus, the antenna beamwidth is the deciding factor in determining the maximum coverage distance for a particular MCS and transmit power. Hence the value of Ω_{max} depends on the data rate and intended distance to be covered by the transmitter. The link budget at the receiver which is at a distance d from the transmitter can be given by Friis' transmission formula,

$$P_r(d) = P_t + G(\Omega_t) + G(\Omega_r) - PL_0 - 10\alpha \log_{10}(d) - X_\sigma - LM. \tag{2.34}$$

Where, P_t is the transmit power, $G(\Omega_t)$ and $G(\Omega_r)$ are the transmit and receive antenna gains that corresponds to the beamwidths Ω_t and Ω_r of the transmit and receive antennas. $PL_0 = 10\alpha \log_{10}(\frac{4\pi}{\lambda})$ is the reference path loss at a distance of 1 m. LM is the link margin, used to compensate for the alignment errors [42]. X_σ is the fading loss and α is the path loss exponent. If RS is the receiver sensitivity for a given MCS, then for satisfactory signal reception, $P_r \geq RS$. The value of RS is given in IEEE 802.11ad [7] for each MCS with a particular noise figure and packet error rate.

Fig. 2.10 shows the relation between required transmit antenna beamwidth for a given receiver beamwidth, MCS and intended coverage range. Curves are plotted for three MCS and intended distances of 5 m, 10 m and 15 m. It can be observed that MCS0 which is a low data rate MCS can operate at relatively wider beams as compared to the higher order modulation schemes MCS2 and MC13. In this way, for given STAs beamwidths, data rate and intended transmission distance,the maximum allowed beamwidth Ω_{max} can be selected.

To determine the beamwidth of QO levels, we start with Ω_{min} for the first sector and keep increasing the beamwidth by $\Delta\Omega$ (the differential beamwidth) until the throughput reaches its maximum value. As we know, with a increase in beamwidth, first the CSMA/CA throughput increases because adequate number of STAs are accommodated in a QO sector, but, when we keep increasing the beamwidth, after a certain beamwidth, the CSMA/CA throughput starts decreasing due to the increase in collisions. The detailed algorithm is described in Algorithm 1.

- **Step 0)** *Initialization (see line 1)*:

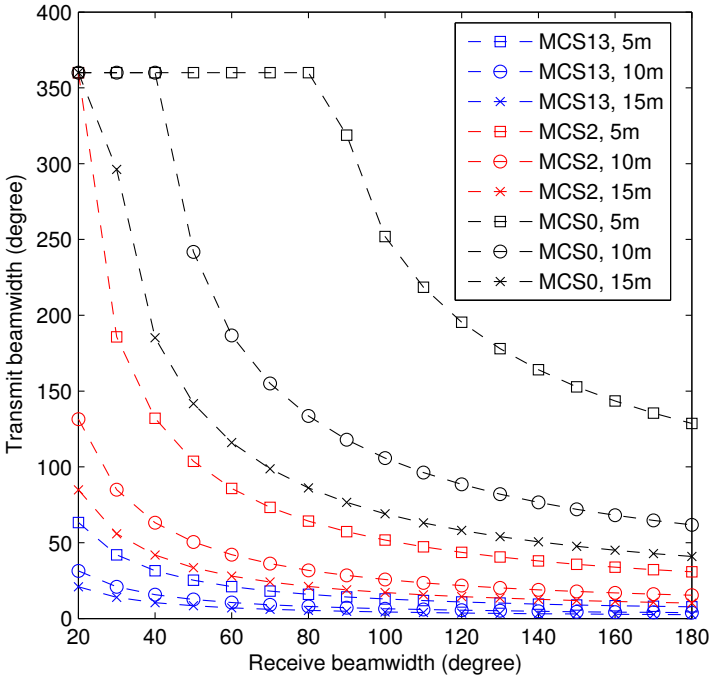

Figure 2.10: Required Rx/Tx beamwidth for different Modulation schems.

During the association process (A-BFT duration), STAs discover the PCP/AP and train their beams with PCP/AP using the SLS procedure. During the SLS process, the PCP/AP collects the angle information (i.e., angle w.r.t the position of PCP/AP) of all the STAs which are associated with the PCP/AP. Let A represent the set of angular information $\beta_j (j = 1, 2 \ldots, n)$ of all the n STAs associated with the PCP/AP.

- **Step 1)** *evaluation for the minimum beamwidth Ω_{min} (see line 3)*:

  Starting with a beamwidth Ω_{min}, PCP/AP calculates the number of devices in this beam area and hence the CSMA/CA throughput. Rename this beamwidth as Ω_p (i.e., past value) and corresponding throughput as U_p.

- **Step 2)** *increment by the differential beamwidth $\Delta\Omega$ (see line 4)*:

  Take Ω_p and U_p as reference values. Then, increase the beamwidth by $\Delta\Omega$, the new beamwidth is denoted as Ω_n (since $\Omega_n = \Omega_p + \Delta\Omega$, more devices are likely to be included in the increased beam area). Calculate the CSMA/CA throughput denoted as U_n.

- **Step 3)** *determine the appropriate QO beamwidth (see line 5 - 10)*:

Compare U_n and Ω_n with U_p and Ω_{max}, respectively. if $U_n \geq U_p$ and $\Omega_n \leq \Omega_{max}$, set $U_p = U_n, \Omega_p = \Omega_n$ and go to Step 3. Otherwise, select $\Omega_k = \Omega_p$ as the optimum beamwidth and n_k STAs for the k^{th} sector (initially, k=1).

- **Step 4)** *iteration to include all the STAs (see line 2 and 12)*:

  After deciding the beamwidth for the k^{th} sector, go to Step 2. Take the end point of the previous QO sector as the starting point for the next QO sector. Repeat the same procedure to decide the beamwidth for the $k + 1^{th}$ sector. Repeat the same procedure until all the devices are included or the complete area around the PCP/AP is traversed.

Algorithm 1 Adaptive QO beamwidth determination

1: **initialize** $A := \{\beta_i | 1 \leq i \leq n\}$, Ω_{min}, $\Delta\Omega$ and Ω_{max};
2: **while** $A \neq \emptyset$ **do**
3: $\Omega_p \leftarrow \Omega_{min}$ and calculate U_p;
4: $\Omega_n \leftarrow \Omega_p + \Delta\Omega$ and calculate U_n;
5: **if** ($U_n \geq U_p$ and $\Omega_n \leq \Omega_{max}$) **then**
6: $\Omega_p \leftarrow \Omega_n$, $U_p \leftarrow U_n$ and go to step 4;
7: **else**
8: $\Omega_k \leftarrow \Omega_p$;
9: count n_k, the number of STAs in the beam area
10: **end if**
11: $A := A - n_k$
12: go to step 2 and repeat the procedure for $(k + 1)^{th}$ sector;
13: **end while**
14: **return** $\Omega, n_k := \{\Omega_k | 1 \leq k \leq TotalSector\}$;

2.6.2. Computation of required CBAP duration for individual sectors

Let n_{id} be the sum of the expected number of idle slots in each backoff stage and n_b the sum of the expected number of busy slots in each backoff stage. Let T_{idle} and T_b represent the idle time slot duration and average busy slot duration, respectively. Since a busy slot can be part of a successful transmission or a collision, hence, $n_b = n_{col} + n_{suc}$ (n_{col} and n_{suc} are collision and successful slot counts respectively). Thus, the total expected CBAP duration T_{CBAP} can be expressed as,

$$T_{CBAP} = n_{id}T_{id} + n_bT_b. \tag{2.35}$$

Let there be a total of N requests to be completed. In order to ensure all the requests (on average) to be successfully transmitted, the sufficient and necessary condition is $n_{suc} \geq N$, i.e., the total number of successful transmissions should be at least equal to the expected number of transmission requests.

If m is the maximum packet retry limit, the average number of backoff slots before an STA successfully transmits a packet can be expressed as,

$$n_{id} = \sum_{0}^{m} P(TX = i|success)E[B_i], \tag{2.36}$$

where $P(TX = i|success)$ is the probability that an STA successfully transmits a packet in the i^{th} backoff stage and is expressed as a conditional probability $P(TX = i|success) = \frac{p^i(1-p)}{1-p^{m+1}}$. $E[B_i]$ is the average number of backoff slots accumulated by a device in the i^{th} backoff stage. Assuming that the backoff selection mechanism is uniformly distributed over the backoff window $[0, W_i - 1]$, $E[B_i]$ can be expressed as:

$$E[B_i] = \frac{1}{2}\sum_{0}^{i}(W_i - 1), 0 \leq i \leq m, \tag{2.37}$$

Therefore, now substituting the value of $E[B_i]$ from (2.37) and $P(TX = i|success)$ in (2.36), n_{id} can be obtained.
A busy slot can have two possible states, i.e., either a collision or a successful transmission. Therefore, the busy slots can be modeled as a Bernoulli random variable with $p_{suc/busy}$ and $p_{col/busy}$ as probability of a successful transmission and collision in a given busy time slot, respectively. Expressions for $p_{suc/busy}$ and $p_{col/busy}$ can be derived as,

$$p_{suc/busy} = \frac{P_{suc}}{1 - P_{idle}} = \frac{n_k\tau(1-\tau)^{n_k-1}}{1-(1-\tau)^{n_k}}, \tag{2.38}$$

and,

$$p_{col/busy} = \frac{P_{col}}{1 - P_{idle}} = \frac{1 - n_k\tau(1-\tau)^{n_k-1} - (1-\tau)^{n_k}}{1-(1-\tau)^{n_k}}. \tag{2.39}$$

From the definition of the Bernoulli trials, the expected number of successful slots can be given as, $n_{suc} = n_b p_{suc/busy}$. In order to calculate the minimum required CBAP duration we have to calculate the minimum required number of busy slots (denoted as $n_b[min]$), which would ensure that the average number of successful slots becomes equal to the average number of CBAP requests N in a given CBAP duration. Hence, $n_b[min]$ is equal to,

$$n_b[min] = \frac{N}{p_{suc/busy}}. \tag{2.40}$$

On substituting the value of n_b from (2.40) and n_{id} from (2.36) into (2.35), we can calculate the minimum required CBAP duration for the completion of the given number of requests. If we assume that, on average, each STA should be able to complete one request in the allotted CBAP time, N can be replaced by the total number of STAs n_k in a QO level to calculate the minimum average required CBAP time for that QO level.

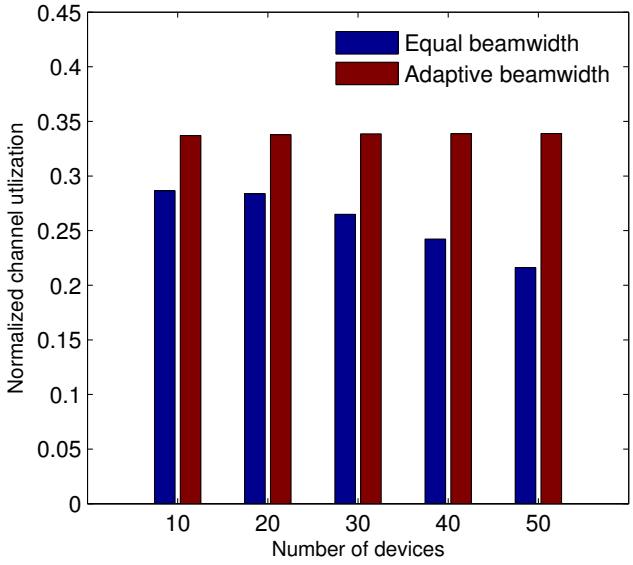

Figure 2.11: Comparison of the CBAP channel utilization for the adaptive and fixed QO beamwidths.

2.7. Numerical results and discussion

We simulate a conference room environment (radius=10 m) for different numbers of STAs with the PCP/AP placed at the center as shown in Fig. 2.2. The fixed beamwidth of all the STAs is assumed to be equal and taken as 60°. The location of an STA is identified by the Euclidean distance and angle from the PCP/AP. The Euclidean distances of STAs from the PCP/AP are uniformly distributed in the range [1,10 m], while angles (at which STAs are distributed) are generated from a Gaussian distribution with mean equal to 180° and a standard deviation of 90°. Thus, this ensures an uneven distribution of devices (some regions are densely packed while some are not). All the parameters values are taken from IEEE 802.11ad [7] and listed in Table 2.1. Both, the minimum beamwidth Ω_{min} and differential beamwidth $\Delta\Omega$ are assumed equal to 20°. To calculate the minimum required CBAP duration, the total number of requests per QO level are taken equal to the number of STAs in that QO level. For the fixed beamwidth, per QO level beamwidth is assumed to be 90° while for the adaptive beamwidth, each QO level has a different beamwidth and decided using Algorithm 1.

Fig. 2.11 shows the CBAP channel utilization for the fixed and the adaptive beamwidth QO levels. It is clear that the adaptive beamwidth approach performs better than the fixed beamwidth. The reason behind this is that the adaptive beamwidth approach always tries to accommodate STAs in such a manner that maximum channel time is utilized. If the number of STAs are increased, throughput of fixed beamwidth approach deteriorates, but adaptive beamwidth approach

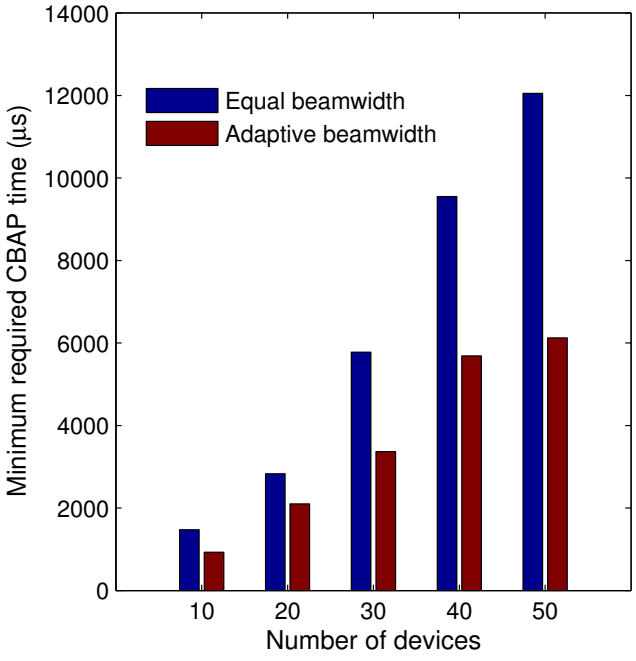

Figure 2.12: Comparison of the minimum required CBAP duration for the adaptive and fixed QO beamwidths.

is able to maintain a fair throughput. This is because the fixed beamwidth QO levels suffer increased collisions due to more number of STAs, while the adaptive beamwidth approach is able to reduce the beamwidth in heavily populated regions and thus restricting the number of STAs under the each QO level. This minimizes the collisions and maintains a steady throughput which is 20-30% more than the fixed beamwidth sectors. Fig. 2.12 shows the minimum required CBAP duration for successful transmission of all the generated requests. It shows that, using the adaptive beamwidth approach, the required CBAP duration is considerably reduced as compared to the fixed beamwidth approach. For example, when the total number of STAs are 50, required minimum CBAP duration is about 40-50% less for the adaptive beamwidth approach. It is evident from the results that as the number of STAs increases, the difference between the output of two approaches widens (for both channel utilization and minimum required CBAP duration). Hence it is clear that adaptive beamwidth QO levels help to reduce the required CBAP duration and maintain the steady channel utilization with an increase in the number of STAs. Therefore, in the regions having a high STA density, it is better to narrow down the QO levels beamwidths to reduce the collisions. This shows that the spatial distribution of nodes should be taken into account while granting channel access during the CBAP.

2.8. Conclusions

To solve the problems associated with the unique propagation characteristics of mmWave signals, directional antennas with dynamic beam steering have beem proposed. The use of directional antennas has a strong impact on the design of mmWave medium access mechanisms. IEEE 802.11ad has proposed a hybrid MAC protocol consisting of both the CSMA/CA and the fixed TDMA based channel access mechanisms. Although the IEEE 802.11ad MAC is backward compatible with IEEE 802.11b/g/n/ac, the DCF of IEEE 802.11ad has significantly distinct features as compared with that of IEEE 802.11b/g/n/ac. Due to the inherent directionality of APs and STAs, all the STAs cannot simultaneously listen to and hear from the AP. Hence, the area around an AP is divided into different sectors to ensure the complete coverage. Consequently, the CSMA/CA based medium access is provided in a round-robin fashion in different sectors leading to a significantly different DCF. This requires new methods of performance analysis that can accommodate the unique features of the IEEE 802.11ad MAC protocol.

In this chapter, we proposed an analytical model to characterize the throughput and delay performance of the IEEE 802.11ad MAC protocol. The proposed model based on a three-dimensional Markov chains takes into account the details of the IEEE 802.11ad MAC protocol and allows us to investigate the impact of different factors attributed to the use of directional antennas. By solving the 3-D Markov chain, we provide accurate analytical expressions for the channel utilization and MAC delay of the IEEE 802.11ad MAC protocol. Our analytical results show that the number of QO sectors has a significant impact on the channel utilization and MAC delay performance. It is shown that by choosing an appropriate QO beamwidth, an efficient channel utilization can be ensured. We proposed an adaptive QO level beamwidth selection algorithm considering spatial distribution of STAs which is able to achieve a significant improvement in the MAC throughput and required CBAP duration. Numerical evaluations have shown that as compared to the fixed beamwidth allocation, the adaptive beamwidth allocation improves the channel utilization up to 20-30% and reduces the required CBAP duration by 40-50%.

Further, we have shown that the MAC delay of the contention based access is highly influenced by the total allocated time for the contention periods in a beacon interval. The presence of the non-contention mode of access can result in longer MAC delays for the CSMA/CA packets. Hence, apart from the QO beamwidths, the division of the total BI duration into a contention and a non-contention part is also an important design parameter for efficient channel utilization while satisfying the delay requirements. In our analytical model, we have assumed a perfect line-of-sight path availability between STAs and the PCP/AP, neglecting the packet failures due to blockages. Further analysis is required where the impact of blockages need to be investigated on the MAC protocol performance. This can be done using the proposed Markov chain model with the provision for an extra probability variable in each of the head-of-the-line states that accounts for the blockage effects.

3

Trade-offs in Millimeter Wave Directional Links

In this chapter, we analyze the trade-offs associated with highly directional millimeter wave (mmWave) links, i.e., high gain resulting from narrow beamwidths versus the corresponding beam searching overhead and susceptibility to beam misalignment. We present a novel capacity modeling framework for mmWave links considering beamwidth, beam searching overhead and beam misalignment. We show that the narrowest possible beamwidth may not always result in the best link throughput. Our results illustrate that there is an optimum beamwidth after which, the effects of beam setup time and random antenna misalignments take precedence and deteriorate the actual link throughput. We also use commodity IEEE 802.11ad hardware to conduct experiments to assess the impact of beam searching and misalignment on 60 GHz directional links. Further, we propose a misalignment-aware beamwidth allocation mechanism which stabilizes the 60 GHz link performance under misalignment conditions. Our analysis emphasize the need for carefully considering the beam alignment and searching overheads while choosing the beamwidths of highly directional mmWave links.

3.1. Introduction

To compensate for the high free-space path loss at mmWave bands, directional antennas using narrow beamwidth pencil beams are employed. Since antenna gains and beamwidths are inversely proportional to each other, the common assumption is that narrow beamwidth antennas always perform better than wider beamwidth antennas. However, there are two important factors that affect the performance of a directional link:

(i) *Beam setup time*– The mmWave standards (IEEE 802.11ad [7] and IEEE 802.15.3c [5]) provide beam forming protocols to find the best transmit (Tx) and receive (Rx) beam directions. The beam search space increases with

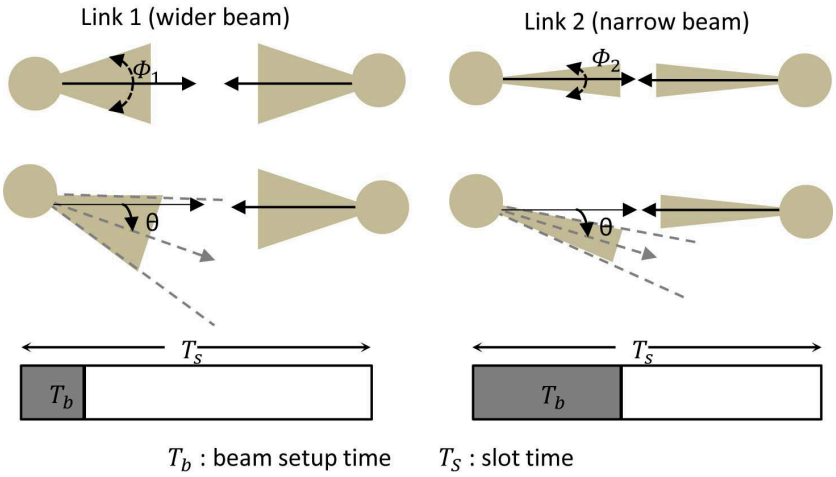

Figure 3.1: Impact of misalignment on mmWave links with different beamwidths.

the decrease in the beamwidths of the Tx and Rx antennas. A considerable fraction of time is wasted in each slot searching the best direction for beamforming. Hence the beam search time contributes significantly to the communication overhead. Although this could be neglected in the static case, for links with mobile stations this is an important aspect.

(ii) *Beam misalignment* – The issue with narrow beamwidth directional links is the frequent misalignment caused by various factors such as orientation error, random movements, vibrations, etc. If the beamwidth is very small (1°-5°), even a small misalignment can result in highly unstable links causing loss of throughput.

Fig. 3.1 illustrates the effects of misalignment on two mmWave links with different beamwidths and equal transmit power. Link 1 employs wider beamwidth antennas than Link 2. This means that the Tx and Rx antenna gains of Link 2 are higher than those of Link 1. However, the link set up time for Link 2 is higher than that of Link 1, causing a higher beam searching overhead for Link 2. Furthermore, Link 2 is more susceptible to antenna misalignment compared to Link 1 and this can lead to an unstable Link 2. Therefore, misalignment and beam searching overhead must be taken into account when modeling the capacity of narrow pencil beam mmWave links.

To the best of our knowledge, there is no prior work that has considered the consequential trade-offs, i.e., beam searching overhead and susceptibility to misalignment due to the use of high gain pencil beams. The existing analytical

models either consider the beam searching overhead [24, 25, 26, 27] or the misalignment [28, 43, 29], separately. Therefore, there is a need for considering both these aspects together. Further, it is also interesting to find the limits on the beamwidth *vis-à-vis* achievable throughput.

Our main contributions are:

(i) We perform extensive measurements to investigate the initial user association time and the beam setup time using commodity IEEE 802.11ad hardware. As compared with the existing experimental evaluations of 60 GHz devices [44, 45, 46, 47, 48], we are the first to measure the beam setup overhead in absolute time units for the commodity IEEE 802.11ad hardware.

(ii) We model the capacity of mmWave links by jointly considering the antenna misalignment, beam training overhead and time slot lengths.

(iii) We conclude that narrow beams result in unstable links with reduced link capacity due to antenna misalignment and high beam training overhead. In such conditions it is advantageous to use moderately narrow beams rather than the high resolution pencil beams for better link quality.

(iv) We propose a mechanism to stabilize the 60 GHz link performance under misalignment conditions which results in a significant improvement in link capacity.

3.2. Related work

Analytical modelling of 60 GHz directional links:
The use of highly directional antennas induces many challenges for network design, medium access control and mobility management due to significantly different constraints at 60 GHz [16], compared to microwave frequencies. As explained in the previous section, one of the major challenges of employing narrow beamwidth antennas is the initial link set up. To solve this issue, a MAC-layer-based two-stage beam searching mechanism, employing exhaustive search, has been proposed [22]. For each beam direction, pre-defined beam steering antenna weight vectors (amplitude and phase configurations) are defined which is also called beam Codebook. This approach has been first included in the 60 GHz standard IEEE 802.15.3c. A slightly different version of this approach is adopted in IEEE 802.11.ad. MAC layer beamforming is chosen over PHY layer beamforming due to the following reasons: (i) antenna structures will have a direct impact on PHY level beamforming hence it would be difficult to implement a standard beamforming procedure; and (ii) angle-of-arrival or angle-of-departure based methods using signal processing algorithms require complex computations to calculate the antenna weight vectors that can lead to high energy consumption in 60 GHz circuits. Therefore, to overcome the dependence on antenna structures and to avoid power-hungry signal processing methods, MAC-layer based beamforming is preferred in IEEE 802.15.3c and 802.11ad.

To reduce the beam searching overhead, a new search technique has been proposed in [24], which uses *iterative subspace partitioning*. Furthermore, it proposes a different beam searching methodology for fixed and adaptive modulation schemes resulting in considerable reduction of the beam searching time. Bin Li, *et al.* [25] have also suggested an optimized search algorithm to improve the beam training time using a modified version of the Rosenbrock numerical algorithm.

A completely different approach employing 2.4/5 GHz signals to assist the mmWave beamforming has been proposed in [26], which reduces the beam training overhead. It is shown that the direction of 60 GHz transmissions can be inferred from 2.4/5 GHz transmissions. To analyse the mmWave link performance for variable beamwidths, a randomized exclusive region-based protocol is proposed in [49]. An enhanced version of [49] is proposed in [50]. However, a perfect link alignment is considered and beam searching overhead is neglected. Analysis of directional networks considering beam misalignment, using stochastic geometry, has shown that a slight misalignment can have a significant impact on the availability of links [28, 43, 29]. However, the beam searching overhead is not considered in these works. The impact of beam searching on mmWave links employing the IEEE 802.15.3c is considered in [27, 51], however, antenna misalignment is neglected. To fully characterize the behavior of mmWave links, antenna misalignment and beam searching overhead must be jointly considered.

Experiments using 60 GHz devices:
In [44], Wilocity 802.11ad hardware (Dell 6430u laptop and D5000 docking station) is used to characterize the performance of 60 GHz links in outdoor picocells. However, the focus of this work was to study the communication range, throughput and blocking effects. Furthermore, only TCP-level performance is traced using a packet analyzer and initial user association time and re-beamforming time are not investigated. Recently, a measurement-based study concluded that the antenna misalignment and beam searching overhead have extremely adverse effects on the performance of IEEE 802.11ad links and can lead to a significant degradation in the link throughput [45]. However, in this paper custom designed non-IEEE 802.11ad hardware and horn antennas are used to emulate the phased array operation, thus impact of misalignment and beam searching overhead using IEEE 802.11ad is not shown. A few other studies [46, 47, 48] have used commodity IEEE 802.11ad hardware to measure the 60 GHz link performance but experiments are limited to average throughput and range measurements only. However, in this thesis we performed experiments using commodity IEEE 802.11ad hardware specifically focussing on IEEE 802.11ad beamforming mechanism to measure the time taken in initial user association, i.e., device discovery; and the time taken in re-beamforming if misalignment is introduced.

3.3. The trade-offs in mmWave beamforming protocols

We consider an IEEE 802.11ad based 60 GHz mmWave Personal Basic Service Set (PBSS) as shown in Fig. 3.2. The one of the STAs in a PBSS acts as the

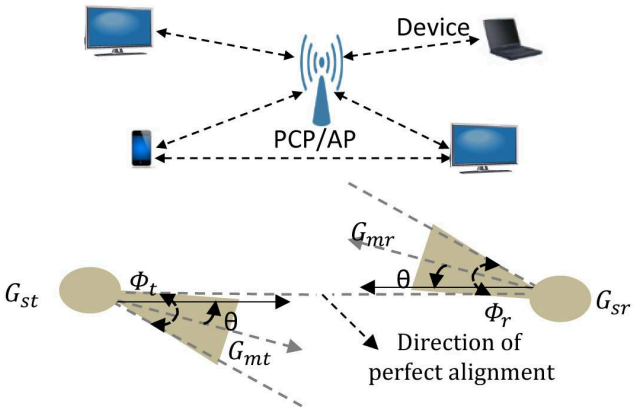

Figure 3.2: IEEE 802.11ad network architecture.

PBSS control point/Access Point (PCP/AP) to coordinate the channel access. In particular, we focus on the service periods (SP) part of the IEEE 802.1ad Beacon Interval (BI) where narrow beamwidth pencil beams are used for the high speed data transmission. The IEEE 802.11ad BI is depicted in Fig. 3.3. The detailed description of the different parts of a BI is already explained in the Chapter 2 (Section 2.3).

To initiate the high speed data transfer in an allocated time-slots during the SP, the IEEE 802.11ad specifies a two-stage beamforming procedure. In the first stage, STAs perform a coarse sector training to find the best Tx and Rx sectors using relatively wide beamwidths, i.e., coarse sector beamwidth. In the second stage, STA pairs perform the beam training mechanism to find the best receive and transmit pencil beams using the beam searching protocol. Once the highest resolution Tx and Rx beams are found, high speed data transmission is initiated. The detailed description of the beamforming procedure can be found in [7].

As shown in Fig. 3.2, we denote the main lobe Tx and Rx antenna gains for the given half-power beamwidth (HPBW) ϕ and antenna misalignment value θ by $G_{mt}^{\phi_t}(\theta)$ and $G_{mr}^{\phi_r}(\theta)$ for the transmitters and receivers, respectively. The subscript 'm' stands for main lobe, and subscripts 't' and 'r' stand for transmitter and receiver, respectively. The angle θ is measured from the axis of perfect alignment to the antenna bore-sight. We assume constant side lobe antenna gain patterns for the transmitter and receiver denoted by $G_{st}^{\phi_t}$ and $G_{sr}^{\phi_r}$, respectively.

Let P_t be the transmit power and G_c be the channel gain, then using the Friis' free-space path loss model, the received power at a distance d from the transmitter is given by,

$$P_r = G_t G_r G_0(\lambda, d) P_t, \tag{3.1}$$

here, λ is the wavelength of the carrier signal and α is the path loss exponent. $G_0(\lambda, d) = \left(\frac{\lambda}{4\pi d}\right)^{\alpha}$ captures the overall effect of free-space path loss and prop-

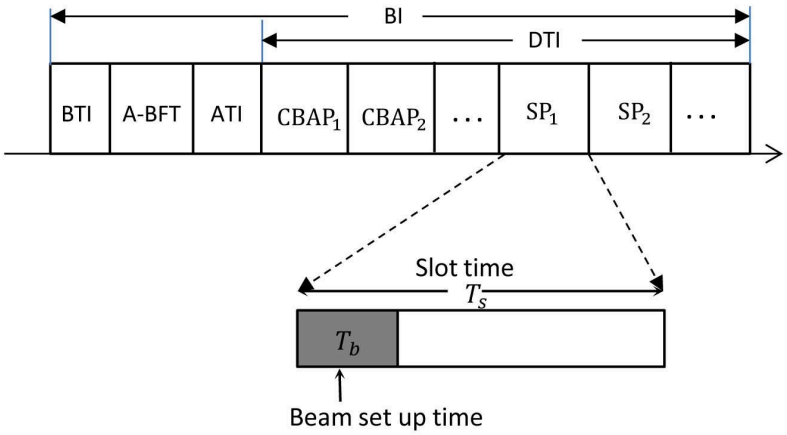

Figure 3.3: IEEE 802.11ad beacon interval.

agation loss over the distance d between transmitter and receiver. Further, the achievable link rate (bits/ Hz), according to Shannon's capacity theorem can be given by,

$$R = \log_2\left(1 + \frac{P_r}{N_0 W}\right), \tag{3.2}$$

where, N_0 is the one-sided power spectral density of white Gaussian noise and W is the signal bandwidth.

3.3.1. Beam misalignment

The antenna elements of an antenna array can be dynamically configured to facilitate varying level of beamwidths and different beam directions. The wider beams can cover large angular areas around transmitters but with smaller range, while very narrow pencil beams can pinpoint on a small region of interest at greater distance. The transmission and reception characteristics of a directional antenna exhibit reciprocity which means that both Tx and Rx gains are achieved using a directional antenna.

Communication using narrow beams require strict alignment of Tx and Rx antennas to ensure the signal reception in the direction of maximum radiation. This makes narrow beams extremely sensitive to beam misalignment. There are many factors which can contribute to antenna misalignment such as estimation errors, user movement, device orientation error, etc. To analyze the impact of antenna misalignment on antenna gains, analytical models of real world antennas are required. In general, it is difficult to capture all the essential characteristics of a real world antenna in a simple mathematical model. The simplest antenna model widely used in the literature employ a circle plus cone model [27] in which the antenna main lobe and the side lobes are represented by constant gain values where the main lobe gain is much higher than the side lobe gain. This model is not suitable to study the effects of antenna misalignment because any value of

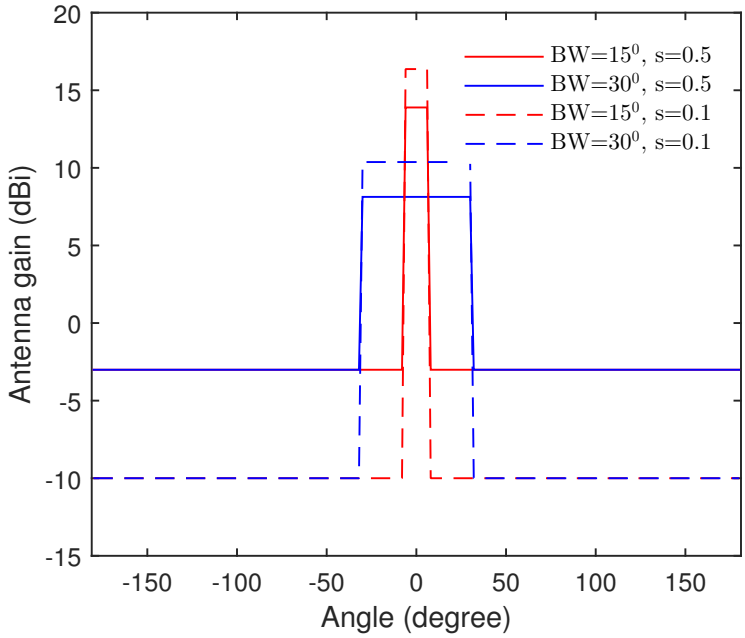

Figure 3.4: Ideal cone-plus-circle antenna gain patterns.

misalignment smaller than the main lobe beamwidth would be unnoticed due to its constant main lobe gain. This antenna model is represented as follows,

$$G^{\phi}(\theta) = \begin{cases} \frac{2\pi-(2\pi-\phi)s}{\phi}, & |\theta| \leq |\frac{\phi}{2}|, \\ s, & |\theta| \geq |\frac{\phi}{2}|, \end{cases} \tag{3.3}$$

here, $0 \leq s \leq 1$ is the gain of the side-lobe. For narrow-pencil-beam antennas $s << 1$, which implies negligible side-lobe radiation thus confining transmitted power to the antenna main lobe. Therefore, the above model can be called an ideal directional antenna model which provides a basic understanding of the radiation patterns of directional antennas.

Fig. 3.4 depicts the radiation pattern of an ideal cone plus circle antenna for beamwidth values of 15° and 30° for a side lobe gain s equal to 0.5 and 0.1. From the radiation patterns, it is evident that this model is an on-off model with constant main and side lobe gains. This model is not suitable for the analysis of wireless systems with adaptive modulation schemes where multiple values of antenna gains based on the Tx-Rx alignment with respect to antenna bore sight can be utilized to adjust the modulation and coding schemes. Hence we consider another antenna model as follows.

A relatively practical antenna model is proposed in IEEE 802.15.3c [5], which uses a Gaussian main lobe instead of constant main lobe radiation pattern. This

antenna model has achieved good agreement with the measured data [5]. The analytical model is represented as,

$$G^{\phi}(\theta) = \begin{cases} G_m^{\phi}(\theta) = \left(\frac{1.6162}{\sin(\phi/2)}\right)^2 \exp^{-K_1\left(\frac{\theta}{\phi}\right)^2}, & |\theta| \leq 1.3\phi, \\ G_s^{\phi} = \exp^{-2.437}\,\phi^{-0.094}, & |\theta| > 1.3\phi, \end{cases} \tag{3.4}$$

here, ϕ is the half-power beamwidth (HPBW) which is the angle between the half-power (-3 dB) points of the antenna main lobe and $K_1 = 4\log_e 2$. The antenna main lobe gain depends on 'θ' which is Tx-Rx alignment angle with respect to antenna bore-sights. θ can also be referred to as antenna misalignment. The main lobe beamwidth ϕ_{ML} of such an antenna is determined using the -20 dB levels relative to the main lobe peak values and is roughly equals to 2.6ϕ. In Fig. 3.5(a), we have marked the -3 dB and -20 dB points for beamwidth ϕ=15°. Fig. 3.5(a) shows the main lobe gain variations with the misalignment with respect to antenna bore-sight angle for different values of HPBW ϕ. We can observe that the gains of narrow beamwidth antennas decrease faster than the wider beamwidth antennas. This implies that the high gain narrow beam antennas are highly susceptible to misalignment errors. Due to beam misalignments, effective Tx and Rx antenna gains would be less than the expected antenna gains for given Tx and Rx beamwidths resulting in transmission errors. Unlike the ideal cone-plus-circle antenna model where the antenna gain has binary values, the Gaussian main lobe model offers different antenna gains for the different values of beam misalignments. This in turn would result in multiple levels of received power at the receiver rather than simple on-off states. This is particularly useful when adaptive modulation and coding schemes (MCS) are used. 60 GHz standards such as IEEE 802.11ad and IEEE 802.15.3c have provisions for adaptive MCS based on the link quality to provide variable data rates ranging from tens of Mb/s to multiple Gb/s.

Fig. 3.5(b) shows the link capacity as a function of beamwidth for different values of misalignment θ at a distance of 5 m. The link capacity represented by (3.2) is evaluated using (3.1) and (3.4). Identical antenna gain and misalignment values are considered for Tx and Rx. It can be observed that for the higher values of the beam misalignment, wider beamwidths result in better link quality than the narrow beamwidths. This can be attributed to the higher misalignment sensitivity of narrow beamwidth antennas. The beam misalignment depends on various factors such as mobility, channel estimation error, vibration due to wind in case of a pole mounted mmWave base station, orientation errors due to device holding patterns of users, and imperfections of antenna array fabrication process, etc [52].

If half of the antenna main lobe beamwidth is less than the maximum possible misalignment, the antenna main lobe pointing error could lead to link failure. If $|\theta_{max}|$ is the maximum misalignment, to ensure the link availability, the following condition should be satisfied,

$$\frac{\phi_{\mathrm{ML}}}{2} \geq |\theta_{max}|. \tag{3.5}$$

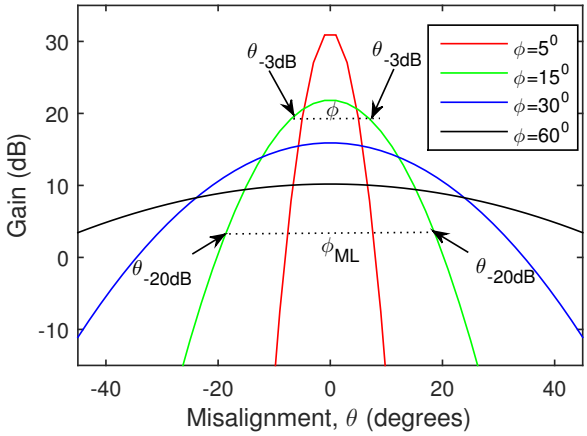

(a) Gain vs beam-misalignment for different beamwidths.

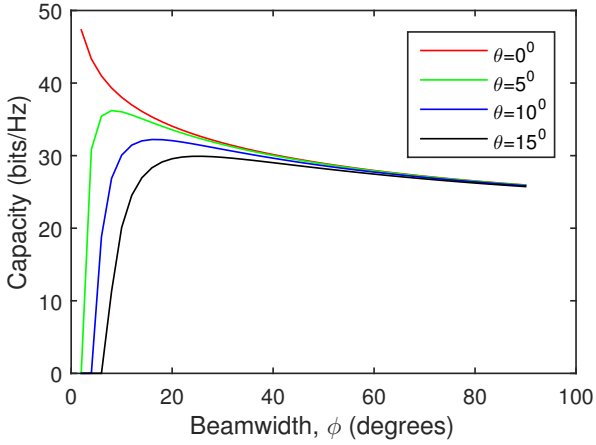

(b) Link capacity vs beamwidth for different misalignments.

Figure 3.5: Effect of beam-misalignment on antenna gains and link capacity.

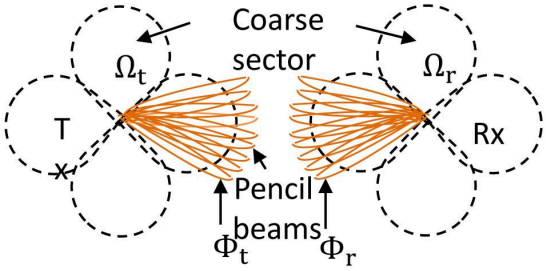

Figure 3.6: IEEE 802.11ad antenna sectors and beams.

In case of a Gaussian main lobe with HPBW ϕ, the main lobe width $\phi_{\mathrm{ML}} = 2.6\phi$.

3.3.2. Beam training overhead

In order to determine best Tx and Rx beam directions, mmWave standards such as IEEE 802.15.3c and IEEE 802.11ad have proposed beamforming protocols which use multi-level beamforming procedures. A pair of STAs that wants to communicate with each other starts scanning using wider beamwidths called quasi-omni (QO) levels or sector levels. For example, Beamwidths of a QO or sector level could be equal to 180° or 90°. Once a transmitter and receiver have found their best Tx and receive Rx sectors, they can further narrow down their beamwidths to form high resolution directional links using narrow pencil beams. Beamwidths of narrow pencil beams depend on the number of antenna array elements. For example a 32 element (8×4) planar antenna array can have a beamwidth equal to 10°. With more antenna elements, beamwidths up to 1° to 5° can be achieved.

Fig. 3.6 illustrates the sector level and beam level beamwidths of a Tx-Rx pair. A coarse beamwidth sector contains many fine beams. Training sequences are transmitted and received in all the possible directions to find the best Tx and Rx directions. In the IEEE 802.11ad beam searching protocol, sector level training is generally performed during the ABFT part of the BI (see Fig. 3.3). However, training for narrow pencil beams is performed during the start of the allocated time slot during an SP. Let Ω_t and Ω_r be the sector level Tx and Rx beamwidths, respectively. Let ϕ_t and ϕ_r be the beam level Tx and Rx beamwidth, respectively. Then, the beam search space consists of $\frac{\Omega_t}{\phi_t}$ Tx beams and $\frac{\Omega_r}{\phi_x}$ Rx beams. T_B, the total time required to find the best Tx and Rx beams using the

IEEE 802.11ad beam searching protocol can be expressed as,

$$T_B = \left(\frac{2\pi}{\Omega_t} + \frac{2\pi}{\Omega_r}\right) T_p + \left(\frac{\Omega_t}{\phi_t} + \frac{\Omega_r}{\phi_r}\right) T_p, \tag{3.6}$$

where, T_p is the time required to transmit a beam training packet.

As shown in Fig. 3.3 a time-slot T_S allocated to a device pair consists of two parts: (i) beam training interval, T_B, and (ii) high-speed data transmission interval, $T_S - T_B$. This implies that the beam training time T_B is a necessary overhead which impacts the average achievable data-rate during the allocated time-slot T_S. From (3.6), we see that the value of T_B depends on the Tx and Rx beamwidths considering a fixed pilot transmission time. The beam-search space increases as the beamwidth decreases. This forces a trade-off between the high data rate that could be achieved by the narrow pencil beams and the required beam training duration.

Let $T_B^{\phi_t,\phi_r}$ be the beam training duration for given Tx/Rx beamwidths, then the fraction of allocated time slot T_S which is used for data transmission is given by,

$$\eta(\phi_t, \phi_r) = \left(1 - \frac{T_B^{\phi_t,\phi_r}}{T_s}\right). \tag{3.7}$$

Hence, the achievable data-rate R^{ϕ_t,ϕ_r} (bits/slot/Hz) for given Tx-Rx beamwidths is given by,

$$R^{\phi_t,\phi_r} = \eta(\phi_t, \phi_r) \log_2\left(1 + \frac{P_r}{N_0 W}\right), \tag{3.8}$$

where, P_r is the received power and is given by (3.1).

Fig. 3.7 shows the impact of beam-training overhead on total achievable data throughput for the given slot durations. Here, we have assumed perfect antenna alignment by employing the antenna gain $G_m^{\phi}(0)$ from (3.4). We can see that using very narrow beams can result in less link capacity than the wider beamwidths. The effect of beam training overhead is more pronounced for smaller time slot lengths. Here, we have considered the 2-D beamforming in which beam search space is limited only to the azimuth plane. However, if 3-D beamforming is employed, beam searching would be performed in both azimuth and elevation plane -resulting in even higher beam training overhead.

3.4. Experimental study of user association and misalignment in IEEE 802.11ad

3.4.1. Hardware details

We use the commercial 60 GHz Wireless Docking Station Dell WLD15 [53] that acts as a PCP/AP and a Dell laptop (Latitude E7450) that acts as an STA. The laptop and docking stations are equipped with Intel Tri-Band Wireless-AC 17265 [54] 60 GHz radio chipsets having 2×16 planar antenna array with an azimuth beamwidth of 120° and elevation beamwidth of 30°. Its beamforming

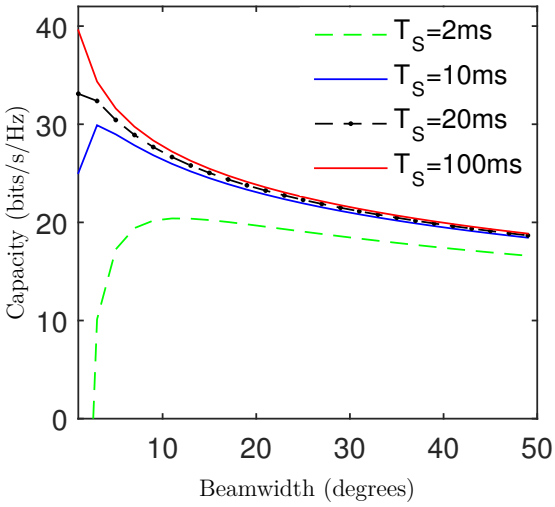

Figure 3.7: Impact of beam-searching overhead on the link capacity.

and rate adaptation mechanisms are adopted from the IEEE 802.11ad standard. Both devices support the use of 3 possible channels in 60 GHz band. For our experiments, we used Channel 3 with the center frequency of 62.64 GHz. The link quality performance is represented by the normalized signal quality parameter on a the scale of 0 to 10. The signal quality is measured at interval of 20μs.

3.4.2. Methodology

The information about IEEE 802.11ad connection between the laptop and the docking station is provided by the Intel Wireless Dock Manager API. The API reports the normalized signal quality on a scale of 0 to 10 acquired from the 60 GHz wireless card. In order to get the signal quality information, we decompiled the WiGig wrapper (WiGigSDKWPFWrapper.dll) which provides the access to the IEEE 802.11ad driver. Through the GetCurrentConnectionInfo class in the wrapper, the signal quality parameter is retrieved. We recorded the signal quality at intervals of 20μs to track the changes in signal quality during the initial user association and re-beamforming procedure.

Table 3.1: IEEE 802.11ad user association time.

Tx/Rx Distance (m)	1	4	10
Best case (ms)	146.28	153.34	172.12
Worst case (ms)	386.14	375.56	324.58
Average (ms)	247.47	245.4	243.75

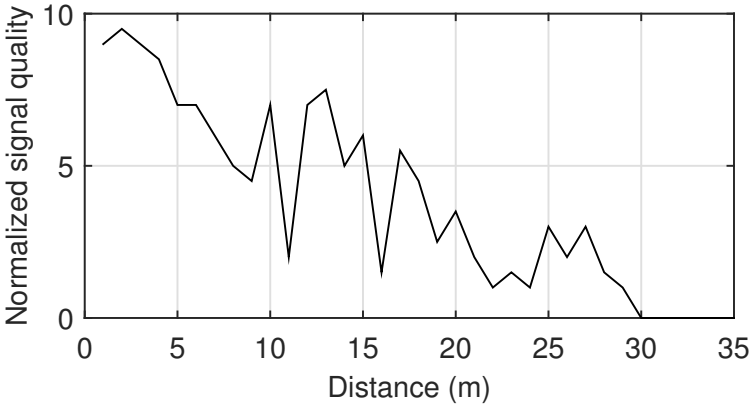

Figure 3.8: Measured INTEL's IEEE 802.1ad chipset signal quality over distance.

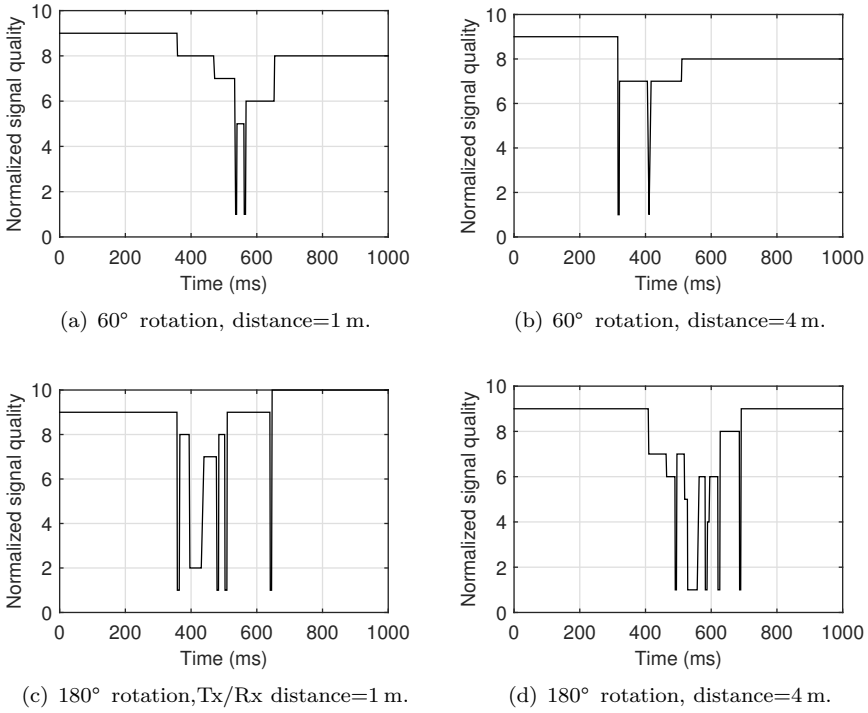

(a) 60° rotation, distance=1 m.

(b) 60° rotation, distance=4 m.

(c) 180° rotation,Tx/Rx distance=1 m.

(d) 180° rotation, distance=4 m.

Figure 3.9: Representative measurements showing signal quality fluctuation caused by misalignment.

3.4.3. Measurement results

In our experimental setup both the devices are placed at a height of 75 cm above the floor. We also make sure that there is no potential 60 GHz interfering device operating in the environment as well as no obstacles between the docking station and the laptop so that direct beam connection between the laptop and the docking station can be established. The measurements are repeated 10 times and the signal quality is monitored for a total duration of 10 s in each iteration. Before assessing the user association and re-beamforming performance, we measured the communication range of these devices in a corridor and found that maximum distance is 30 m (see Fig. 3.8). Since the corridor width is only 3 m, effects of multipath arising due to the signal bouncing off the walls are visible in the experimental results. Beyond a distance of 30 m, the docking station and the laptop could not discover each other.

Initial user association

This experiment is performed by resetting (turning-off and turning-on) the docking station. Initially the docking station is turned-off. Once the docking station is turned-on, the laptop and the docking station try to establish the IEEE 802.11ad connection. The signal level from the IEEE 802.11ad interface of laptop is continuously monitored at discrete time intervals of 20μs. We measure the time difference between the final stable signal value and the first registered signal value.

Table 3.1 shows the association time for distances of 1 m, 4 m and 10 m. The average association time at all the three distances is almost equal which is logical because the IEEE 802.11ad uses two-stage fixed beamwidth searching mechanism. However, the worst case and the best case measurements shows opposite trends with respect to distance. The best case association time is least for 1 m distance while worst case association time is least when the Tx-Rx distance is 10 m. A possible reason for these differences could be the channel variations because of multipath effects.

Beam misalignment and connection re-establishment

In this experiment, the laptop is rotated complete 360° in discrete angular steps while the docking station is kept in a fixed position. We use two different rotation angle steps: 60° and 180°. The rotational movement is performed in clockwise manner by using a mechanical rotor to introduce misalignment. During the rotation from one step to another step, the 60 GHz connection suffers degradation due to beam misalignment which is indicated by the degradation of the signal quality parameter. Consequently, the laptop and the docking station try to re-align their beams using the IEEE 802.11ad beamforming mechanism in order to retrieve highest achievable signal quality.

Fig. 3.9 shows the snapshots of the effects of misalignment (60° and 180°) on signal quality. We can see that the signal quality nearly drops to zero in both cases of misalignment. Fluctuations in signal levels suggest the presence of multipaths due to reflections from laptop keyboard and room surface as the height of both the docking station and laptop is 75 cm from the floor.

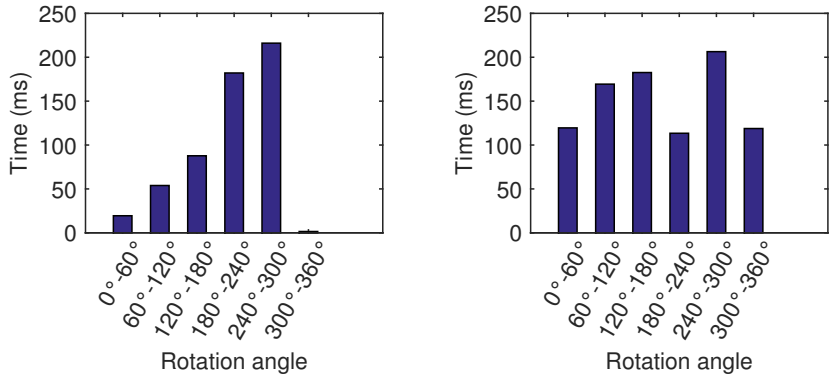

(a) Tx/Rx distance=1 m. (b) Tx/Rx distance=4 m.

Figure 3.10: Average re-beamforming time taken during 60°misalignment.

The average re-beamforming times are shown in Fig. 3.10 and Fig. 3.11. In case of rotation step of 60°, the re-beamforming time significantly differs for each rotation step. Since the IEEE 802.11ad antennas are placed on the lid of the laptop, each rotation step results in a different view of the laptop's antenna array from the docking stations perspective. This could be a reason for the differing re-beamforming times. However, in the case of 180° rotation, the difference in re-beamforming time is small because laptop and docking station directly face each other. These results manifest the randomness in the beam alignment procedure due to channel variations and orientation of devices. Further, the approximate duration of 150–250 ms re-beamforming time is quite high as compared to the numerical estimates of a few milliseconds. Furthermore, these values are quite large for many 5G applications requiring delay of less than 10 ms [55] and thus it requires immediate attention. In the next section, we analyze capacity of 60 GHz links considering above aspects.

3.5. Analytical modelling of link capacity jointly considering beam setup time and misalignment

In this section, we model the capacity (bits/s/Hz) of mmWave links considering the effects of misalignment and beam training overhead together. By substituting antenna gains as a function of misalignment θ and HPBW ϕ into (3.8), the link capacity can be found as,

$$r^{\phi_t,\phi_r}(\theta_t,\theta_r) = \eta(\phi_t,\phi_r)\log_2\left(1+\frac{G_t^{\phi_t}(\theta)G_r^{\phi_r}(\theta)G_0(\lambda,d)P_t}{N_0W}\right). \tag{3.9}$$

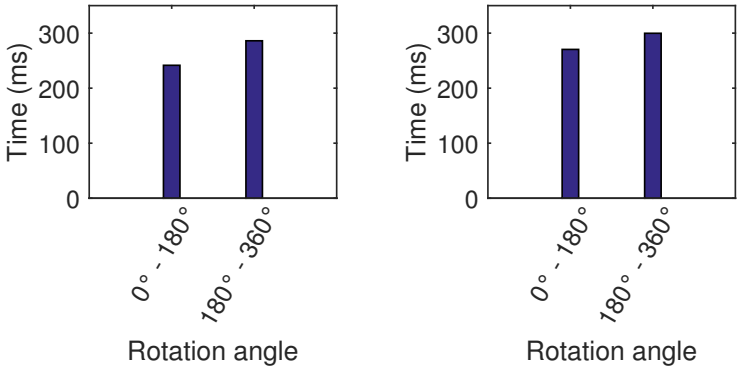

(a) Tx/Rx distance=1 m. (b) Tx/Rx distance=4 m.

Figure 3.11: Average re-beamforming time taken during 180°misalignment.

Where, $G_t^{\phi_t}(\theta)$ is a function of Tx beamwidth ϕ_t and misalignment θ; similarly, $G_r^{\phi_r}(\theta)$ is a function of Rx beamwidth ϕ_r and θ. $\eta(\phi_t, \phi_r)$ depends on sector beamwidths Ω_t and Ω_r, pencil beam beamwidths ϕ_t and ϕ_r, and allocated time slot T_S. Since in most of the mobile scenarios PCP/AP or base stations are usually fixed, only users' devices are prone to misalignment due to movement of users. Therefore, we consider the effect of misalignment at the users-end only and neglect the misalignment of the PCP/AP antennas. Hence $\theta_t = 0$ and $\theta_r = \theta$. By replacing the antenna gain values in (3.9), we get,

$$r^{\phi_t,\phi_r}(\theta) = \eta(\phi_t, \phi_r) \log_2 \left(1 + c_1 \exp\left(-\left(\frac{\theta}{\phi_r}\right)^2\right)\right), \tag{3.10}$$

here, $c_1 = G_0(\lambda, d) P_t \left(\frac{1.6162}{sin(\phi_t/2)}\right)^2 \left(\frac{1.6162}{sin(\phi_r/2)}\right)^2$. It can be observed that the exponential part of (3.10) contains only the Rx misalignment as Tx misalignment is assumed to be zero. For brevity, henceforth, we will represent $r^{\phi_t,\phi_r}(\theta)$ as r and $\eta(\phi_t, \phi_r)$ as η.

Here we may notice that the misalignment θ is a random variable. Hence r^{ϕ_t,ϕ_r}, which is a function of θ, would also be random and let us denote the underlying random variable by R. Let us assume θ is uniformly distributed in the interval $-\theta_m$ to θ_m, then $f(\theta)$, the probability density function (pdf) of θ is,

$$f(\theta) = \begin{cases} 1, & |\theta| \leq \theta_m, \\ 0, & |\theta| > \theta_m. \end{cases} \tag{3.11}$$

Let us represent the transformation function of R and θ by $r = g(\theta)$. Using the definition of the transformation of random variables [56], $f_R(r)$, the pdf of R can

be expressed as,

$$f_R(r) = (-1)^i f(g^{-1}(r)) \frac{\partial}{\partial r} g^{-1}(r). \tag{3.12}$$

Where $i = 0$ if $g(\theta)$ is a monotonically increasing function of θ, and $i = 1$ if it is a monotonically decreasing function of θ. It is evident from (3.10) that $r = g(\theta)$ is a monotonically decreasing function of θ, which is maximum when $\theta = 0$, and minimum when $|\theta| = \theta_m$. Hence, $i = 1$ and r is bounded between $g(\theta_m)$ and $g(0)$. Using the expression (3.10),

$$g^{-1}(r) = \phi_r \left(\ln \frac{2^{\frac{r}{\eta}} - 1}{c_1} \right)^{-\frac{1}{2}}, \tag{3.13}$$

From (3.11), it can be deduced that $f(g^{-1}(r)) = 1$. Hence the pdf of R can be written as $f_R(r) = -\frac{\partial}{\partial r} g^{-1}(r)$.

$$\mathbb{E}[R] = \int_{g(\theta_m)}^{g(0)} r f_R(r) dr. \tag{3.14}$$

Since $f_R(r) = -\frac{\partial}{\partial r} g^{-1}(r)$, $\mathbb{E}[R] = \int_{g(0)}^{g(\theta_m)} r \frac{\partial}{\partial r} g^{-1}(r) dr$. Here $\mathbb{E}[R]$ represents the average link capacity as a function of random Rx misalignment given that the misalignment stays within the main lobe of Rx antenna. Based on the magnitude of maximum antenna misalignment $|\theta_m|$ and Tx and Rx main lobe beamwidths, two scenarios emerge. We capture them using two propositions given below.

Proposition 1. *If $|\theta_m| \leq \frac{\phi_{ML}}{2}$, the expected link capacity is,*

$$r = \mathbb{E}[R]. \tag{3.15}$$

Proof. If the maximum misalignment $|\theta_m|$ during a time slot T_S is less than the half of the main lobe beamwidth 2.6ϕ, then despite the misalignment, Tx and Rx always stay within their main lobe beamwidths. Therefore, the average capacity $r = r_{m,m}^{\phi_t,\phi_r} = \mathbb{E}[R]$. Here, subscripts '$m, m$' implies that both antennas are within their main lobes

Proposition 2. *If $|\theta_m| > \frac{\phi_{ML}}{2}$, the link capacity is,*

$$r = p_{m,m}\mathbb{E}[R] + p_{m,s}\eta \log_2 \left(1 + \frac{G_m^{\phi_t}(0) G_s^{\phi_r} G_0(\lambda, d) P_t}{N_0 W} \right). \tag{3.16}$$

Proof. If maximum $|\theta_m| > 1.3\phi$, we have two cases: (i) with a probability $p_{m,m} = \left(\frac{1.3\phi_t}{\theta_m}\right)$, both Tx and Rx stays within their main lobes. The link capacity in this case is given by (3.14) as $r_{m,m}^{\phi_t,\phi_r} = \mathbb{E}[R]$. (ii) with probability $p_{m,s} = \left(1 - \frac{1.3\phi_t}{\theta_m}\right)$, Rx stays in its side lobe. Side lobe gain is always a constant irrespective of the magnitude of the misalignment (recall (3.4)). Since we

have assumed misalignment free Tx, the capacity can be calculated using (3.9) as $r_{m,s}^{\phi_t,\phi_r} = \eta \log_2\left(1 + \frac{G_m^{\phi_t}(0) G_s^{\phi_r} G_0(\lambda,d) P_t}{N_0 W}\right)$.
Considering both these cases, average capacity can be expressed as, $r = p_{m,m} r_{m,m}^{\phi_t,\phi_r} + p_{m,s} r_{m,s}^{\phi_t,\phi_r}$.

To analyze the impact of beamwidth on the capacity of directional mmWave links employing IEEE 802.11ad beam searching protocol, we assume a fixed coarse sector level beamwidth Ω for both the Tx and Rx antennas. We assume that the Rx misalignment is uniformly distributed in the range $[-\theta_m, \theta_m]$. Based on the Tx and Rx antenna beamwidths, we consider two configurations as follows: (i) Rx capable of forming pencil beams and Tx using the coarse beamwidth; and (ii) both the Tx and Rx using pencil beam antennas having equal beamwidths ϕ.

3.5.1. Pencil beam reception and coarse-sector transmission

In this configuration, a coarse-sector beamwidth (wider beamwidth) is used for transmission while narrow beamwidth pencil-beam is used for reception. Therefore, $\phi_r = \phi$, $\phi_t = \Omega$, $G_{mr} = G_m^{\phi}(\theta)$, $G_{mt} = G_m^{\Omega}(0)$, $G_{sr} = G_s^{\phi}$. based on the misalignment, following two cases are possible:
Case-1: $|\theta_m| \leq 1.3\phi$**.** In this case the link capacity can be calculated by replacing Tx gain by $G_m^{\Omega}(0)$ and Rx gain by $G_m^{\Omega}(\theta)$ in (3.15).
Case-2: $|\theta_m| > 1.3\phi$**.** In this case the average capacity can be calculated using (3.16) as $r = p_{m,m} r_{m,m}^{\Omega,\phi} + p_{m,s} r_{m,s}^{\Omega,\phi}$ where $p_{m,m} = \left(\frac{1.3\phi}{\theta_m}\right)$ and $p_{m,s} = 1 - p_{m,m}$.

3.5.2. Equal beamwidth pencil beam Tx and Rx

In this configuration, both the Tx and Rx employ narrow pencil beams of equal beamwidth, i.e., $\phi_t = \phi_r = \phi$. Thus, the antenna gain can be written as, $G_{mr} = G_m^{\phi}(\theta)$ and $G_{mt} = G_m^{\phi}(0)$ and $G_{sr} = G_s^{\phi}$. Again we have two cases here.
Case-1: $|\theta_m| \leq 1.3\phi$**.** In this case the procedure for calculating the link capacity is similar to that of the previous configuration (see Section 3.5.1) except that the Tx beamwidth value Ω should be substituted by ϕ.
Case-2: $|\theta_m| > 1.3\phi$**.** In this case the average capacity can be calculated using (3.16) as $r = p_{m,m} r_{m,m}^{\phi,\phi} + p_{m,s} r_{m,s}^{\phi,\phi}$ where $p_{m,m} = \left(\frac{1.3\phi}{\theta_m}\right)$ and $p_{m,s} = 1 - p_{m,m}$.

3.6. Numerical results and discussions

We used MATLAB to numerically evaluate the impact of misalignment and beam searching overhead on the link capacity for different Tx and Rx beamwidths. We used transmit power $P_t = 10\,\text{mW}$, Tx-Rx distance $d = 5\,\text{m}$, bandwidth $W = 2.16\,\text{GHz}$ and coarse sector beamwidth $\Omega = 90°$. Using the IEEE 802.11ad recommendations 'T_p' the time required to transmit a beam training packet is fixed to be $20\mu\text{s}$. The duration 'T_S' of the allocated slot-time is taken as 10 ms and 1 s. The beam misalignment θ is considered to be uniformly distributed in the interval $-\theta_m$ to θ_m.

Fig. 3.12 shows the link capacity for pencil beam transmission and coarse

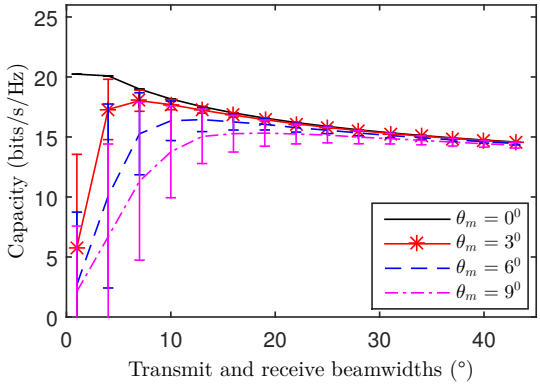

(a) Slot time=10 ms.

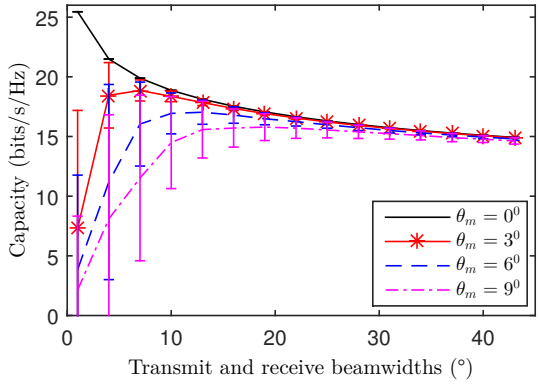

(b) Slot time=1 s.

Figure 3.12: Link capacity for pencil beam reception and coarse-sector transmission.

sector reception. In Fig. 3.12(a), the optimum Tx beamwidth values are 3°, 7°, 10° and 15° for misalignment θ_m equal to 0°, 3°, 6° and 9°, respectively. It is evident from Fig. 3.12(a) and Fig. 3.12(b) that the antenna misalignment has a significant impact on the link capacity for smaller beamwidths. For $\theta_m = 3°$, the link capacity deteriorates if the beamwidth decreases below 5°. For $\theta_m = 9°$, the link capacity at beamwidth=15° is 60% better than the link capacity at 5° beamwidth. We can see that as the beamwidth decreases, the standard deviation increases at a fast rate.

If we compare Fig. 3.12(a) with Fig. 3.12(b) for perfect alignment ($\theta_m = 0°$), it can be observed that the $T_S = 1$ s results in a better link capacity than $T_S = 10$ ms. For $T_S = 1$ s and $\theta_m = 0°$, the link capacity monotonically increases with a decrease in Tx beamwidth. This happens because a slot of longer duration will be less affected by the beam searching overhead compared to the slot of

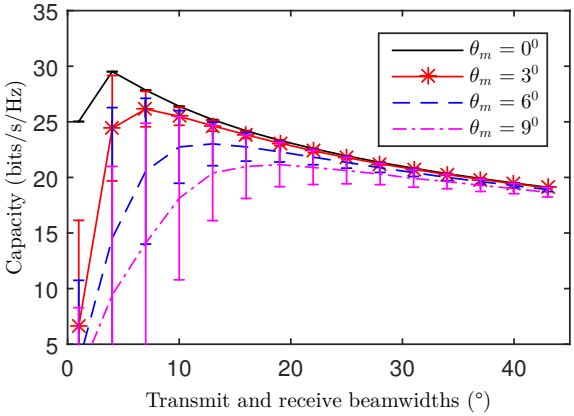

(a) Slot time=10 ms.

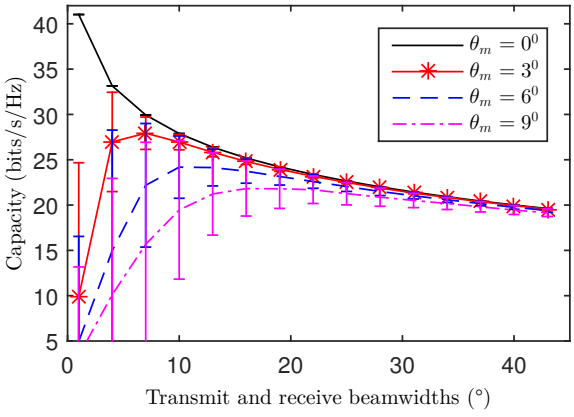

(b) Slot time=1 s.

Figure 3.13: Link capacity for pencil beam transmission and reception.

shorter duration. Moreover, a coarse sector beamwidth is used for Tx, hence beam searching overhead does not affect much for T_S=1 s and $\theta_m = 0°$. This suggests that if antenna misalignment does not exist, then the lowest possible Tx beamwidth would result in the best link capacity if the allocated time slot is sufficiently large and coarse sector reception is used.

Fig. 3.13 shows the link capacity when both the transmitter and receiver employ narrow pencil beam antennas. In this case, the link capacity is even more sensitive to the misalignment θ_m and deteriorates faster compared to the coarse sector transmission. In Fig. 3.13(a) where $T_S = 10$ ms, the link capacity for perfect alignment ($\theta_m = 0°$) decreases after a certain beamwidth. On the other hand, for the perfect alignment scenario, in Fig. 3.13(b) where $T_S = 1$ s, the link capacity monotonically increases with the reduction in antenna beamwidth. Furthermore, irrespective of the slot length T_S, an increase in misalignment θ_m always deteriorates the link capacity which is evident by the large difference in minimum and maximum link capacity for smaller beamwidths. This manifests the dominance of beam misalignment over the high gain of narrow beamwidth antennas.

3.7. Misalignment-aware beamwidth adaptation mechanism

As discussed above, beam misalignment leads to a significant reduction in achievable link capacity. Misalignment has two major consequences: (i) effective Tx/Rx gains are reduced; and (ii) frequent re-beamforming is required to correct the antenna alignment if the misalignment is severe. Here, we propose a simple mechanism (see Algorithm 1) to adapt Tx/Rx beamwidths to ensure a misalignment-resilient mmWave link.

The idea is to maintain a stable link quality by adjusting beamwidths such that the effect of misalignment is minimized. We propose to monitor the average received signal strength ($\overline{\text{RSSI}}$) for each time slot. If $\overline{\text{RSSI}}$ is below an expected threshold RSSI_{th}, beamwidth is increased by $\Delta\phi$. To determine the initial Tx/Rx beamwidths ϕ_t, ϕ_r, only the beam searching overhead is considered. As transmission progresses, the impact of misalignment is measured by monitoring the average RSSI during each time slot. If $\overline{\text{RSSI}} < \text{RSSI}_{\text{th}}$, the Tx and Rx beamwidths are increased by $\Delta\phi$, and $\overline{\text{RSSI}}$ is monitored again in the next time slot. The beamwidth adjustment procedure is repeated until $\overline{\text{RSSI}}$ becomes greater than RSSI_{th}. Once the measured average RSSI becomes greater than the expected threshold RSSI, beamwidth adaptation is completed. In our simulations, RSSI_{th} is calculated as the average expected received signal strength considering antennas pointing randomly within the entire main lobe beamwidth, i.e., $\theta \in [-1.3\phi, 1.3\phi]$.

$$\text{RSSI}_{\text{th}} = \frac{1}{(\frac{2.6\phi}{\Delta\theta} + 1)} \sum_{\theta=-1.3\phi}^{1.3\phi} G_{mt}^{\phi_t}(\theta) G_{mr}^{\phi_r}(\theta) G_0(\lambda, d) P_t.$$

Where $\Delta\theta$ is the sampling interval and $\frac{1}{(\frac{2.6\phi}{\Delta\theta}+1)}$ is the number of samples. In our calculations, we considered $\Delta\theta = 2°$. To evaluate our algorithm, we simulated

Algorithm 1 Beamwidth adaptation algorithm

1: Begin with the Tx/Rx beamwidths determined by (3.8) for the given slot duration T_S;
2: Monitor the average signal strength $\overline{\text{RSSI}}$ during transmission;
3: **if** $\overline{\text{RSSI}} < \text{RSSI}_{\text{th}}$ **then**
4: $\phi_t = \phi_t + \Delta\phi$ and $\phi_r = \phi_r + \Delta\phi$;
5: Go to Step 2;
6: **else**
7: Stop the beam adaptation mechanism;
8: **return** ϕ_t, ϕ_r;
9: **end if**

IEEE 802.11ad link in MATLAB using the Gaussian antenna model with both Tx and Rx having the same beamwidth. In the first experiment we used ϕ=2° and ϕ=7° in the next. Beamwidths are obtained from (3.8) for T_S=1 s and T_S=10 ms, respectively. We considered uniformly distributed misalignment in the interval $-\theta_m$ to θ_m, and $\Delta\phi$=2°. All the other parameters are same as in the previous section. For ϕ=2°, θ_m=2° and θ_m=10°. For ϕ=7°, θ_m=7° and θ_m=15° are considered. In each case the simulation time is 10 time slots.

It can be seen in Fig. 3.14 that the beamwidth adaptation mechanism gradually reaches the best achievable link capacity by adjusting Tx/Rx beamwidth such that misalignment errors do not result in link outages, and frequent re-beamforming is avoided. The signal strength is monitored during each time slot, and if it is below the defined threshold, Tx/Rx beamwidths are increased to accommodate the misalignment. In case of 7° beamwidth, the adaptation mechanism improves the link capacity by 20% (see Fig. 3.14(a)) to 100% (see Fig. 3.14(b)). For 2° beamwidth similar results are observed where we see that link capacity improves by 50% (see Fig. 3.14(d)) to 200% (see Fig. 3.14(d)). If we compare Fig. 3.14(c) and Fig. 3.14(d), we observe that in Fig. 3.14(c) highest capacity is achieved in 2nd slot while in Fig. 3.14(d) it takes 5 slots to achieve the highest capacity. This is due to the high misalignment in the latter case and beamwidth adaptation needs more slots. On the other hand, if beamwidth adjustment is not performed, misalignment leads to persistently weaker links due to reduced antenna gain and frequent re-beamforming.

3.8. Conclusions

mmWave communications has now become an inextricable part of 5G communications to support multi-Gbps data transmission. To compensate for the additional free-space path loss at mmWave frequencies, the use of narrow beamwidth directional antennas has been proposed. The narrow beamwidth directional links are highly sensitive to beam misalignment. Furthermore, the beam searching

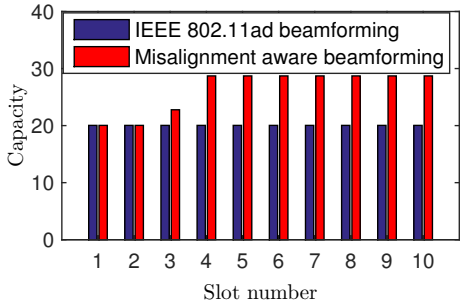

(a) ϕ=7°, θ_m=7°.

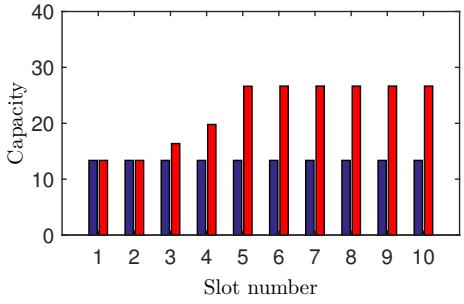

(b) ϕ=7°, θ_m=15°.

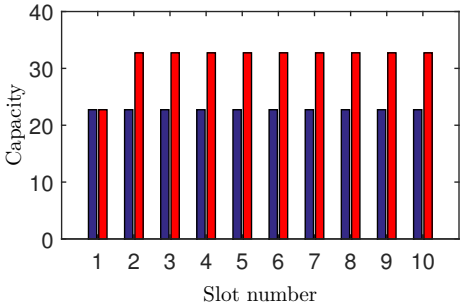

(c) ϕ=2°, θ_m=2°.

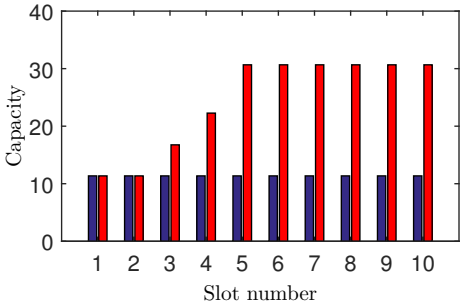

(d) ϕ=2°, θ_m=10°.

Figure 3.14: Performance of misalignment-aware beamwidth adaptation mechanism.

mechanism employed to find the best Tx and Rx beam directions results in high overhead that limits the actual data transmission capacity. We used commodity IEEE 802.11ad hardware to measure the re-beamforming time when link alignment is disturbed. Our measurement results show that it takes considerable time (100 ms–300 ms) to re-align the IEEE 802.11ad links. Hence, efficient beamforming technologies are needed to realize mmWave based mobile networks in 5G communications.

Most of the available literature on mmWave communications has focused on the physical characteristics of mmWave transmission, however, these have a deep impact on the Link/MAC layer. In this chapter we addressed this problem by jointly considering the Link/MAC layer mechanisms and the physical layer characteristics. We provided a novel capacity modeling framework for the mmWave links considering the trade-offs between Tx-Rx beamwidths, beam searching overhead, antenna misalignment and allocated slot duration. Our analysis provides important insights into the behaviour of directional mmWave links. It is shown that the beam searching overhead and antenna misalignment can deteriorate the expected link capacity by an order of magnitude if extremely narrow Tx-Rx beamwidths (1° to 5°) are used. The analytical results suggest that to exploit the full potential of mmWave communications, Tx-Rx beamwidths must be carefully chosen. In the presence of misalignments, moderately wide beamwidths (15° to 20°) perform better than the narrow beams. Our analytical framework is general enough to be applied to mmWave based WLANs and cellular systems. However, we only considered the performance of a single link. In case of multiple links operating simultaneously, a misaligned link could become a source of interference to other links which were otherwise isolated from each other. This can lead to a decrease in spatial reuse in mmWave communication and needs further investigation.

4

A *Decrease-and-Conquer* based Beam Searching Mechanism for Fast mmWave Link Setup

To establish the narrow beamwidth directional links, the medium access control (MAC) layer beam searching protocols are specified in millimeter wave (mmWave) communications standards. A beam searching protocol determines the best transmit and receive directions by transmitting and receiving training packets in the complete beam-search space. This consumes a very high amount of channel time. In this chapter, we propose a novel multi-level beam searching mechanism based on a *decrease-and-conquer* approach that results in a massive reduction in the number of beam searching packets required to establish the directional mmWave links. For the extremely narrow beamwidths (2°-5°), the proposed algorithm reduces the number of required beam searching packets by 85%-88% as compared to the IEEE 802.11ad beam searching mechanism. This would be extremely beneficial in case of mobile users where frequent beamforming is required. The proposed algorithm is equally effective in the two dimensional (2-D) as well as the three dimensional (3-D) beamforming systems.

4.1. Introduction

To compensate for the high path loss at mmWave bands, directional antennas using narrow pencil beams have been proposed [14, 8]. The high gain pencil beams confine signal power in the desired directions, thus allowing more power to be received at the intended receiver. The higher antenna gains can be achieved either by using special antenna geometries such as horn antennas, or by using

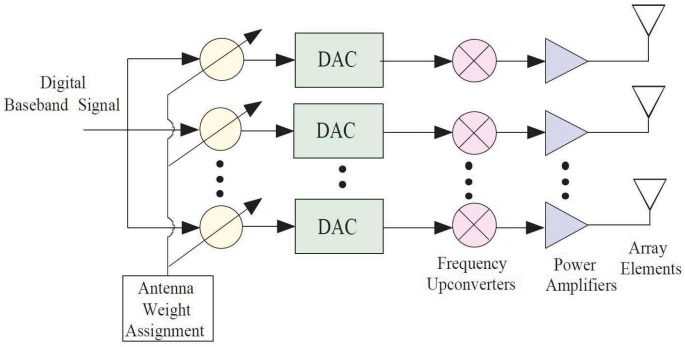

(a) Digital baseband beamforming architecture (transmit side).

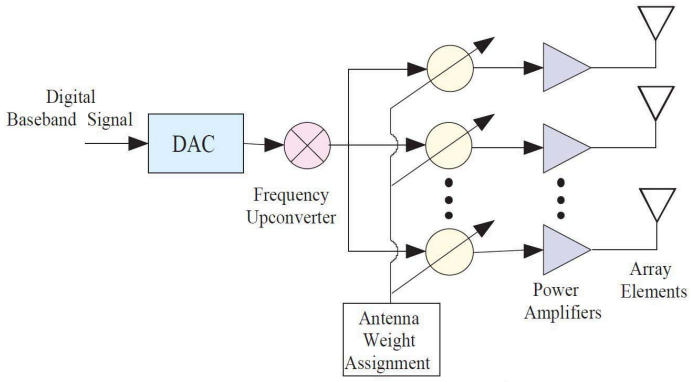

(b) Analog RF beamforming architecture (transmit side).

Figure 4.1: Beamforming architectures

array antennas which can be electronically steered. Thus the antenna structures have a direct impact on how the beamforming is accomplished. In the case of antenna array beamforming, generally the beamforming is accomplished either in digital domain or in the analog domain (see Fig. 4.1). In digital beamforming systems, antenna weight vectors (amplitude and phase configurations) are applied on digital baseband signals where each antenna element requires a dedicated radio frequency (RF) chain that consists of a digital to analog (DAC) converter and a frequency upconverter. On the other hand, analog RF beamforming requires a single RF chain for all the antenna elements. The digital baseband beamforming provides greater accuracy due to the flexibility offered by digital signal processors. Since mmWave systems would consist of a large number of antenna elements, the number of RF chains required becomes much higher as compared to the microwave systems where a few antenna elements are used. A large number of RF chains and enormous operating bandwidth resulting in a very high power consumption and costly systems make digital beamforming an unattractive choice

for the mmWave systems.

To avoid the power-hungry signal processing methods, 60 GHz standards (e.g., IEEE 802.15.3c and 802.11ad) have advocated the use of analog beamforming. Further, to overcome the dependence on the antenna structures, beam searching procedures that works on the medium access control (MAC) layer instead of the physical (PHY) layer are adopted in the above said 60 GHz standards. In the MAC layer beamforming, pre-defined antenna weight vectors (amplitude and phase configurations) are specified for each beam direction. The collection of pre-defined antenna weight vectors is also called the Beam Codebook [22]. The codebook based beamforming employs beam searching protocols to find the best transmit (Tx) and receive (Rx) beam directions. As the Tx and Rx beamwidth decreases, the beam-search space increase which results in a very high beam searching overhead. There exists another variant of beamforming called hybrid beamforming that combines both the analog and digital beamforming [57, 58] to exploit the spatial multiplexing capabilities of mmWave channel for high data rate mmWave mobile cellular communications. However, we mainly focus on improving the beam searching protocol using analog beamforming targeting short range wireless local area network (WLAN) applications.

The IEEE 802.11ad beam searching protocol uses a two stage beam searching approach in which beamwidth is divided in two levels of granularity: (i) sector level searching using coarse beamwidths; and (ii) beam level searching using high resolution pencil beams. When beamwidths become small, the number of training packets required during second stage become very high, which is the main issue with the two level beam searching approach. To solve this problem, we propose a beam searching protocol that employs a multi-stage beam searching procedure instead of the two-stage approach. The proposed beam searching algorithm requires significantly lower number of beam training packets to find the best Tx and Rx beam directions. Our main contributions are:

(i) We propose a multi stage beam searching mechanism employing decrease-and-conquer approach for mmWave beamforming. The proposed mechanism reduces beam searching overhead with smaller beamwidths immensely. The number of required training packets is reduced by 60% for 20° beamwidth and 85-88% for 2°-5° beamwidth as compared to the beam searching protocol specified in IEEE 802.11ad.

(ii) We show that the proposed beam searching algorithm is equally effective in reducing the beam searching overhead for 2D and 3D beamforming.

(iii) The proposed mechanism does not alter the structure of IEEE 802.11ad training packets, hence it can be easily integrated in IEEE 802.11ad standard.

4.2. Related work

The mandatory use of directional antennas at mmWave frequencies makes the beam searching mechanism an important step in establishing highly directional

links and the initial link setup for device discovery. To facilitate the link setup, IEEE 802.15.3c and IEEE 802.11ad have specified beam searching protocols that use exhaustive searching to find the best transmit (Tx) and receive (Rx) directions [5, 7]. The main difference between the IEEE 802.11ad and IEEE 802.15.3c is that the IEEE 802.15.3c beam searching simultaneously search for the best Tx and Rx directions while IEEE 802.11ad does find one at a time. Further, IEEE 802.11ad employ inpacket training where beam directions are switched within a packet. It has been shown that the inpacket training result in an in-consistence performance if multipaths are present [23]. On the other hand, IEEE 802.15.3c uses a packet by packet training procedure resulting in higher searching overhead.

Molisch *et al.* have proposed techniques to reduce the beam searching overhead by using different approaches for the fixed and the adaptive modulation schemes [24]. In case of fixed modulations, the beam searching is stopped when the desired signal to noise ratio is achieved without searching further even if there is a possibility of finding better beam pair. A hierarchical beam searching approach is proposed which is similar to the one we have proposed in this chapter, however we specifically focus on the bisection approach. In case of adaptive modulation, prediction based on historical data is used resulting in considerable reduction in the beam searching time. Bin Li, *et al.* have also suggested an optimized search algorithm to improve the beam training time [25]. A beam searching protocol for scheduling multiple links is proposed [59]. A completely different approach employing 2.4/5 GHz signals to assist the mmWave beamforming has been proposed in [26], which reduces the beam training overhead. It is shown that the direction of 60 GHz transmissions can be inferred from 2.4/5 GHz transmissions. However, all these works except [26] still use the two-stage beam searching protocol incurring considerably higher beam searching overhead. We propose a multi-stage beam searching approach using the divide and conquer approach that significantly minimizes the searching overhead.

The rest of the chapter is organized as follows. Section 4.3 introduces the IEEE 802.11ad beam searching procedure. Section 4.4 presents the proposed decrease-and-conquer based beam searching protocol. Numerical results are discussed in Section 4.5, followed by concluding remarks in Section 4.6.

4.3. IEEE 802.11ad mmWave beamforming protocol

Apart from the Quasi-Omni (QO) beamwidth, IEEE 802.11ad defines two levels of antenna beamwidths denoted as the sector and beam levels as shown in Fig. 4.2. Sector level beamwidth is relatively wider compared to the beam level beamwidth. A sector can contain many high resolution beams. For example, a sector level beamwidth could be 120° or 90° while beam level beamwidth can be 20° or even as low as 1°-5°. In order to establish a highly directional link, IEEE 802.11ad beamforming is performed in two stages employing exhaustive search procedure. A station (STA) starting the beam training[1] is referred as initiator and the

[1]In this chapter beam training and beam searching are used interchangeably.

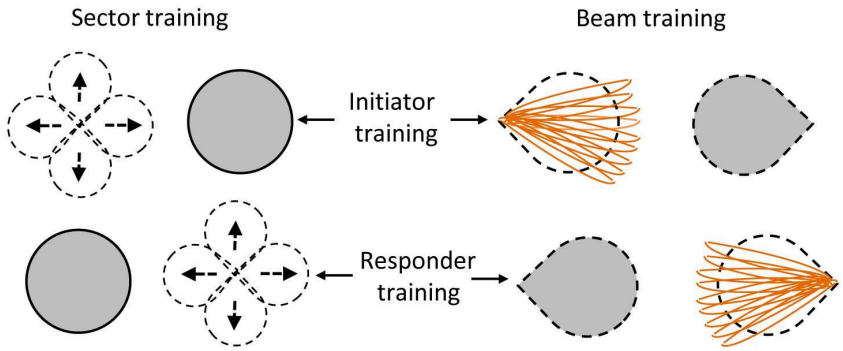

Figure 4.2: Illustration of IEEE 802.11ad beam searching protocol.

recipient is referred as responder.

Fig. 4.2 depicts the BF procedure specified in IEEE 802.11ad assuming symmetrical antenna structures, i.e., the best Tx direction is also the best Rx direction for an antenna. In the first stage, coarse sector training is performed in which best Rx and Tx sectors are chosen by transmitting and/or receiving training packets in all the possible Tx and Rx sectors of initiator and responder. In the second stage, high resolution beam training is performed in which best high resolution Tx and Rx pencil beams are selected within the already selected Tx and Rx sectors. If the initiator is a Personal Basic Service Set Control Point (PCP) , then the first stage of BF, i.e. coarse sector training, is performed during Association Beamforming Training (ABFT) part of IEEE 802.11ad Beacon Interval (BI) and second stage is performed in the beginning of the reserved time slot called Service Periods (SP) part of BI. However, if a non PCP STA is an initiator, then both stages of BF training are performed in allocated SPs.

Let Ω be the sector level beamwidth and Φ be the beam level beamwidth, then number of initiator antenna sectors $N_I^s = \frac{2\pi}{\Omega_I}$, number of responder antenna sectors $N_R^s = \frac{2\pi}{\Omega_R}$, number of initiator beam directions within a sector $N_I^b = \frac{\Omega_I}{\Phi_I}$, and number of Rx beam directions within a sector $N_R^b = \frac{\Omega_R}{\Phi_R}$. Here subscript '$I$' and '$R$' refer to initiator and responder beamwidths, respectively.

Hence, N, the total number of packets transmitted (excluding feedback packets) to attain the given beam resolution is given by,

$$\begin{aligned} N &= a(N_I^s + N_R^s) + a(N_I^b + N_R^b), \\ &= a(\tfrac{2\pi}{\Omega_I} + \tfrac{2\pi}{\Omega_R}) + a(\tfrac{\Omega_I}{\phi_I} + \tfrac{\Omega_R}{\phi_R}), \end{aligned} \tag{4.1}$$

here, $a = 1$ for STAs using symmetrical antenna systems and $a = 2$ for STAs using asymmetrical antenna systems.

For narrower beamwidths such as 1°-5°, the required number of training packet transmissions would be very high and will result in significant beam training overhead. For example, in the case of 2-D beamforming if initial sector beamwidth is 180°, then for Rx and Tx beamwidths of 5°, total number of

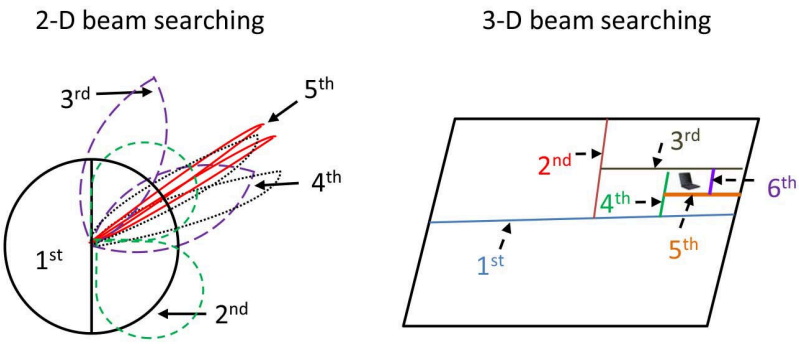

Figure 4.3: Multi-stage decrease-and-conquer beam searching procedure for 2-D and 3-D beamforming.

narrow beams in a sector is equal to 180/5=36. To select the best Tx and Rx beams for the bidirectional link, approximately $(36 + 36) = 72$ training packets would be needed if symmetrical antenna systems are used. However, if asymmetric antenna system is used, the best Rx and Tx configurations will be different for each STA resulting in twice the number, i.e., 144 training packets. If three-dimensional beamforming is used, the beam searching would span over azimuth as well as elevation, thus even higher channel time is consumed in selection of best beams. For example, for a 2° azimuth and elevation beamwidths, 360 training packets are required to find the best Tx and Rx beams if initial azimuth and elevation beamwidth of a QO sector is 180°. Hence, it is important to reduce the beam searching time in order to exploit the high data rate advantage of highly directional mmWave links.

4.4. Multi-stage decrease-and-conquer beam searching protocol

Instead of the two-level beam searching protocol, we propose to use a multi-level beam searching protocol which follows decrease-and-conquer approach to perform the hierarchical narrowing down of beamwidths to increase the beam resolution. The proposed mechanism in a 2-D setting is described in Algorithm 1. Let Γ_T be the target link budget to be obtained by narrowing the initiator and responder beamwidths, and ϕ_{I-min} and ϕ_{R-min} are the minimum[2] obtainable initiator and responder beamwidths, respectively. Beam searching would be accomplished when initiator and responder beamwidths result in sufficient antenna gains such that the achievable link budget $\Gamma(\phi_I, \phi_I) \geq \Gamma_T$.

The first step of the beam searching algorithm is to find the best QO sectors among the $\frac{2\pi}{\Omega_I}$ initiator sectors and $\frac{2\pi}{\Omega_R}$ responder sectors. The values of Ω_I and Ω_R depend on the intended coverage distance. The best initiator and responder QO sectors are determined by transmitting $\frac{2\pi}{\Omega_I} + \frac{2\pi}{\Omega_R}$ training packets. In the

[2]Minimum beamwidth depends on the number of antenna elements in the antenna array.

Algorithm 1 Beam searching mechanism employing decrease-and-conquer approach

Given: Ω_I, Ω_R, $\phi_{I-min}, \phi_{R-min}$, Γ_T;
Find the best initiator and responder QO levels from $\frac{2\pi}{\Omega_I}$ initiator QO levels and $\frac{2\pi}{\Omega_R}$ responder QO levels;
i=0, $\phi_I[i] = \Omega_I$, $\phi_R[i] = \Omega_R$;
while $\Gamma(\phi_I, \phi_R) < \Gamma_T$ **do**
  i++;
  if $\phi_I > \phi_{I-min}$ & $\phi_R > \phi_{R-min}$ **then**
    $\phi_I[i+1] = \frac{\phi_I[i]}{2}$, $\phi_R[i+1] = \frac{\phi_R[i]}{2}$;
    Perform both initiator and responder training;
  else if $\phi_I > \phi_{I-min}$ & $\phi_R \leq \phi_{R-min}$ **then**
    $\phi_I[i+1] = \frac{\phi_I[i]}{2}$, $\phi_R[i+1] = \phi_{R-min}$;
    Perform intiator training only, stop responder training;
  else if $\phi_I \leq \phi_{I-min}$ & $\phi_R > \phi_{R-min}$ **then**
    $\phi_I[i+1] = \phi_{I-min}$, $\phi_R[i+1] = \frac{\phi_R[i]}{2}$;
    Stop initiator training, perform responder training only;
  else
    return $\phi_I = \phi_{I-min}$, $\phi_R = \phi_{R-min}$;
    Required link budget cannot be attained, hence either operate at the attainable data rate or abandon the transmission;
  end if
end while
return $\phi_I = \phi_I[i+1]$, $\phi_R = \phi_R[i+1]$; Stop the beam searching procedure and start transmission.

subsequent beam searching stages beamwidths are halved at each stage resulting in two Tx/Rx directions for initiator and responder STAs (see Fig. 4.3). At every stage, best Tx and Rx directions are selected by transmitting four training packets if symmetrical antenna structures are used. In our algorithm we take care of the situations where both STAs have different minimum beamwidths that depend on the number of elements in respective antenna arrays. In case of different minimum beamwidths, it may so happen that one STA reaches its lowest attainable beamwidth before another STA and hence only one of the STA would participate in the beam training procedure while other STA would use its minimum beamwidth (see the Algorithm 1).

For example, STAs can start with 180° or 90° QO beamwidths resulting in 2 or 4 QO sectors, respectively. This will require $2+2=4$, or $4+4=8$, training packet transmissions in first stage, respectively. Once the best Tx and Rx QO sectors for the first stage are known, in the subsequent stages, each sector is divided into two parts, where total 4 training packets are required to find the best Tx and Rx sector until the minimum possible beamwidth level is reached. Else, if required link strength is achieved before reaching the narrowest beamwidth level (see Algorithm 1 and Fig. 4.3). Similar procedure is applicable for 3-D beamforming where beam searching spans over both azimuth and elevation.

Proposition 1. *In case of 2-D beamforming, the total number of training packets required to establish a directional link is* $\left(2aL + 2a\left(\frac{2\pi}{\Omega}\right)\right)$. *Here,* Ω *is the QO sector beamwidth for Tx and Rx;* $'\phi'$ *is the beamwidth of Tx and Rx pencil beams, and* $L = \left\lceil \log_2 \frac{\Omega}{\phi} \right\rceil$.

Proof. In case of 2-D beamforming with initial sector beamwidth Ω for both Tx and Rx, total number of training packets transmitted are $2\left\lceil \frac{2\pi}{\Omega} \right\rceil$. If the final beamwidth is ϕ, then total number of beamforming stages required to reach the beamwidth value of ϕ would be $L = \left\lceil log_2 \frac{\Omega}{\phi} \right\rceil$. Apart from the first stage, each successive stage would require four training packets. □

Corollary 1. *For the 3-D beamforming case, if* ϕ^{az} *is the azimuth beamwidth and* ϕ^{el} *is the elevation beamwidth of the Tx and Rx using pencil beam antennas, then the total number of training packets required to establish the link is* $\left(2aL + 2a\left(\frac{2\pi}{\Omega^{az}} + \frac{2\pi}{\Omega^{el}}\right)\right)$. *Here* Ω^{az} *and* Ω^{el} *are the azimuth and elevation QO sector beamwidths, respectively, and* $L = \left\lceil \log_2 \frac{\Omega^{az}}{\phi^{az}} \right\rceil + \left\lceil \log_2 \frac{\Omega^{el}}{\phi^{el}} \right\rceil$.

Proof. The proof of this corollary is similar to the proof of Proposition 1 except extending the search in one more dimension, i.e., elevation. □

4.5. Performance analysis

We used MATLAB to numerically evaluate the proposed beam searching scheme and to compare it with the IEEE 802.11ad beam searching protocol. We assumed an ideal directional antenna model with constant main lobe gain and without

any side lobes. The initial QO sector beamwidth is assumed to be 180° for both the Tx and Rx antennas. Fig. 4.4 shows the comparison for 2-D beamforming. The vertical axis represents the beam searching counts, i.e., the total number of training packets sent for both the protocols while horizontal axis depicts the beamwidths of Rx and Tx antennas, which are assumed to be equal.

It is evident from Fig. 4.4 that for narrow pencil beams, large number of training packets are sent before the narrow beamwidth link is established, if IEEE 802.11ad beamforming protocol is used. On the other hand, decrease-and-conquer beam-searching demonstrate huge reductions in the number of required training packets. The number of stages for decrease-and-conquer beamwidth depends on the initial sector beamwidth and the width of the narrow pencil beam as explained in the Proposition 1. As beamwidth decreases, the number of training packets increase steeply in the case of IEEE 802.11ad because beam search space is inversely proportional to the beamwidth of narrow beams. On the other hand, decrease-and-conquer beam searching uses multi-stage approach where each stage has only two Tx and Rx sectors which requires only four training packets at each stage and number of stages is equal to $\log_2 \frac{\Omega}{\phi}$, resulting in approximately 60% decrease for 20° beamwidth and 85% decrease for 5° beamwidth in required number of training packets.

Fig. 4.6 shows the results for 3-D beamforming employing IEEE 802.11ad beam-search protocol (left) and the proposed decrease-and-conquer beam-search protocol (right). The vertical axis (perpendicular to the plane of the paper) represents beam searching counts. The axes on the plane of the paper show the azimuth and elevation beamwidths. We assume a 90° beamwidths in both

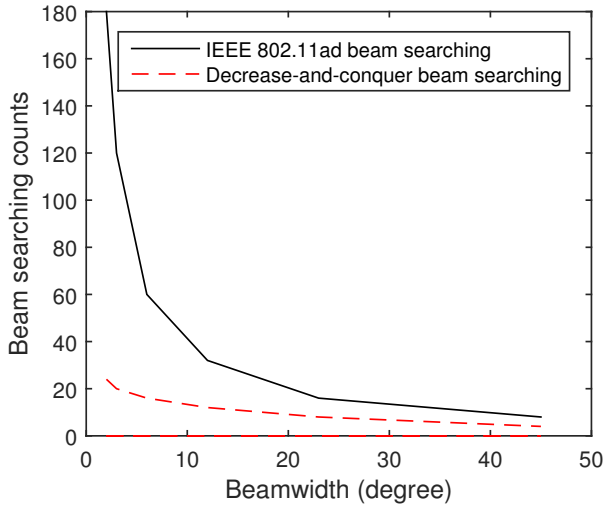

Figure 4.4: Comparison of IEEE 802.11ad beam searching protocol with the proposed beam searching protocol for 2-D beamforming.

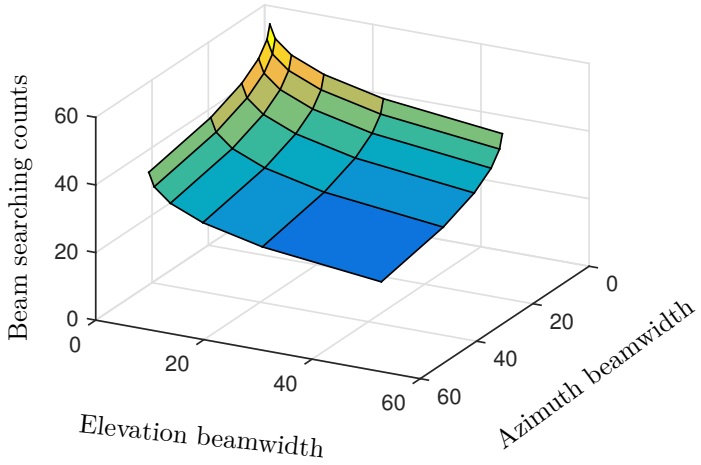

(a) Proposed beam searching

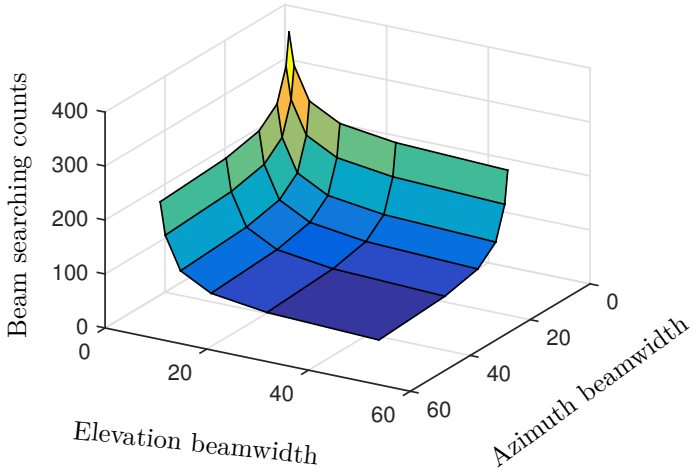

(b) IEEE 802.11ad beam searching.

Figure 4.5: Comparison of IEEE 802.11ad beam searching protocol with the proposed beam searching protocol for 3-D mmWave beamforming.

the azimuth and elevation directions for the first stage sectors. Compared to the 2-D beamforming where only beam searching in a single direction (azimuth) is required, 3-D beamforming requires searching in two different directions, i.e., azimuth as well as elevation. Hence, huge number of training packets are sent when beamwidths are small which is evident from the Fig. 4.5. However, multi-

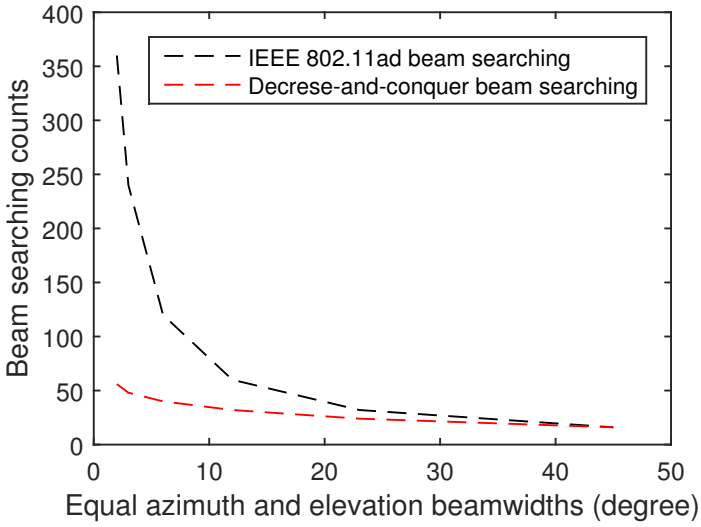

Figure 4.6: Comparison of IEEE 802.11ad beam searching protocol with the proposed beam searching protocol for 3-D mmWave beamforming with equal azimuth and elevation beamwidths.

stage decrease-and-conquer beam searching results in a massive reduction in the required number of training packet transmissions.

To provide a clearer picture, Fig. 4.6 shows comparison between IEEE 802.11ad beam searching and the proposed beam searching mechanism a 3-D beamforming scenario for equal azimuth and elevation beamwidths. It can be seen that up to 88% reduction in required number of training packets is achieved for a 2° beamwidth. Thus, enormous reduction in the required training packets can be achieved even in case of 3-D beamforming by using the multi-stage beam searching approach. Also, the proposed mechanism does not modify IEEE 802.11ad training packets, hence it can be easily integrated with the IEEE 802.11ad MAC protocol.

4.6. Conclusions

Finding the best transmit and receive beam directions is a prerequisite to establish a multi-Gbps mmWave wireless link employing narrow beamwidth antennas. Beam searching protocols have been proposed to find the best Tx/Rx directions that use training packets to assess the link quality for different Tx and Rx directions. This results in a significant communication overhead. The beam searching procedure will be more often needed if links are not static. Thus it is important to have beam searching protocols that results in a minimum overhead.

In this chapter, we proposed a beam searching protocol for millimeter wave communications using pencil beam antennas. The proposed mechanism employs

decrease-and-conquer approach for selection of best beams. It outperforms the 60 GHz IEEE 802.11ad beam searching protocol in terms of required number of training packets to find the best transmit and receive beam directions. The number of required training packets are reduced by 60% for 20° beamwidth and 85-88% for 2°-5° beamwidth as compared to IEEE 802.11ad beam searching protocol. We have shown that the proposed mechanism is equally effective in reducing the beam seaching overhead in both 2-D and 3-D beamforming systems.

Although the proposed multi-stage beam searching results in a significant reduction in the required number of training packets, the practical implementation needs efficient beam codebook design. Since each stage of beam searching uses a different beamwidth, the number of active antenna elements would also vary at each of these beam searching stages. Thus, new switching based beamforming architecture is required that can ensure the required beam patterns at every stage of beam searching mechanism by selecting appropriate number of antenna elements.

5

Sensor-Assisted Proactive Beam Switching in 60 GHz Communications

In Chapter 3 and 4, we investigated the impact of beam misalignment and beam searching overhead on the narrow beamwidth millimeter wave (mmWave) links. If misalignment is severe, beam searching is instantiated to re-orient the antenna beams in the desired directions. This frequent re-beamforming amounts to significant communication overhead as well as a poor quality of experience. In this chapter, we propose to use the motion sensors available in mobile devices to initiate proactive beam switching. Using the data from motion sensors, next desired beam orientation is predicted and beam switching is performed without interrupting the data transmission. Once a directional link is established, the proposed scheme results in much less invocation of the re-beamforming mechanism to maintain the link alignment.

5.1. Introduction

Maintaining the receive (Rx) and transmit (Tx) beam alignment is highly important in mmWave directional links to leverage the multi-Gbps wireless capacity offered by the large available bandwidth. To maintain the beam alignment, the IEEE 802.15.3c [5] and IEEE 802.11ad [7] standards provide beam-tracking mechanisms. During the beam searching phase, apart from the best Tx and Rx beam directions, the second best beam directions are also determined as backup. In beam-tracking mechanisms, special sequences are used to evaluate the link strength. These beam tracking sequences can be either part of the data packets or be transmitted as independent packets. The tracking mechanism senses the current link quality by observing signal to noise ratio of a tracking packet. If the tracking mechanism observes a sufficient link quality degradation, the link

switches to the second best (backup) beam directions determined during the beam searching phase. However, if the chosen beams (after switching) do not provide sufficient link quality, the beam searching mechanism is invoked again to find a fresh set of best beam directions. If very narrow beamwidth antennas are used, maintaining the link alignment could be very difficult due to the slightest movement of devices. Thus frequent beam searching would be triggered to re-align the link. This limits the achievable link throughput as a considerable amount of channel time is wasted in maintaining the alignment. Generally, misalignment happens due to the movement of users or a change in the device holding pattern.

We propose to use motion sensors (accelerometer, gyroscope and magnetometer) to identify and correct the link misalignments. We use sensor data to find user movement and reconfigure the beam directions to maintain a steady link quality. Generally, the link degradation primarily happens either due to blockage or due to beam misalignment. When use commonly found motion sensors in mobile devices to distinguish the cause of link degradation. This is done by using the simple classification technique to find if there is any movement (translation, rotation) or it is caused by blockage. Once it is established that the device movement has occurred, we differentiate the translational movement from the rotational movement, and use this information to resolve the misalignment by reorienting the Tx and Rx beams in the expected directions. This is accomplished by predicting the next beam-pair based on the movement data and switch the beams before the link quality drops significantly. We call it *proactive* beam switching because it is done before the link breaks and that too without using the IEEE 802.11ad beam tracking and searching mechanisms. We summarize our contributions as follows:

(i) We use the motion sensor data to determine the cause of link degradation, i.e., whether it is caused by blockage or misalignment. Further, we determine the cause of misalignment, i.e., translational movement or rotation movement.

(ii) Using the historical movement data, we predict the next location/orientation of the mobile device.

(iii) By using the prediction results indicating next location/orientation of the mobile device, proactive beam switching is facilitated, that results in significant reduction in re-beamformings.

By using an example scenario, we show that the sensor-assisted proactive beam switching can avoid frequent link disruptions. It reduces re-beamformings instances along the path traversed in the example scenario and results in a lower beam searching overhead and a better user experience. Since presently there is no mobile device available that has 60 GHz radio implemented, we used a Samsung smart phone to collect the motion sensor data along the example path. Further, we used a radio simulation tool to gather 60 GHz received power data

by mapping this example path in the radio simulation tool. We merged the collected sensor data and received signal power in MATLAB to simulate the beam switching mechanism. This work is mainly performed as an M.Sc. thesis project undertaken by Mr. Arjen Doff under my supervision. We would like to explicitly express that in this work, we do not provide a generalized solution for the sensor-assisted beam switching, rather, we, using an example path scenario, show that using motion sensors are helpful in facilitating the beam switching.

5.2. Related work

Exploiting data gathered from motion sensors to re-orient the beam direction is an idea less explored. Only a few papers [60, 61, 62, 63] have explored the relation of mobility and beam switching in 60 GHz communication. In [60] the rate at which the received signal power changes is monitored to identify the error type affecting the link. In [61], the impact of device mobility on 60 GHz link quality is explored. It is shown that circular (rotational) motion has more impact than the linear motion on the 60 GHz link quality, which prompts frequent re-beamformings. It is argued that the motion aspects should be included in the 60 GHz beam-tracking and MAC protocols. In [60], the causes of link degradation in 60 GHz directional communications are investigated and concluded that it is very important to differentiate between link degradation due to blockage and link degradation due to beam misalignment because of device movement. The importance of identifying the cause of link degradation is highlighted because correction mechanisms are different in case of blockage, translational movement and rotational movement. In [62], the idea of utilizing the motion sensors for beam tracking in mmWave networks is presented. The data gathered from accelerometer, gyroscope and magnetometer is used to reorient the beam direction if user movement is observed. An attitude heading reference system and zero velocity detector data are used to accurately determine the device movement. A similar method for mmWave beam-tracking employing motion sensors is presented in [63]. However, both of these works use sensor data for beam-tracking only and reactive beam switching is performed. On the other hand, we propose proactive beam switching by predicting the next location/orientation of the mobile device using motion sensor data, which avoids link disruptions and reduces the re-beamforming instances.

5.3. Motion sensors and movement classification

In this section, we first introduce the motion sensors used to identify the movement of a mobile device. It is followed by the description relation between type of movement (translational, rotational, or both) and the required beam switching actions (Tx beam switching, Rx beam switching, or both the Tx and Rx beam switching) in 60 GHz directional links.

5.3.1. Sensors

A smartphones has many sensors, among which *accelerometers*, *gyroscopes* and *magnetometers* can be seen as the most relevant to detect motion. Gyroscopes measure angular velocity in rad/s based on the Coriolis force while accelerometer measures the linear acceleration in m/s^2. The magnetometer can be used as a digital compass. Both the accelerometer and the gyroscope data are used in the error identification phase and are represented by $\boldsymbol{a} = [a_x, a_y, a_z]$ and $\boldsymbol{g} = [g_x, g_y, g_z]$ corresponding to the x, y, and z directions, respectively.

To retrieve useful information from these sensors it is possible to combine the data from two or more sensors. The combination of these sensors is referred to as a virtual sensor. The *rotation vector sensor* is such a virtual sensor, where accelerometer, gyroscope and magnetometer data are fused. The rotation vector sensor gives the orientation of the device relative to the East-North-Up coordinates, and is represented as $\boldsymbol{\epsilon} = [\phi, \theta, \Psi]$. The azimuth angle ϕ will be used in the movement prediction phase to determine the direction of movement.

5.3.2. Types of movements

When a mobile station (STA) and an access point (AP) are connected, we assume their beams are perfectly aligned. However, translational or rotational movement results in link degradation due to misalignment of Tx and Rx beams. If the STA starts to move in a linear direction, both the STA and the AP need to change beam direction, as can be seen in Fig. 5.1.

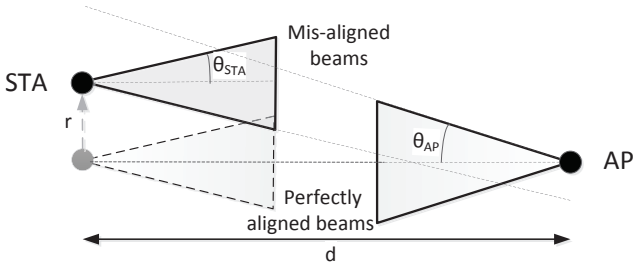

Figure 5.1: Illustration of beam misalignment due to translational movement.

On the other hand, when the STA only experience rotation movement, we only need to change the beam direction of the STA, as can be seen in Fig. 5.2. It

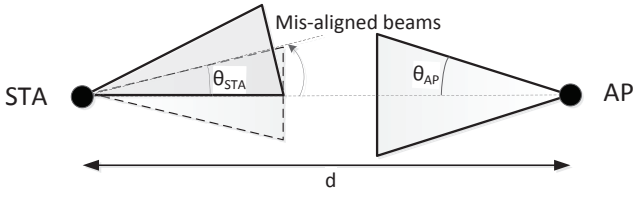

Figure 5.2: Illustration of beam misalignment due to angular movement.

can be easily seen that the STA should switch its beam if it has rotated more than θ_{STA}. To get an understanding of how often beam switching needs to be done, angular speeds were measured [60]. Table 5.1 shows the necessity of performing

Table 5.1: Angular displacement of a smartphone under different activities.

Activities	Angular displacement in 100 ms
Reading, web browsing (no change of orientations)	$6° - 11°$
Reading, web browsing (horizontal from/to vertical orientation changes)	$30° - 36°$
Playing games	$72° - 80°$

frequent re-beamforming due to rotations if no additional information is known. This was also explored and shown in [61] where beam switching needed to be done every 14-54 ms during rotations, depending on the antenna setup.

5.4. Identifying and predicting movements

The first objective is to identify what caused the error: translational movement, rotational movement or blockage. The secondary objective is to predict the next beam sector/beam-pair when we know the origin of the error.

5.4.1. Identify error

The first phase is to identify the error by performing activity recognition to detect if the user is standing still, moving straight, turning or both turning and moving. A simple, yet very effective algorithm used in activity recognition is k-nearest neighbors (k-NN) [64] which uses a feature vector to identify features specific to a certain activity.

Let k be the number of nearest neighbors and $\boldsymbol{T} = \{\boldsymbol{x}_1, \boldsymbol{x}_2, \ldots, \boldsymbol{x}_N\}$ be the training samples collected from the accelerometer or gyroscope. $\boldsymbol{x}_i = (\boldsymbol{f}_i, c_i)$, where $\boldsymbol{f}_i$ is the feature vector of the training samples $\boldsymbol{x}_i$ and c_i is the class that $\boldsymbol{x}_i$ belongs to. The feature vector was chosen to contain the mean and standard deviation of the accelerometer data $\boldsymbol{a}$ and the gyroscope data $\boldsymbol{g}$, as well as the maximal autocorrelation of the accelerometer data $\boldsymbol{a}$ to better detect the steps taken by a user. Thus $\boldsymbol{f} = [\mu_{\boldsymbol{a}}, \mu_{\boldsymbol{g}}, \sigma_{\boldsymbol{a}}, \sigma_{\boldsymbol{g}}, \max(R_{\boldsymbol{a}})]$.

A new sample $\hat{\boldsymbol{x}} = (\hat{\boldsymbol{f}}, \hat{c})$ is classified as shown in ALGO. 1. Multiple measures of distances can be used to calculate the distance $d(\hat{\boldsymbol{f}}, \boldsymbol{f}_i)$ between the feature vector of the input sample and the training samples. We use the l^2 norm, where the distance d is calculated as $d(\hat{\boldsymbol{f}}, \boldsymbol{f}) = \sqrt{\sum_{j=1}^{n} |\hat{f}_j - f_j|^2}$. Here $n = 15$ is the length of the feature vector.

Blockage can also indirectly be detected using sensors. If the signal-to-interference-plus-noise ratio (SINR) drops and the device does not measure any movement, it is apparent that the beam was blocked. Note that this conclusion

Algorithm 1 k-NN

1: **for each** $\hat{\boldsymbol{x}} = (\hat{\boldsymbol{f}}, \hat{c})$ **do**
2: Calculate the distance $d(\hat{\boldsymbol{f}}, \boldsymbol{f}_i)$ between $\hat{\boldsymbol{x}}$ and all $\boldsymbol{x}_i$ in $\boldsymbol{T}$.
3: Sort $\boldsymbol{T}$ ascending based on the distance $d(\hat{\boldsymbol{f}}, \boldsymbol{f}_i)$.
4: Select the first k samples from $\boldsymbol{T}$, these are the k points closest to $\hat{\boldsymbol{x}}$.
5: Assign a class to $\hat{c}$ based on the majority vote of the k classes.
6: **end for**

is only valid if we assume movement and blockage do not occur at the same time. If they do occur at the same time, it will be difficult to identify the source of the error.

5.4.2. Movement prediction

After the cause of link degradation is known, i.e., whether its caused by device movement or by blockage due to obstacles, appropriate actions are needed. If device movement is the cause of the link degradation, the next step is to predict the next best beam-pair based on the measurements from the sensors. Usually, according to IEEE 802.11ad, every time the signal power severely drops, the exhaustive beam searching is performed. However, we propose to use sensor data to determine the next beam directions in the following two ways:

Simple prediction

In this method, the next beam sector is predicted by extrapolating the current beam sector and the previous beam sector. It does not takes into account the device orientation information. If we take $\boldsymbol{S_c} = [x_c, y_c]^T$ as the current sector and $\boldsymbol{S_p} = [x_p, y_p]^T$ as the previous sector. Then the next sector $\boldsymbol{S_n}$ is calculated as

$$\boldsymbol{S_n} = \begin{bmatrix} x_n \\ y_n \end{bmatrix} = \begin{bmatrix} x_c + \mathrm{sgn}(x_c - x_p) \\ y_c + \mathrm{sgn}(y_c - y_p) \end{bmatrix},$$

where $\mathrm{sgn}(*)$ is the signum operator. As an example, if the user moves from beam sector $[x_p, y_p]^T = [3, 1]^T$ to $[x_c, y_c]^T = [3, 2]^T$, the next beam sector is predicted to be $[x_n, y_n]^T = [3, 3]^T$. This method works well if the user is always walking in one direction, however if turns are made this method will wrongly predict the next beam-pair.

Sensor prediction

The second prediction method uses the azimuth angle information obtained from the rotation vector sensor in the device. The rotation vector sensor gives the orientation of the device. We use change in the azimuth angle as an indication of the change in the direction of the mobile device. The azimuth angle information provided by the rotation vector sensor only influences the beam direction of mobile device if there is no translational movement is observed. The prediction

of the next beam sector $\boldsymbol{S_n}$ is calculated from this direction as follows:

$$\boldsymbol{S_n} = \begin{bmatrix} x_n \\ y_n \end{bmatrix} = \begin{bmatrix} x_c + \text{nint}(\sin\phi) \\ y_c + \text{nint}(\cos\phi) \end{bmatrix},$$

where nint$(*)$ is the nearest integer, or round function and ϕ represents the azimuth angle of the device orientation.

5.5. Test setup

For the prediction phase, without loss of generality, the following example scenario is assumed. A user device (STA) is connected to a 60 GHz AP located at the center of the ceiling. The user starts to move, which means the directional beam of the AP is no longer aligned with that of the user. Consequently, a dip in the signal power is observed triggering the need for switching the beam direction of AP and the mobile device.

In order to simulate the 60 GHz network with mobility we used two stages. The first stage is to gather data from a simulated environment using a verified radio frequency propagation simulator, called Radiowave Propagation Simulator (RPS) [65], which provides close to real 60 GHz signal strength at various locations on a floor plan. The second stage consists of collecting *real* experimental sensor data from the user assuming the user is moving along the path shown in Fig. 5.3(a) using the motion sensors in a Samsung Galaxy SIII smartphone.

In RPS a room is created with material properties of glass, concrete and wood as shown in Table 5.2. A 100×100 grid is placed at a height of 1.5 m to simulate

Table 5.2: Dielectric properties of materials in 60 GHz [66].

Material	Thickness (m)	ϵ_{Re}	ϵ_{Im}
Concrete wall/ceiling	0.3	6.14	-0.3015
Wooden floor	0.2	2.81	-0.0964
Wooden door	0.04	2.81	-0.0964
Glass window	0.02	4.58	-0.0458

possible positions and height of users when holding a mobile device. RPS is able to measure the signal power at every position in this grid. A directional transmit (TX) antenna is placed in the middle of the room at a height of 4 m, which acts as an AP. The AP antenna can be directed at 25 different sectors, such that a 5×5 grid is created as shown in Fig. 5.3. The TX antenna pattern is Gaussian as is also assumed in the task group IEEE 802.11ad (TGad) channel model [67].

The receive (RX) antenna pattern of the device has an elevation beamwidth of 180°and azimuth beamwidth of 30°. The parameters for the RPS setup are shown in 5.3.

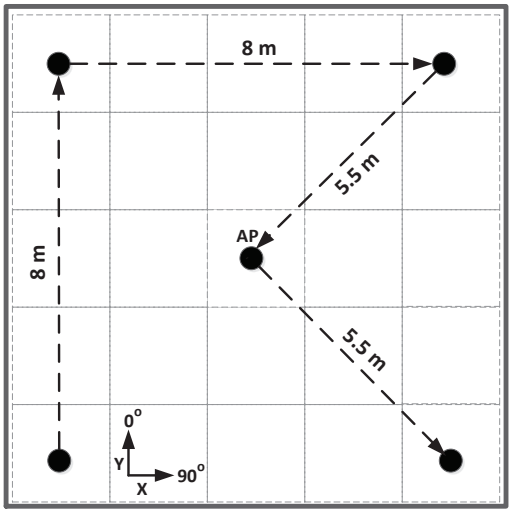

(a) The test setup in the room showing the 5×5 grid and the route.

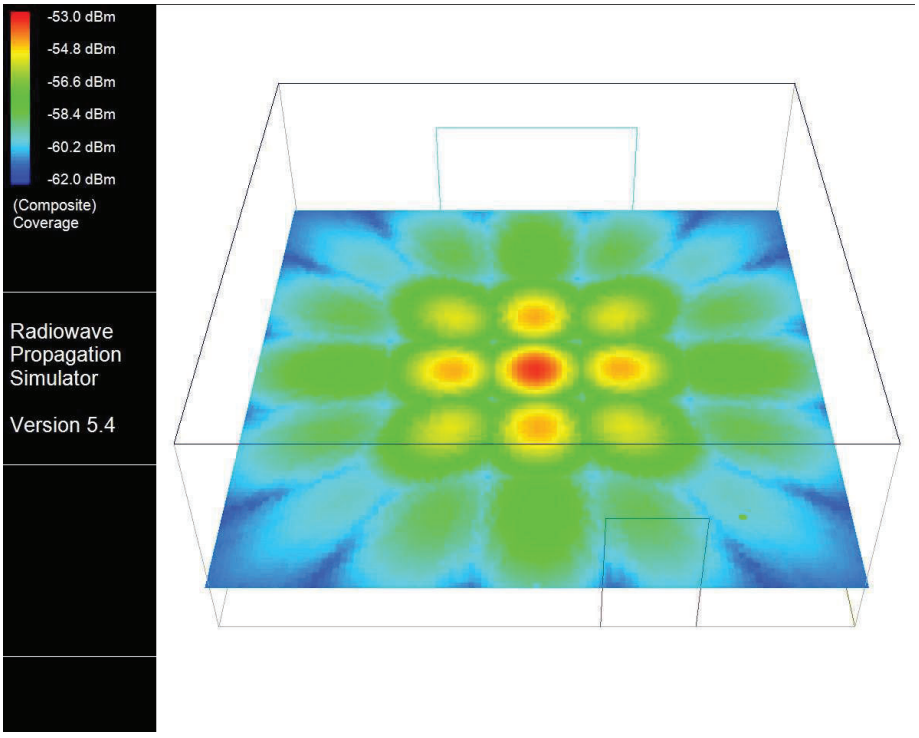

(b) The received power.

Figure 5.3: The example path and the received power using RPS.

Table 5.3: RPS parameters.

Room dimensions	$10 \times 10 \times 4$ m
Carrier frequency	60 GHz
TX half-power beamwidth (HPBW)	30°
TX power	10 dBm
TX antenna gain	14 dB
RX antenna gain	14 dB
Noise figure	10 dB
Antenna polarization	Left hand circular

To predict the next beam sector, it is assumed that the direction of the user with respect to the AP can be measured directly using the azimuth angle of the device given by the rotation vector sensor. This is of course an abstraction of reality where the user may hold the device in a tilted manner. We used fastest sampling rate for sensors as specified in the data sheet (100 Hz for accelerometer and 200 Hz for gyroscope and orientation sample collection), as is shown in Table 5.4.

Table 5.4: Sensor parameters.

Sensor	Ideal rate (Hz)	Actual rate (Hz)
Accelerometer	100	90
Gyroscope	200	180
Orientation	200	180

We superimposed the mobile device sensor data and the received signal strength indication (RSSI) values from RPS in Matlab to simulate the beam switching events. To identify cause of misalignment (rotational movement or translational movement), mean and standard deviation of the accelerometer and gyroscope sensor values as are chosen as features for the k-NN classifier which have shown good results as reported in [68]. The autocorrelation of the accelerometer data was also used as a feature to detect the steps taken by a user.

To increase the scale of the experiments with respect to a single simple route, a RWPM was used such that statistical analysis on the different prediction methods can be done. In the RWPM the orientation of the device is assumed to be known. The details of the simulations using RWPM are presented in the next section.

5.6. Experimental results

5.6.1. Identifying errors

The activity recognition was done by sampling the sensors for 10 min while doing the activities: (i) standing still, (ii) turning, (iii) moving straight or (iv) both turning and moving. The training vectors were generated from the first 5 min of

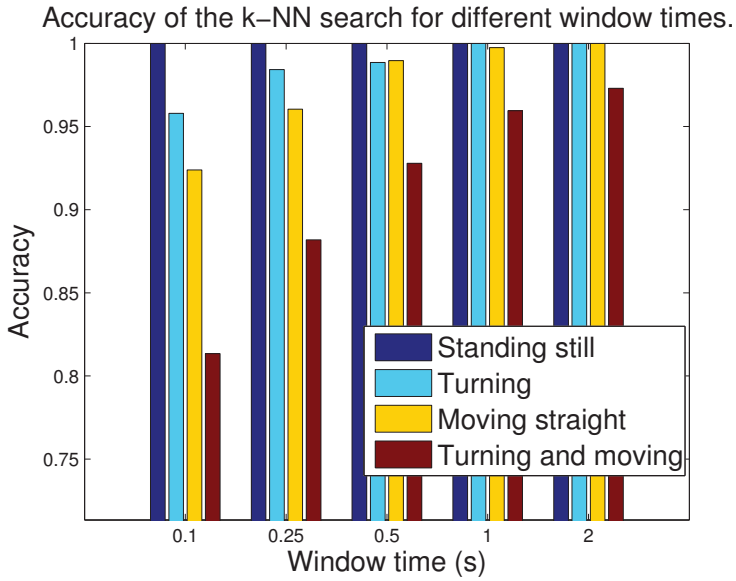

Figure 5.4: The accuracy of the k-NN search for different window sizes.

the recorded samples. For the last 5 min a k-NN search, with $k = 3$ was applied. The accuracy of the k-NN search for different window sizes can be seen in Fig. 5.4. A window size of 100 ms means we are trying to detect the activity from the last 100 ms.

From Fig. 5.4 it can be seen that an accuracy of 100% can be achieved when the user is standing still. This means we were always able to identify if the user was standing still. Turning could be identified with an accuracy of 96-100%. Moving straight was detected with an accuracy of 92-100%. It can be observed that the combination of turning and moving was the hardest to detect with only 81% to 97% accuracy. As was also explored in [68] the window size has a big impact on the results. Basically there is a trade-off between accuracy and speed. When the window size decreases, the activity will be recognized faster, however the results will be less accurate and vice versa.

From Table 5.1 we observe that angular movement can happen rapidly. This means that the window size of 100 ms is not enough when the movement is faster. The accelerometer is sampling at roughly 100 Hz, which means 10 samples are taken every 100 ms. To further increase the reaction time for activity recognition, we need to decrease the window size to 10 ms. Meaning we would observe barely 1 sample in a window, which is not sufficient to recognize an activity. To overcome this limitation the sampling rate of the sensors needs to be increased. If the sampling rate is increased, faster and more accurate results can be obtained.

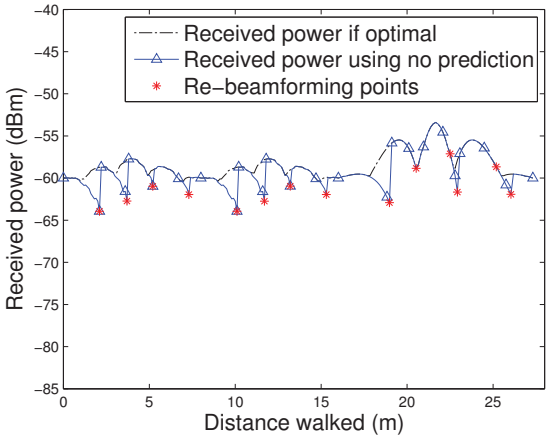

(a) No prediction.

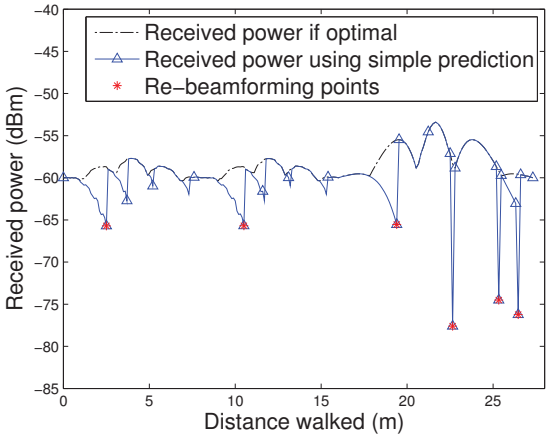

(b) Simple prediction.

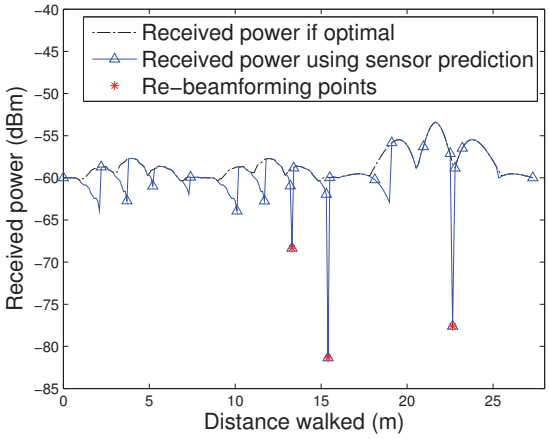

(c) Prediction using sensors.

Figure 5.5: The received power along the route of 5.3(a) using $P_{Dth} = -3\,\text{dBm}$ and $P_{Rth} = -65\,\text{dBm}$.

5.6.2. Movement prediction

To understand the impact of movement prediction, a route was specified as shown in Fig. 5.3(a). This route does not contain any obstacles. Every prediction method is activated only when the received power drops by a certain threshold P_{Dth} – the drop-off threshold. A forced re-beamforming is done if the received power reaches the re-beamforming threshold P_{Rth}. For this scenario we chose $P_{Dth} = -3\,\text{dBm}$ and $P_{Rth} = -65\,\text{dBm}$.

The received power along the route of Fig. 5.3(a) for the simple and sensor prediction methods is shown in Fig. 5.5. Re-beamforming needs to be done if a switch is made to a wrong beam sector or if the re-beamforming threshold is reached. These locations are indicated with a red star in Fig. 5.5(a), Fig. 5.5(b) and Fig. 5.5(c).

Using no prediction as seen in Fig. 5.5(a), re-beamforming is used every time the signal power drops by more than 3 dBm. This results in re-beamforming having to be performed 14 times along the route. In contrast, Fig. 5.5(b) shows that using a simple prediction method, only 6 re-beamformings are needed along the route. The number of re-beamforming along the route is reduced to 3 if the sensor prediction method is used.

It is not always possible to predict and switch the beam to better beam-pair in terms of received power. This causes sudden drop in power as shown in Fig.5.5(b) and Fig. 5.5(c). The sudden drop in signal power is undesired because it forces re-beamforming. Thus in order to minimize this signal power dip it is advised that the prediction methods incorporate a simple beam-pair test to see if the predicted beam-pair actually increases the link quality.

5.6.3. Simulation with RWPM

To analyse the improvement due to sensor prediction on the number of re-beamforming we used the RWPM to simulate the user movement. 100 waypoints were randomly generated in the room and for different drop-off thresholds the number of re-beamformings was calculated. This was repeated 100 times to obtain a statistically significant mean and standard deviation as shown in 5.6. At every step along the route it is evaluated if re-beamforming is needed. We use the distance of the route to normalize the number of re-beamforming, such that a percentage of re-beamforming is obtained. From Fig. 5.6 it can be seen that when using sensor prediction and $P_{Dth} = -4\,\text{dB}$, 0.5% re-beamforming is needed. With no prediction the re-beamforming increases to 6% for the same P_{Dth}. This means the overhead due to re-beamforming is up to 12 times lower if sensors are used under the condition that the RX device is omni-directional. The gain is expected to increase if directional antennas are used.

The minimum re-beamforming percentage of 0.5% is obtained at $P_{Dth} = -4\,\text{dBm}$ using sensor based prediction. This is because, for higher drop-off thresholds ($P_{Dth} = -3\,\text{dBm}$ to $-1\,\text{dBm}$) beam switching is triggered too often, increasing the re-beamforming percentage. The increase in re-beamforming for lower drop-off thresholds ($P_{Dth} = -10\,\text{dBm}$ to $-5\,\text{dBm}$) can be attributed to two reasons. First, as P_{Dth} is decreased, the forced re-beamforming threshold

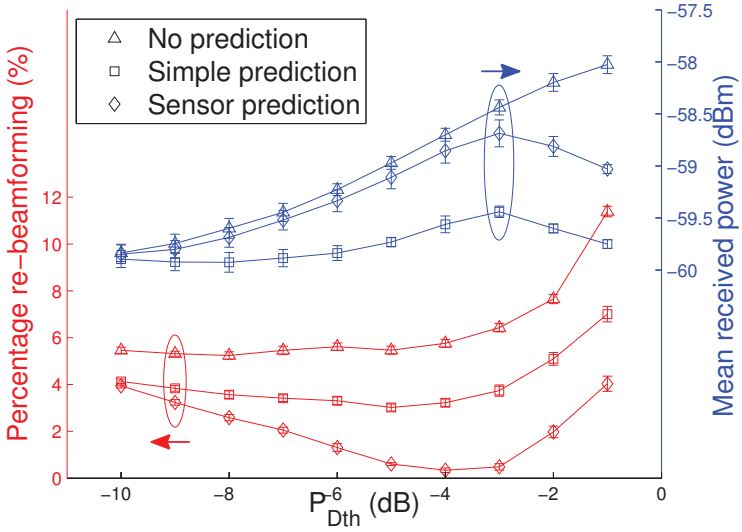

Figure 5.6: The percentage of re-beamforming and mean received power v/s the drop-off threshold P_{Dth} in the RWPM, for the simple and sensor-assisted prediction methods with $P_{Rth} = -65\,\text{dBm}$.

P_{Rth} will be reached more often resulting in triggering frequent re-beamforming. Second, the low P_{Dth} causes the AP to wait too long to switch beams. If it takes too long to switch beams based on the prediction, the predicted beam is more likely to be misaligned, which leads to re-beamforming.

The trade-off can be seen when looking at the mean received power along the route as shown in Fig. 5.6. If sensor prediction is employed, the mis-predictions cause the mean received power to be lower compared to no prediction. Still, for $P_{Dth} = -10\,\text{dBm}$ to $-3\,\text{dBm}$ the difference in mean received power between sensor prediction and no prediction is no more than 0.5 dBm.

In Fig. 5.6 we see it is possible to obtain a favorable P_{Dth} in terms of both re-beamformings and received power. Using sensor prediction, the mean received power is maximized at $P_{Dth} = -3\,\text{dBm}$ and the re-beamforming percentage is minimized at $P_{Dth} = -4\,\text{dBm}$.

5.7. Conclusions

To exploit the full potential of the large available bandwidth in the mmWave bands, it is important to maintain the strict alignment of narrow beamwidth transmitter and receiver antennas. The beam misalignment due to user movements can result in a severe link degradation and requires solutions to maintain the beam alignment. In this chapter, we showed that by using the commonly available motion sensors in the mobile devices, it is possible to predict the device movements and pro-actively realign the beams without disrupting the connection.

We demonstrated that by predicting the next location/orientation of a mobile device using motion sensors data, proactive beam switching can be facilitated which has shown significant reduction in the re-beamforming instances along an example path.

This work takes the first steps to incorporate sensor data as a means of improving network performance. However, further research is required to fully incorporate this scheme. For example, we have used k-NN to differentiate between the translational and rotational movements, however the drawback of k-NN is the need for training. Further, in our simulations we have assumed that the AP has the full knowledge of the mobile sensor data to predict the next beam sector. However, the IEEE 802.11ad standard has no data/control field wherein the sensor data can be transmitted. This means either the IEEE 802.11ad data frame needs to include the sensor data in a dedicated field or the sensor data needs to be transmitted in a separate packet. More investigation is thus required to incorporate our findings. The prediction methods in the case of simultaneous blockage and movements also need to be investigated further.

6

CogCell: A Hybrid 2.4/5 GHz and 60 GHz Indoor Network Architecture

In the preceding chapters, we focussed on the medium access control and beam alignment aspects of narrow beamwidth millimeter wave (mmWave) links considering the IEEE 802.11ad specifications. Although mmWave communications in the unlicensed 60 GHz band is an obvious choice for multi-Gbps indoor wireless access, providing a 'WiFi like' seamless connectivity in indoor environments is challenging because of the 60 GHz signals' inability to penetrate walls. To solve this problem, IEEE 802.11ad provides a fast session transfer (FST) mechanism to switch from 60 GHz band to 2.4/5 GHz bands to leverage the benefits of robust coverage provided by 2.4/5 GHz bands. However, the proposed FST mechanism considers a single 60 GHz Access Points (AP) working within the coverage range of a 2.4/5 GHz AP. Since every room or area separated by walls requires a dedicated 60 GHz AP, multiple 60 GHz APs fall within the coverage range of one 2.4/5 GHz AP. We consider this aspect, and propose CogCell, a novel indoor architecture with a 2.4/5 GHz control-plane covering multiple 60 GHz APs supporting the data-plane. We show that the proposed architecture makes device discovery faster and promises a better medium access control. We also make a provision for 60 GHz data-plane fallback to 2.4/5 GHz if 60 GHz links cannot be established. We show that the proposed CogCell architecture enabling cognitive interplay between 2.4/5 GHz and 60 GHz bands will improve the user experience in future indoor/hospot communications.

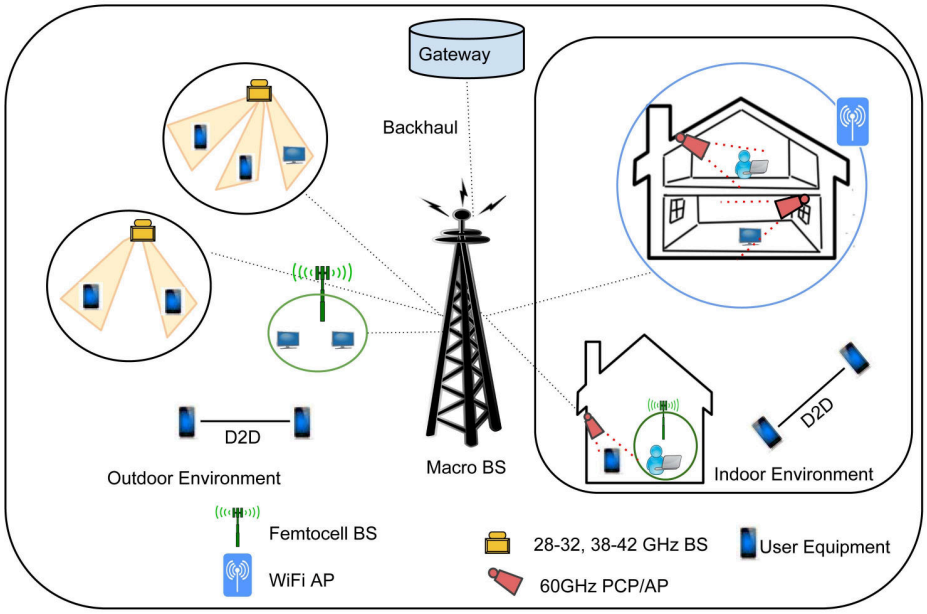

Figure 6.1: A 5G scenario with multiple radio access technologies.

6.1. Introduction

5G networks aim to achieve ubiquitous communication between anybody and anything, anywhere and at anytime [69]. The performance requirements are far beyond what is offered by current systems – in particular a 1000x increase in network capacity is targeted. All this requires new network architectures, new spectrum and technologies [70]. mmWave frequencies (30 GHz to 300 GHz) are being explored as alternatives for both outdoor and indoor communication due to the huge bandwidth they provide. Licensed 28–30 GHz and 38–42 GHz bands have been proposed for outdoor cellular networks [8], while the unlicensed 60 GHz band is being investigated for indoor communication [71]. Moreover, 2G, 3G and 4G access interfaces will have to be integrated with the new technologies to ensure the support of legacy systems. Fig. 6.1 shows 5G communication scenario, where multiple radio access technologies, i.e., 60 GHz Wireless Local Area Networks (WLAN), 2.4/5 GHz WiFi, 28-30 or 38–40 GHz outdoor mmWave base stations (BSs) and macro and femto cell BSs are present. For an efficient spectrum utilization, multiple licensed as well as unlicensed bands will need to work in cohesion to support diverse applications and services. mmWave based mobile communication (28-32 and 38-42 GHz spectrum) and WLANs at 60 GHz will coexist with the legacy cellular networks and WLANs.

To exploit the available spectrum across the various frequency bands, a highly flexible communication interface is required which can support multiple RATs

for various, possibly very different, services at the same time. For example, machine-to-machine (M2M) communication will have infrequent small packets with low data rates but with critical latency requirements. On the other hand, video applications, e.g., 4K video, have some latency requirements, can tolerate errors to an extent, but will require very high data rates. Web browsing and file sharing applications, on the other hand have again different requirements. In case of M2M, signaling and control mechanisms employed in current networks would cause high overheads. Furthermore, to enable device-to-device (D2D) communications which uses direct communications between devices in proximity without involving BSs, very efficient signaling mechanisms are required so that spectrum utilization can be increased.

To address these challenges, instead of a rigid and infrastructure-centric approach adopted by previous generations, device- and user-centric architectures are being advocated for 5G, in order to better support ubiquitous and seamless communication. Legacy 2G, 3G and 4G systems covering large areas were envisioned to serve both indoor and outdoor environments likewise [70]. However, in the 5G-era, 80% of traffic is expected to be generated in indoors [72]. Usually most of the high data rate applications such as large file transfer, high definition video streaming and conferencing would be used indoors. Therefore, 5G networks must take care of the distinction between indoor and outdoor traffic. To tackle this problem, high capacity indoor local small cells are required that can provide multi-Gb/s connectivity with better coverage. The 60 GHz frequency band has emerged as the most promising candidate for the high speed indoor communications due the availability of a large bandwidth. The 60 GHz standards IEEE 802.15.3c [5] and IEEE 802.11ad [7] have already been completed, promising data rates up to 5-7 Gb/s for a range of 10 to 20 m. Since IEEE 802.11ad is backward compatible with IEEE 802.11b/g/n/ac, it has emerged as a better candidate for 5G indoor communications than IEEE 802.15.3c. However, there remain several issues which need to be addressed to realize multi-Gb/s 60 GHz indoor networks based on the IEEE 802.11ad. Let us discuss these issues.

Access delay: IEEE 802.11ad divides the area around an access points (AP) in sectors, e.g., a sector can span over 60°or 90°. CSMA/CA-based random access is used during predefined time periods – in each sector in a round robin fashion – called Contention Based Access Period (CBAP). A device has to wait for the CBAP period allocated to its sector. For example, if each sector spans an angle of 90°then there are four sectors. Thus, if a device generates a request just after the allocated CBAP period for its sector, it has to wait until the next three CBAP periods have passed. This introduces a considerable delay before the request is fulfilled.

Re-beamforming: Although the peak PHY data rate promised by IEEE 802.11ad is about 7 Gb/s, realizing a seamless multi-Gb/s WLAN system providing a sustained peak data rate is difficult. 60 GHz links are highly susceptible to blockage caused by obstacles such as humans, furniture, walls, etc. Further, communication using narrow beams has to track moving devices to maintain the link [14, 73]. With narrow beams, beam misalignment caused by small movements result in

broken links. If a device moves away from the beam coverage area, an exhaustive beam-search is required, resulting in excessive delays and communication overhead. It is therefore important to keep beam alignment in order to maintain a stable link.

Handover: While using directional antennas at 60 GHz, device discovery by the AP is challenging due to the required strict alignment of receiver and transmitter antennas. Further, 60 GHz signals do not penetrate walls, there will be many isolated from each other 60 GHz APs in an indoor area. This results in frequent handovers when a user moves. When moving from the coverage area of one AP to another's, one should be able to quickly reconnect with another AP. To ensure this, efficient mobility management, fast discovery and authentication mechanisms are needed. Since the data rate is very high, a small interruption in signal coverage can lead to the loss of a large amount of data. Further, frequent device discovery and association also leads to excessive energy consumption resulting in fast battery drain.

To address these challenges associated with the standalone operation of 60 GHz indoor wireless access, we propose CogCell, a 2.4/5 GHz assisted 60 GHz picocellular network architecture. This is similar to the existing macro-assisted small cells – also called *phantom cells* architecture, for 5G outdoor networks [74]. In this approach, the control-plane and data-plane are decoupled. The macro cell covering a large area is responsible for the control and management functions, while small cells are used solely for providing high data rate communications. Usually small cells remain in a turn-off state to save energy. We got the inspiration to propose our CogCell architecture from the *phantom cells* concept, however we have tailored it to indoor environments to benefit from the ubiquity of WiFi, operating at the 2.4/5 GHz bands and the high data rate capability of the 60 GHz band. To the best of our knowledge, there is no prior work on hybrid 2.4/5 and 60 GHz network architecture for indoor communications. In our proposed architecture, the 60 GHz band is used for high speed data communication (data-plane traffic) while 2.4/5 GHz WiFi is used for control purposes (control-plane traffic). In the absence of a 60 GHz link, 2.4 GHz can also be used as a fallback data-plane option in CogCell architecture making the best of both worlds. Several, isolated from each other, 60 GHz picocells are controlled by a single WiFi AP. This facilitates faster device discovery and excellent mobility management of the room-level picocells. The proposed architecture provides the following benefits:

i Better spectrum utilization by switching between 2.4/5 GHz and 60 GHz bands for control and data transmission, respectively.

ii Faster device discovery leading to a speedy network association and reduced latency in medium access.

iii Provision for opportunistic fall-back of the 60 GHz data-plane to the 2.4/5 GHz band for data transmission, when a 60 GHz link is not available.

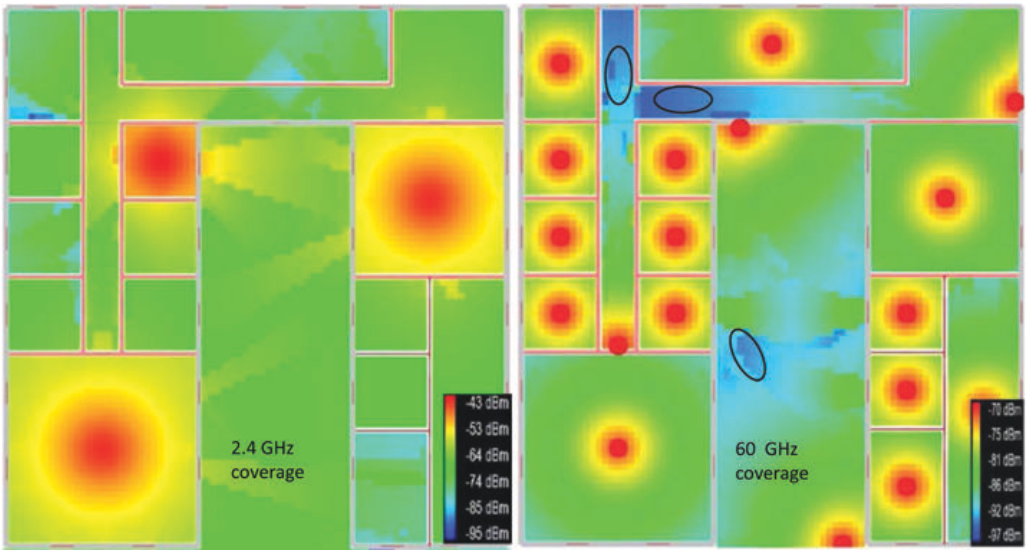

Figure 6.2: Signal coverage comparison at 2.4 GHz and 60 GHz.

6.2. Indoor networks based on the combination of WiFi and 60 GHz

In this section we analyze and motivate the choice of a hybrid 2.4/5 GHz and 60 GHz network architecture by discussing the capacity and coverage limitations of 2.4/5 and 60 GHz signals, respectively. We illustrate that 2.4 GHz and 60 GHz systems are complementary in terms of coverage and capacity, and explain how the proposed CogCell architecture enables the interplay of both to provide a seamless multi-Gb/s indoor wireless connectivity.

Complementarity of 2.4 and 60 GHz

Fig. 6.2 depicts the coverage of 2.4 GHz and 60 GHz signals in an indoor environment with dimension 40 m×40 m and internal walls shown in the figure. We employed Radio-wave Propagation Simulator (RPS) [75] to generate the heatmap of the coverage provided by 2.4 GHz and 60 GHz transmitters. We placed three antennas transmitting at 2.4 GHz and 18 antennas (one in the every room) transmitting at 60 GHz. The position of the transmitters corresponds to the centre of the red circles. RPS uses ray tracing to determine the coverage in the indoor area. To calculate the signal power, reflections up to second order are considered and all the antennas are assumed to be omnidirectional. The transmission power of antennas is 10 dBm. It is clear that three antennas operating at 2.4 GHz are sufficient to cover the whole area. On the other hand, at 60 GHz every room needs a dedicated 60 GHz antenna. A significant fraction of the 60 GHz signal power is absorbed by the walls. This is illustrated by the black ellipses over the blue colored areas in Fig. 6.2.

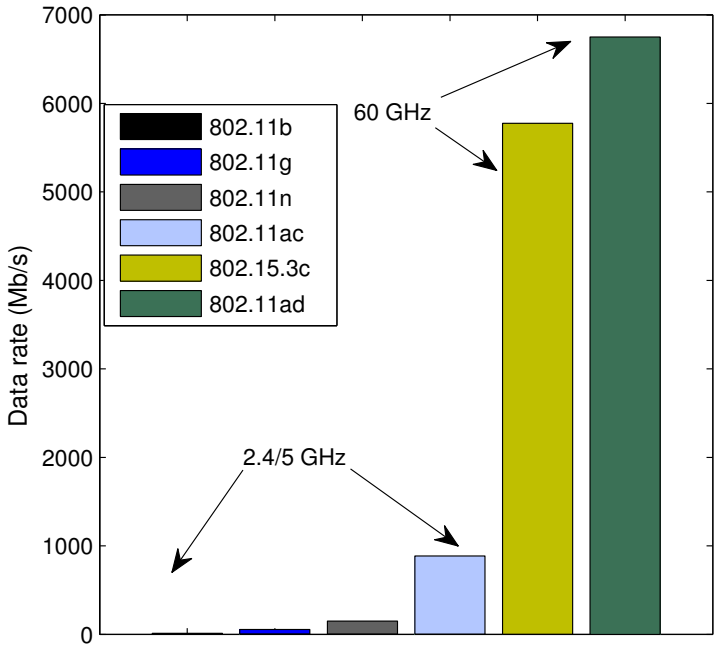

Figure 6.3: Comparison of peak data rates at 2.4/5 GHz and 60 GHz based on the IEEE 802.11 b/g/n/ac/ad and the IEEE 802.15.3c.

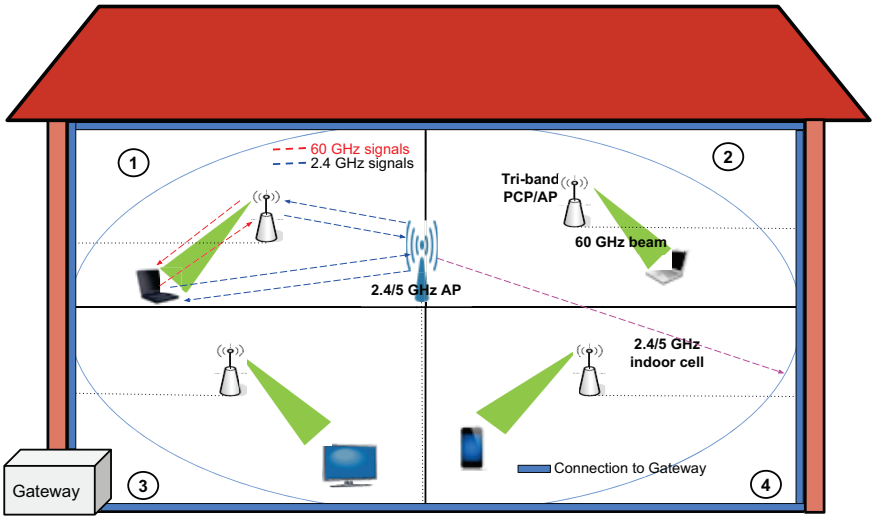

Figure 6.4: Cogcell architecture exhibiting the interplay of 2.4 and 60 GHz frequency bands.

Fig. 6.3 compares the maximum data rates promised by different WLAN standards operating in the 2.4/5 GHz and 60 GHz frequency bands. Even though IEEE 802.11n and IEEE 802.11ac use very sophisticated PHY layer techniques such as MIMO, MU-MIMO, channel bonding, and frame aggregation at the MAC layer, the expected data rate is much lower compared to what can be achieved at the 60 GHz frequency band.

It is evident that the 2.4 GHz and 60 GHz signals complement each other in terms of capacity and coverage. The capacity of 60 GHz signals is at least ten times higher than the 2.4 GHz systems. Thus a hybrid solution, involving 2.4 GHz transmission assisting the 60 GHz devices can be very effective. Almost every consumer electronic device, such as smartphones, tablets, laptops, cameras, etc., is equipped with WiFi and this trend is expected to continue. Hence, assistance of 2.4/5 GHz band for 60 GHz communications seems a pragmatic solution.

6.3. Hybrid 2.4 and 60 GHz WLAN Architecture

In order to create a hybrid architecture, there can be two types of solutions: (i) utilizing the existing 2.4 GHz WiFi and IEEE 802.11ad, and modify them accordingly; or (ii) a new system other than IEEE 802.11b/g/n and IEEE 802.11ad. The former category is more likely to succeed as a majority of wireless communication devices are already equipped with IEEE 802.11b/g/n. Hence we propose to use WiFi as a supportive technology to control the 60 GHz network. One WiFi AP covers several 60 GHz APs and hence, several 60 GHz APs are controlled (medium access control, device discover and mobility management, etc.) by a single WiFi AP. This is the basic idea behind the proposed CogCell architecture.

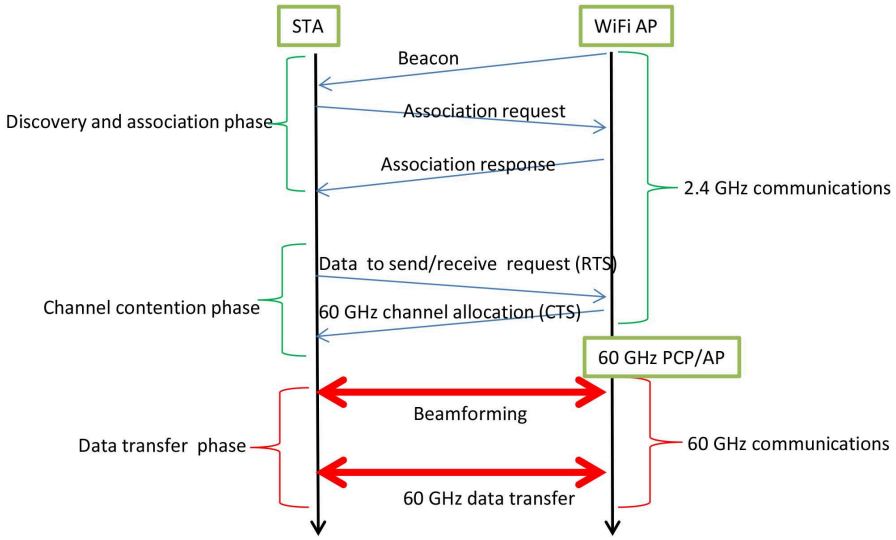

Figure 6.5: Sequence diagram of dual band transmissions in the Cogcell architecture.

Fig. 6.4 shows the conceptual diagram of a CogCell architecture. One 2.4/5 GHz AP covers all 60 GHz coverage area. Further, every area separated by walls has a 60 GHz PCP/AP (802.11ad APs are called PCP/APs) dedicated for high speed data transmission. In a smaller indoor environment such as a small home, a single 2.4/5 GHz AP can be sufficient to provide the coverage but if the indoor area is large (e.g., big office, shopping malls or airports), multiple 2.4/5 GHz APs would be needed to cover the complete area. Moreover, when areas are separated by walls, they always require a separate 60 GHz PCP/APs.

In the proposed CogCell architecture, device discovery, association and channel access requests are transmitted over 2.4/5 GHz channels, while data is transmitted over 60 GHz channels. If a device wants to transmit data, it first sends its request using the 2.4/5 GHz frequency band. Thereafter, the appropriate 60 GHz AP is directed to provide the high speed data transmission. IEEE 802.11ad PCP/APs are tri-band devices, hence WiFi AP can communicate with 60 GHz PCP/AP over 2.4/5 GHz. Fig. 6.5 provides the schematic of the packet transmissions in the CogCell architecture.

6.4. Advantages and Challenges of the Hybrid Architecture

In outdoors, LTE is a better choice than WiFi to support the 60 GHz mmWave small cells because it provides a better coverage (longer range) than WiFi [76]. However, in indoor environments, WiFi is more suitable instead of LTE due to the prevalence of WiFi networks over licensed LTE cells and the potential blockage of LTE signals by the outer walls of the buildings. The propagation of LTE signals

Table 6.1: MAC parameters used in the numerical evaluations.

Parameters	Typical values	Parameters	Typical values
Control frame transmission rate	1 Mbps	Retry limit[2.4 GHz]	5
WiFi data rate	54 Mbps	CW_{max}[60 GHz]	16
SIFS[2.4 GHz]	10μs	CW_{max}[2.4 GHz]	256
SIFS[60 GHz]	3μs	RTS	20 Bytes
Slot time[2.4 GHz]	20μs	CTS	14 Bytes
Slot time[60 GHz]	5μs	ACK	14 Bytes
DIFS[60 GHz]	SIFS + Slot time	PHY Header	16 Bytes
DIFS[2.4 GHz]	SIFS + 2×Slot time	MAC Header	24 Bytes
RIFS	30μs	WiFi data	1024 Bytes
CW_{min}[60 GHz]	8	Association request	1024 Bytes
CW_{min}[2.4 GHz]	32	Association response	16 Bytes
Retry limit[60 GHz]	5	Sector sweep and feedback frame	1024 Bytes

in indoor environment is highly dependent on the building materials and signals can get severely attenuated. Furthermore, a WiFi control-plane is more suitable for indoor mobility management because of its localization capabilities which are accurate up to a few meters [77]. It also helps in handovers between 60 GHz APs, where room level positioning accuracy is required. Let us now discuss the advantages and challenges of interplay between WiFi and 60 GHz as follows.

6.4.1. Advantages of the hybrid architecture

Firstly, isolated (behind the walls) 60 GHz APs still facilitate a seamless WLAN experience to the indoor users. Secondly, device discovery and association are easily performed over 2.4/5 GHz. As users move from one room to another room, they are still covered by the same 2.4 GHz AP. Thirdly, information sent over the 2.4 GHz channel helps in 60 GHz beamforming procedure using the location based beamforming. It has been demonstrated in [78, 26], that it is possible to infer the direction of 60 GHz transmissions using the 2.4/5 GHz transmissions that can reduce the link setup overhead by avoiding exhaustive beam searching. Instead of using the two-level exhaustive beam searching specified in the IEEE 802.11ad, devices estimates the approximate directions of each other using 2.4/5 GHz frames and narrow down the beam-search space. Generally, 2.4/5 GHz communications (IEEE 802.11n, IEEE 802.11ac) employ multiple antennas through which the approximate direction of arrival can be obtained. Using this rough estimate of direction of arrival, the search space of exhaustive beam searching for 60 GHz is reduced.

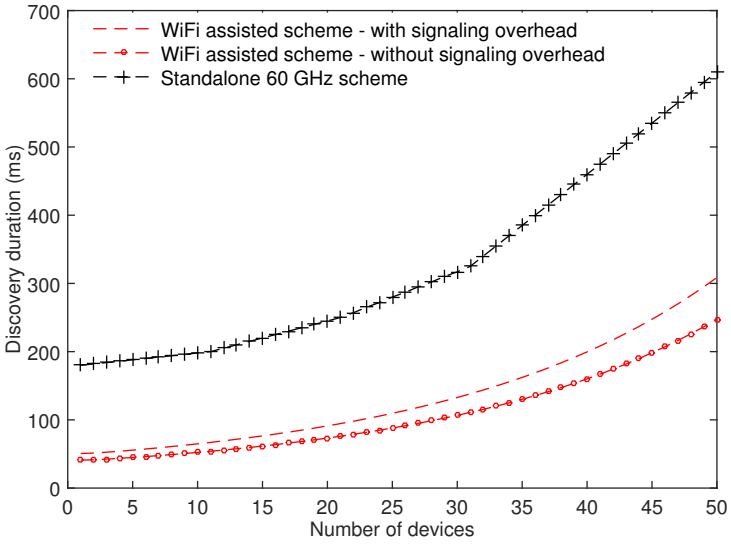

Figure 6.6: Average device discovery vs number of devices.

To assess the improvement in device discovery, we used MATLAB for numerical evaluations. We considered an indoor scenario of four rooms with a central 2.4/5 GHz controller and four 60 GHz PCP/APs capable of 2.4/5 GHz transmissions. The devices are uniformly distributed throughout the indoor area. We assumed that devices can infer the rough sector estimates using 2.4 GHz transmissions employing the mechanism proposed in [26]. In our evaluation, sector level beamwidth of all the devices and PCP/AP is assumed to be 60°. Further it is assumed that the traffic on WiFi band only consists of the 60 GHz discovery frames. We used Bianchi's [18] model to calculate the packet transmission collision probabilities. All the simulation parameters are listed in Table 6.1.

Fig. 6.6 shows results for the WiFi assisted device discovery mechanism. The results are compared with the standalone 60 GHz directional device discovery scheme proposed in [79]. It can be observed that the WiFi assisted scheme is nearly 150% to 300% faster than the 60 GHz directional device discovery scheme. The results also show the effect of signaling overhead due to the 2.4 GHz control frame transmissions which is obtained by including the time required for transmission of extra WiFi frames needed for communications between central WiFi controller and the tri-band 60 GHz PCP/APs. Apart from a faster device discovery, the CogCell architecture can also reduce the channel access delay because a device can place the data transmission request over 2.4/5 GHz channel whenever it wants. It does not need to wait for the alignment of its antenna array with that of the PCP/AP. On the other hand, in sectorized MAC protocols such as IEEE 802.11ad, a device has to wait for channel access if the 60 GHz AP is serving a different sector other.

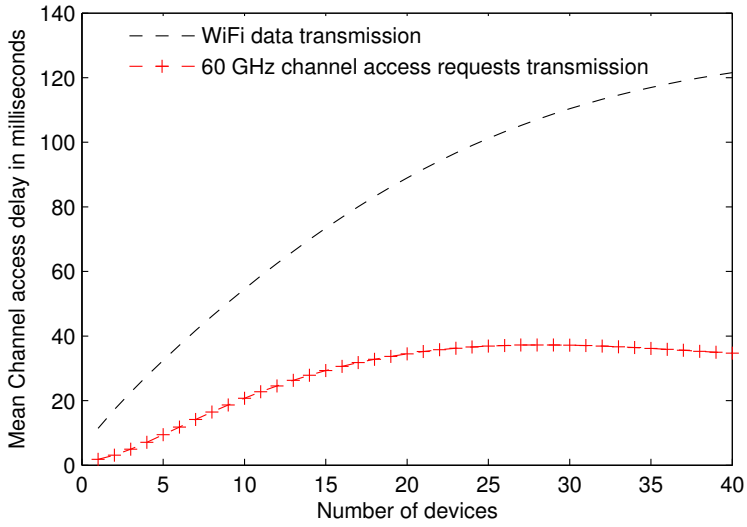

(a) Channel access delay.

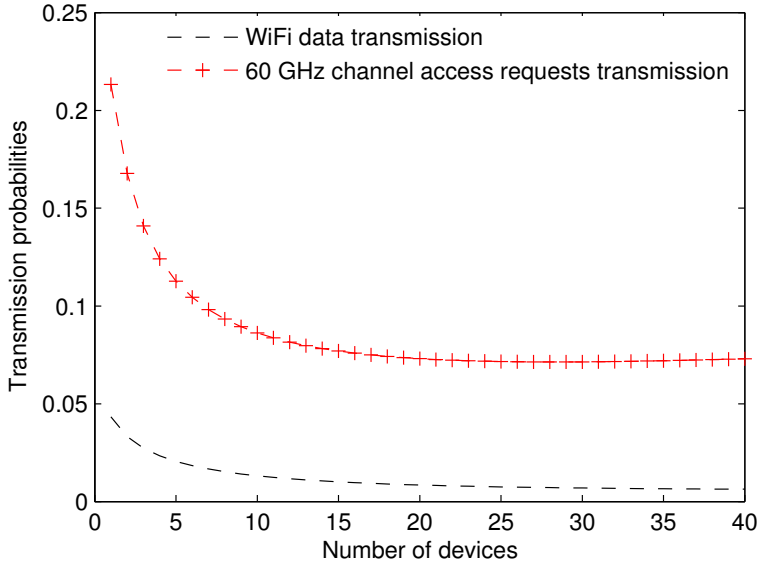

(b) Transmission probabilities of 60 GHz channel requests and WiFi data frame.

Figure 6.7: Channel access delay and transmission probability performance using prioritization.

6.4.2. Challenges of the hybrid architecture

The hybrid 2.4/5 GHz and 60 GHz network has many challenges also. The number of WiFi devices in indoors is rapidly increasing due to the increased use of WiFi in consumer appliances and smart home communication infrastructure. Therefore, a large number of WiFi devices can hinder the control-plane communication meant for quickly accessing the 60 GHz data-plane. Hence it is important to ensure that the 2.4/5 GHz control-plane does not become a bottleneck in accessing the 60 GHz channels. To address this issue, we propose to prioritize the 60 GHz channel access request frames over the usual 2.4 GHz frames. To do so, we define two categories of frames sent over 2.4 GHz channel: (i) 60 GHz channel request frames which are given high priority, and (ii) usual 2.4 GHz channel request frames by non-60 GHz devices. We assign different minimum and maximum contention window sizes, DIFS (distributed coordination function inter frame space), SIFS (inter frame space) and maximum number of retransmissions for these categories, which are shown in Table 6.1. The 60 GHz channel requests are given high priority by selecting a smaller window size and reduced inter frame spacings. A similar scheme is used in IEEE 802.11e [21], where traffic is classified in different access categories to provide the different quality of service to the each access category. It is a well established fact that the traffic prioritization schemes employing differential contention window sizes and inter frame spacings can ensure a higher probability of success with a lesser channel access delay for the high priority traffic class [21]. We used the analytical framework provided in [21] to calculate the transmission probabilities and the medium access delays. To analyze the proposed prioritization scheme, here, we also assumed a four room indoor scenario with uniform device distribution and each room having one 60 GHz PCP/AP. The ratio of 60 GHz devices to WiFi-only devices is assumed to be 1:4.

Fig. 6.7(a) and Fig. 6.7(b) show the MATLAB simulation results for the average channel access delays and transmission probabilities for both type of requests using the CSMA/CA based medium access. It can be seen that a significantly faster channel access and higher transmission probabilities can be guaranteed for the 60 GHz channel requests comparing with that of the ordinary WiFi request frames. This is because the reduced window size results in an increased transmission opportunity and the smaller inter frame spacings ensures a collision free transmission in CSMA/CA based channel access.

Another important challenge using multiple radios simultaneously is the increased power consumption that can drain the batteries of the mobile devices. Hence novel schemes are required to reduce the device power consumption. One possible solution could be to turn on the 60 GHz radio only when data-plane communication is required. Furthermore, the Cogcell architecture envisage data-plane fallback to 2.4/5 GHz if the high speed 60 GHz links cannot be established. This requires intelligent mechanisms to determine when the data-plane fallback should be triggered as the 60 GHz link quality can frequently fluctuate due to the multiple reasons such as antenna misalignment caused by user movement or blockages due to obstacles.

6.5. Conclusions

One of the main objectives of 5G networks is to achieve a 1000x increase in the current network capacity to address the explosive growth of mobile data traffic. The previous generations of communications (2G, 3G and 4G) did not differentiate between indoor and outdoor environment and assumed the same set of services for both. Since most of the high data rate applications such as HD video streaming/conferencing and gaming are used indoors, it is expected that the indoor traffic will overwhelmingly dominate (80%) the total data traffic in 5G era. Since, 5G communications aim to use mmWave frequencies for multi-Gbps wireless access, heavy attenuation of mmWave signals from building materials requires a separate network design approach for indoor environments.

The massive available bandwidth in the unlicensed 60 GHz band makes it an ideal choice for multi-Gbps indoor wireless access. However, providing a 'WiFi like' seamless indoor connectivity is still a challenge because every room or areas seperated by walls require dedicated APs. These closely spaced behind the walls APs remain isolated from each other as signals cannot penetrate walls. In this chapter, we proposed CogCell, a novel indoor network architecture for indoor communications that uses 2.4/5 GHz bands to control the 60 GHz APs. The CogCell architecture envisages the interplay between 2.4/5 and 60 GHz bands with a 2.4/5 GHz control-plane covering multiple 60 GHz APs supporting the data-plane. The CogCell provides a seamless multi-Gb/s WLAN experience at 60 GHz frequency bands and reduces device discovery and channel access delays. If 60 GHz links cannot be established, 60 GHz data-plane fallback to 2.4/5 GHz is also provisioned. Since the standalone operation of 60 GHz wireless access is not sufficient due to its poor coverage, we show that the 2.4/5 GHz assisted 60 GHz communications can be a potential alternative to leverage the multi-Gbps capacity provided by 60 GHz frequency band. Moreover, the hybrid network architecture also brings many new challenges. For example, the simultaneous use of multiple radios would result in high power consumption that need to be tackled. Furthermore, the coexistence with the IEEE 802.11 networks need to be carefully considered when designing the functionalities of the control-plane and data-plane.

7

A 60 GHz Radio over Fiber based Indoor Network Architecture

In indoor environments, every room or area separated by walls requires at least one dedicated millimeter wave (mmWave) access point (AP) due to the mmWave signals' inability to penetrate walls. This results in frequent handovers, causing a lot of overhead, and high deployment costs. On the other hand, in the 5G era, data traffic generated indoors is predicted to be about 80% of the overall data traffic. Hence, cost effective and easily managed high speed indoor wireless solutions are required.

As a solution, we propose in this chapter a 60 GHz wireless indoor network architecture –employing radio-over-fiber (RoF) technology based implementation of the cloud radio access network (C-RAN) [80] –called micro C-RAN (μC-RAN). The purpose is to exploit the cost effective centralized baseband processing and adaptive resource allocation capabilities of the C-RAN architecture. In this chapter, we discuss in detail the requirements and research challenges for various system modules such as remote beamforming and medium access mechanisms and the corresponding solutions provided by the μC-RAN architecture. We also investigate the feasibility of the IEEE 802.11ad MAC protocol for the proposed μC-RAN architecture, considering both carrier-sensing multiple-access with collision avoidance (CSMA/CA) and fixed time division multiple access (TDMA) schemes. We show that the throughput performance of the CSMA/CA based channel access is highly dependent on the fiber length as compared to the TDMA based channel access. We show that the μC-RAN architecture provides a seamless 60 GHz multi-Gbps wireless connectivity with adaptive capacity allocation capability due to the provision of a centralized network management. The centralized baseband processing leads to simple APs resulting in a cost effective

network deployment and energy efficient operation.

7.1. Introduction

The 60 GHz signals' inability to penetrate walls requires line-of-sight (LOS) communication [31]. Therefore, indoor areas separated by walls require the installation of multiple APs to provide an uninterrupted coverage. Further, due to the limited coverage of 60 GHz signals, the overlapping area among 60 GHz APs is very small. This triggers frequent handovers when a user moves from the coverage area of one AP to the one of another AP. The frequent association and disassociation with APs results in a significant loss of data and thus a degraded quality of experience for the user. To make network management easy, a centrally managed network architecture with simple APs (cost effective) is highly desirable. Such an architecture can provide smooth handovers and optimize the bandwidth and energy resources in response to change in traffic demand. The C-RAN architecture has emerged as one of the most promising centralized network architectures because it enables efficient baseband processing and dynamic resource allocation in ultra-dense small-cell deployment. The concept of C-RAN is inspired by the centralized cloud principle where storage and computing resources are shared to ensure efficient utilization of the available resources. Similarly to the cloud principle, C-RAN offers centralized baseband processing (BBU) for many remote radio heads (RRHs) to increase the energy efficiency and allow lower hardware investment. Here RRHs are similar to the traditional BSs, but with reduced functionality. Since RRHs are centrally managed, adaptive resource allocation and coordinated scheduling leads to enhanced spectral efficiency. We conclude that C-RAN architecture is an attractive alternative for the 60 GHz wireless local area networks because:

(i) It provides centralized baseband processing leading to simpler (inexpensive) APs resulting in a reduced CAPEX. Further, the energy efficient BBU operations result in a reduced OPEX.

(ii) It is capable of adaptive resource allocation as the centralized BBU can allocate resources (baseband processing, capacity, etc.) on-demand based on the dynamics of traffic in time and space.

(iii) The centralized network management facilitates smooth handovers among closely spaced APs.

The radio over fiber (RoF) technology is seen as an attractive option to implement the C-RAN based architectures due to the cost effective centralized baseband processing and the provision of relatively simple transceiver modules coinciding with the main objectives behind the C-RAN network architecture [81, 82, 80]. In RoF systems, radio signals are transmitted over fiber by modulating the optical carrier with the radio signals [83, 84]. All the functioning related to the radio access control, signal generation, distribution and baseband processing is done in a centralized point. The simple remote radio units (RAUs) installed at the

remote locations, e.g., in every room, demodulate (optical-to-electrical conversion) the RoF signals and transmit the radio signals. The proposed μC-RAN architecture employs RoF to realize a cost effective multi-Gbps 60 GHz wireless indoor network. Our contributions in this chapter are the following:

(i) We propose a network architecture for 60 GHz indoor radio access. We describe in detail the function of each of the system modules such as signal generation, the wireless access interface and the network management.

(ii) Considering the use of directional antennas at 60 GHz frequency band, we propose a novel true-time-delay (TTD) based beamforming module that can be remotely configured.

(iii) We investigate the applicability of the IEEE 802.11ad MAC protocol in the proposed architecture and establish the impact of the fiber length on the performance of the CSMA/CA and TDMA based medium access schemes.

7.2. Related work

C-RAN has the potential to increase both the energy and the spectral efficiency of mobile networks [80]. There are many alternatives available to connect the BBUs with RRHs (fronthauling) such as existing copper cables, wireless fronthaul at microwave frequencies, optical fiber and recently mmWave wireless. However, it has been argued that optical fiber and mmWave wireless are future-proof fronthaul candidates, due to the high bandwidth [80, 85]. Since mmWave signals cannot penetrate walls, optical fiber is the only choice for high speed in-building signal distribution making RoF-based implementation a suitable candidate for a centrally managed indoor network. There are many articles available in the literature on RoF technology for the mmWave frequency bands [86, 87, 88, 89]. The majority of these papers focus on wireless service delivery for long distances emphasizing the physical (PHY) layer. A novel 40 GHz frequency band RoF architecture is proposed in [86]. It integrates optical and wireless signal delivery. Techniques for remote radio signal generation, up-conversion and wavelength division multiplexing (WDM) are presented. A hybrid star-tree based network architecture is proposed in [88]. It incorporates WDM for optical carrier and sub carrier multiplexing for radio signals. In [89], authors have evaluated the performance of IEEE 802.15.3c Physical layer modulations and coding schemes.

Some researchers have investigated the use of popular MAC protocols in the WLANs. In [90], the performance of an RoF network employing IEEE 802.11a/g MAC is investigated and the feasibility of 802.11a/g in an RoF network was demonstrated using an experimental setup. In [91], an indoor network architecture based on RoF technology is proposed. In [92], the performance of ETSI HiperLAN/2 and IEEE 802.11 is examined. It is also shown that centralized MAC protocols are better suited for RoF indoor networks. All these works summarized above provide standalone and isolated analysis either at the medium access control (MAC) layer or PHY layer. Further, the impact of directional antennas on the network building blocks is not considered ehich is an important

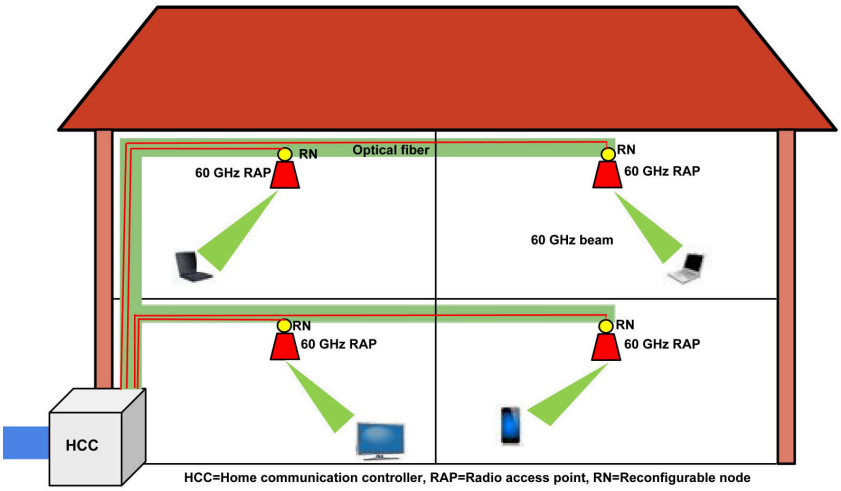

Figure 7.1: A schematic of μC-RAN architecture.

factor in 60 GHz communications. On the other hand, we provide a unified view of the 60 GHz RoF indoor/hotspot network architecture. The unified view means we simultaneously consider the physical layer, medium access control and network architecture aspects rather than the standalone perspective at each layer.

7.3. System architecture

Fig. 7.1 shows the schematic diagram of a μC-RAN indoor network architecture. The centralized home communication controller (HCC) is responsible for radio access control, signal generation, distribution and processing. It corresponds to the BBU of the C-RAN architecture. HCC monitors the communication needs of the wireless devices spread over the indoor area and takes care of setting up the communication links with these devices through the radio access points (RAPs). Here, a RAP corresponds to the RRH part of the C-RAN architecture. Every room or partition has at-least one RAP, which provides wireless connectivity to all the devices in its coverage area and is connected to the HCC through an optical fiber via the optical network Nodes (RNs). In the next section, we provide a detailed description of the different system modules of the proposed μC-RAN architecture.

7.4. HCC, RAP and RN: structure, functions and requirements

The HCC acts as a central control and management unit while the RN and RAP perform the functions of the remote control unit and the radio access point. The

detailed functions of HCC, RN and RAP are elaborated in the following section[1]

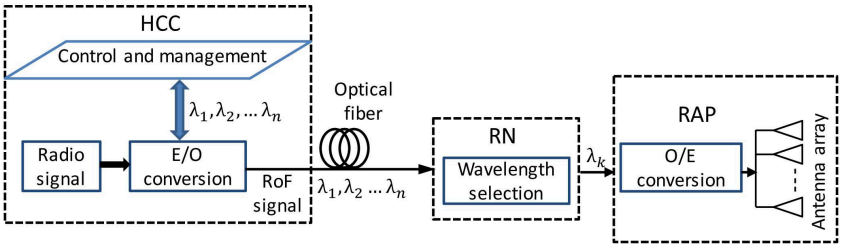

Figure 7.2: An illustration of μC-RAN building blocks.

7.4.1. Home communication controller (HCC)

The HCC performs network management, routing, switching, baseband processing and up-conversion and finally modulates the 60 GHz RF signal on an optical carrier. The main function of the HCC is to reconfigure the transparent fiber network for these RF signals (see Fig.7.2). Since the RF signal up-conversion is accomplished at the HCC, the proposed architecture falls in the category of analog ROF systems. On the other hand, the RF up-conversion at the RAP falls in the category of digital RoF which is mainly suitable for long distance RoF communications [95].

7.4.2. Radio Access Point (RAP) and Reconfiguration Node (RN)

The reconfigurable node (RN) and remote antenna point (RAP) are principally depicted in Fig.7.2. The RN performs wavelength selection and beam-steering (by introducing phase differences) while the RAP performs optical-to-electrical (O/E) conversion and transmits the radio signal. The RN is defined as a remote unit to configure the RAP. Its main functions are control signal detection, processing and wavelength insertion. The control signals are used to transmit the commands to the RN for dynamic reconfiguration of wavelengths. The feedback control signals (uplink), e.g., to convey status information, are also sent back to the HCC via the RN. Apart from the wavelength reconfiguration, the RN would also support the control signal delivery for the antenna array in order to allow beam-steering and beam-forming.

The main components of the optical interface for control signal delivery (detection and insertion) between HCC and RN are an asymmetric splitter, a selecting filter (optional) and a low-speed optical detector (photo-diode). The optical-electrical (demodulation of RoF signal) conversion is realized by using a

[1]This section is a joint effort by the SOWICI project partners from TU Eindhoven, TU Delft and UTwente. The main contributions are provided by TU Eindhoven and can be found in[93, 94]. It is kept in this thesis provide a complete overview of the proposed architecture.

photo-diode. For uplink transmission, the wireless signal is received by an antenna array and is then down-converted and, via an optical modulator, converted from electrical to optical. The modulated optical signal is then transmitted back) to the HCC. In the practical case, the RN and RAP are placed in the same location and thus can be integrated.

7.4.3. Beamforming and beamsteering

Radio beams can be steered by phased array antennas where controlled differences in the phases between the radio signals radiated by the antenna elements determine the shape and direction of the beam. For this, accurate and tunable shifting of phases needs to be accomplished. This is particularly challenging when large bandwidth mmWave radio signals, with complex modulation formats, are involved and when fast beam steering is required. Traditionally, beamforming is realized by electronic circuits. A time delay or phase shift can be realized at different stages [96]. The radio frequency (RF) beamforming realizes beamforming at RF frequencies and is done fully in a analog way [97]. Another emerging technique for beamforming is to use optical circuits. Beamforming by optical techniques is achieved by deploying bulky dispersive fiber delay lines [98], and dispersive micro-ring structures [99] that deal only with 1-dimensional beam steering.

In case of broadband 60 GHz communication, electronic beam steering is not the best option as the phase shifter circuitry highly depends on the signal frequency [98]. A large bandwidth signal may result in beam squinting caused by frequency dependent behavior of the phase shifter circuitry. Further, controlling the beam-steering from the HCC in electronic beamforming is a difficult task, requiring strictly synchronized control signals. Apart from the dynamic capacity allocation capability, the simplicity of the RAPs is considered to be the most important feature of the RoF architectures. However, beamforming modules increase the complexity of 60 GHz RAPs significantly. Hence, it is important to have the beamforming done in such a way that the RAPs are kept simple. Therefore, we adopt optical phase shifters for beamforming in the μC-RAN architecture. We use a true-time-delay (TTD) based beamforming [100, 101] which exploits the wavelength-dependent dispersion property of fiber to steer the antenna beams in different directions. By employing TTD beamforming, beam steering can be remotely controlled from the HCC by changing the optical wavelengths thus resulting in a simpler RAP module by avoiding extra control signaling requiring strict synchronization.

Fig. 7.3 shows the schematic diagram of a TTD beamformer. When the RoF signal impinges on the arrayed waveguide gratings (AWG), delays are introduced $\Delta\tau$ which depend on the wavelength of optical RoF signal. In Fig. 7.3 we can see that RoF signals with wavelengths λ_1, λ_2, λ_3 and λ_4 are subject to different delays $\Delta\tau$, $2\Delta\tau$, $3\Delta\tau$ and $4\Delta\tau$, respectively. RoF signals follow a path with specific delay $\Delta\tau_i$ depending on the wavelength of the signal. The beam steering angle θ_i, due to the specific time delay among array elements, is given by,

$$\theta_i = \sin^{-1}\left(\frac{c.\Delta\tau_i}{d}\right) \tag{7.1}$$

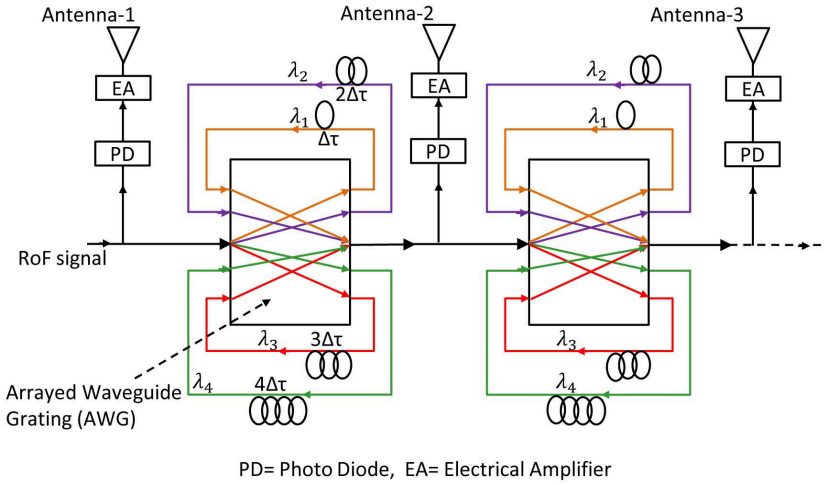

Figure 7.3: TTD beamforming block diagram

here c is the speed of light and d is the spacing among antenna elements. The delay $\Delta\tau_i = D.L_i.\Delta\lambda$ depends on the dispersion introduced by the fiber length where D is the dispersion coefficient of fiber, L_i is the length of the path traversed by the RoF signal of wavelength λ_i, and $\Delta\lambda_i$ is the free spectral range of the AWG. We show an illustration using MATLAB (see Fig. 7.4) to depict the working principle of the TTD beamforming. It is assumed that an 8-elements antenna array is mounted on the ceiling at 4 m height. The antenna main lobe is assumed to be Gaussian and the transmit power is 10 dBm. We used three different wavelengths, λ_1=1540 nm, λ_2=1545 nm, and λ_3=1550 nm, considering a 5 m×4 m room and calculated the received signal power along a line going through the center of the room for three different wavelengths. Please see [94] (a publication by the TU/e SOWICI project partners) for the detailed description of the proposed TTD beamforming. It can be seen from Fig. 7.4 how the change in the wavelength of the RoF signal can steer the radio beam into different directions. Using different wavelengths result in peak power at different locations in the room.

We conclude that the optical TTD beamforming is a promising solution for remotely steering the radio beams and for decreasing the complexity of the RAPs. It can also be employed in 5G networks using mmWave radio frequencies where centralized base-band processing is much needed for closely spaced mmWave base stations. Apart from the feasibility of steering radio beams remotely from the HCC, the TTD beamformer provides squint-free beam steering as the steering angle θ_i in Eq. 7.1 is independent of the radio signal frequency. This is a desired characteristic as 60 GHz signals have a large bandwidth, e.g., IEEE 802.11ad specifies four channels in the 60 GHz band and each of them is 2.16 GHz wide.

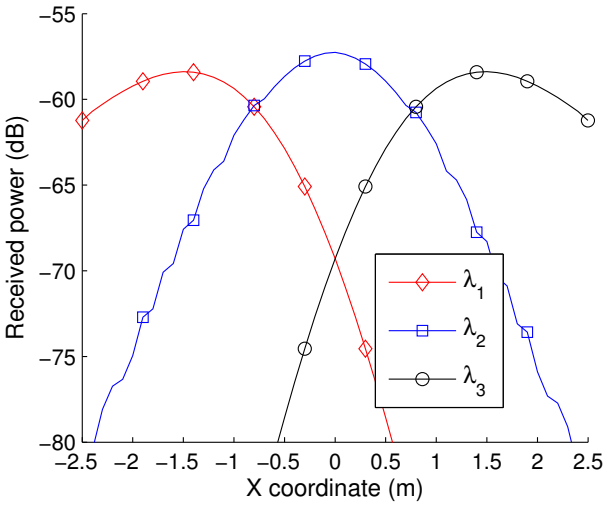

Figure 7.4: Illustration of received power along a line passing through the center of the room for different wavelengths λ_1=1540 nm, λ_2=1545 nm, and λ_3=1550 nm.

7.5. Functional management and communication protocol stack

The HCC contains the control plane functions for optimizing the μC-RAN communication infrastructure with respect to service demands, load balancing and energy consumption. The most important function of the control plane in the proposed 60 GHz RoF architecture is to remotely configure the antenna array of the RAPs to create a beam in the desired direction. In case of the proposed TTD beamformer, it can be obtained by appropriate wavelengths selection. From the wireless access perspective, medium access is also facilitated by HCC. Standards such as IEEE 802.15.3c [5] and IEEE 802.11ad [7] have defined MAC protocols for short range communications at 60 GHz. Because IEEE 802.11ad is backwards compatible with 802.11a/b/g/n, creating the opportunity of fast session transfers between the 2.4/5 GHz and 60 GHz frequency bands, it is preferred over IEEE 802.15.3c. IEEE 802.11ad has proposed three PHYs: a Control PHY with data rate 27.5 Mbps, SC PHY (data rate) and OFDM PHY with peak data rates up to 7 Gb/s.

As explained in Chapter 2 (Section 2.3), the IEEE 802.11ad defines a Personal Basic Service Set (PBSS) which is the operating area of the network formed by 60 GHz wireless stations (STAs). One of the STAs in a PBSS works as the PBSS control point/Access Point (PCP/AP) to coordinate the channel access among STAs. Timing in the IEEE 802.11ad is based on beacon intervals (BIs) set by the PCP/AP. The detailed description of the BI was presented in Chapter 2 (Section 2.3 and Fig. 2.3). The data transfer interval (DTI) part of the BI consist of: contention-based access periods (CBAPs) and service periods (SPs).

The CBAP part employs CSMA/CA based channel access while the SP part uses TDMA based channel access mechanism. In order to incorporate standard wireless MAC protocols in the proposed RoF based architecture, it is necessary to ensure that a smooth medium access is guaranteed. The PCP/AP located in the HCC makes the whole indoor area one PBSS, and is responsible for the coordination amongst the devices in rooms and scheduling 60 GHz data transmissions.

7.5.1. The impact of fiber length

The channel access using CSMA/CA is more complex than the TDMA based access as several IFSs, e.g., DIFS (distributed coordination function inter-frame space), SIFS (standard inter-frame space), MIFS (minimum inter-frame space), etc., are involved. One of the important factors determining the length of these IFSs is the air propagation delay. In RoF networks, the fiber distribution network introduces extra delays preventing the direct use of a wireless MAC protocol in RoF networks. Hence, it is important to investigate the effects of extra delay introduced by fiber on the performance of IEEE 802.11ad MAC protocol.

As explained in the chapter 2, during the CSMA/CA based medium access, if the channel is sensed busy, an STA freezes its backoff counters. But if the channel is found to be idle for a DIFS duration, it resumes decrementing the back-off counter and transmits the frame when the backoff counter reaches zero. The IEEE 802.11ad DIFS duration ranges from 4.2 to 6.5 μs. For a distance of 10 m, the round-trip propagation time in the air(t_{prop}) is 30 ns which is negligible. But in the presence of fiber, the extra propagation delay has to be taken into consideration. In order to allow CSMA/CA to work properly, either the maximum fiber length should be such that t_{prop} does not exceed the DIFS period or DIFS period should be modified. The speed of light in a fiber of refractive index of 1.62 is 194.81 m/μs. Thus, for a DIFS period of 4.2 μs, the maximum allowable fiber length is 427 m to ensure that t_{prop} is always less than the DIFS duration. Otherwise DIFS needs to be increased by the extra delay. However, the acknowledgment (ACK) timeout has to be always increased by the extra delay introduced by the fiber network to avoid unnecessary retransmissions.

Considering the above modifications, we evaluate the normalized throughput performance of the CBAP part and the data throughput of the SP part of IEEE 802.11ad. These are presented next as follows.

7.5.2. CSMA/CA based channel access

The normalized throughput during the CBAP periods employing CSMA/CA is defined as the fraction of time that the channel is used to transmit payload successfully. The channel access during CBAPs is provided in a sector-wise fashion, where STAs in the k_{th} sector compete for the channel time during $CABP_k$. Let T_i, T_c and T_S represent the idle, collision and successful transmission durations, respectively. And P_i, P_c and P_s be the idle channel, collision and successful transmissions probabilities, respectively. Let us represent normalized throughput of

STAs in the k_{th} sector by S_{CABP_k}, which can be calculated as,

$$S_{CBAP_k} = \frac{P_s E[Payload]}{P_i T_i + P_s T_s + P_c T_c}, \tag{7.2}$$

where, $E[Payload]$ is the average size of a payload frame. The transmission probabilities (P_i, P_c and P_s) and the normalized throughput (S_{CABP_k}) are calculated using the expressions derived in Chapter 2 (Section 2.4). T_i, T_c and T_S are calculated using IEEE 802.11ad specification and adjusted with the extra delay introduced due the fiber length. The average normalized throughput S_{CABP} for one RAP is calculated as the average of that of all the RAP antenna sectors.

7.5.3. TDMA based channel access

Further, we evaluate the SPs throughput for the different ACK schemes and the constant physical channel bit error rate (BER). Let the fixed BERs be p_{hdr} and p_{data} for the header and data parts of a frame, respectively. ACK frames are assumed to be sent at the header rates. If L_{hdr}, L_{ack} and L_{data} are the lengths of base header, ACK and data, respectively. Then P_{suc}, the probability of the successful transmission of a frame is expressed as [102],

$$P_{suc} = (1 - p_{hdr})^{(L_{hdr}+L_{ack})} (1 - p_{data})^{L_{data}}. \tag{7.3}$$

Let SP throughput is denoted as S_{SP} which is defined as the effective data rate achieved at the MAC layer. Let T_{avg} be the average time taken in successfully transmitting a frame after n_r retransmissions. If ρ is the SP fraction of a BI, then the average data throughput during SP (S_{SP}) is given by,

$$S_{SP} = \rho \frac{L_{data}(1 - (1 - P_{suc})^{n_r+1})}{T_{avg}}. \tag{7.4}$$

Let T_{suc} is the time of a successful transmission and T_{fail} is the time taken by a failed transmission attempt, then the average time taken by a frame after n_r retransmission attempts is given by,

$$T_{avg} = \sum_{i=0}^{i=n_r} [P_{suc}(1 - P_{suc})^i (iT_{fail} + T_{suc}) + (1 - P_{suc})^{n_r+1}(n_r + 1)T_{fail}]. \tag{7.5}$$

For the Immediate ACK (ImmAck) mechanism, T_{suc} and T_{fail} are given by, $T_{suc-Imm} = T_{pre} + T_{hdr} + T_{data} + T_{ack} + 2SIFS + t_{prop}$ and $T_{fail-Imm} = T_{pre} + T_{hdr} + T_{data} + RIFS + t_{prop}$. Here, RIFS is the retransmission inter-frame space and t_{prop} is the propagation delay given by $t_{prop} = t_{air} + t_{fiber}$. If L_{Fiber} is the length of fiber, t_{fiber} is equal to $L_{Fiber}/194.81$ μs.

Other than the ImmAck, IEEE 802.11ad uses two more ACK mechanisms, delayed ACK and block ACK denoted as DlyAck and BlkAck, respectively. These acknowledgment mechanisms are depicted in Fig. 7.5 by showing the difference

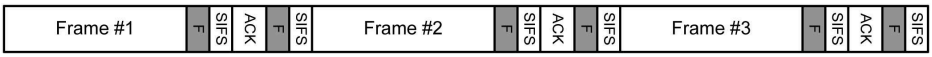

(a) Immediate ACK

(b) Delayed ACK with burst size $K = 3$

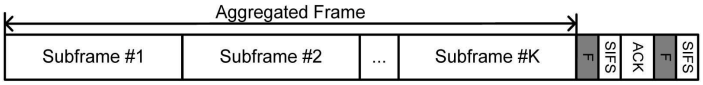

(c) Block ACK

Figure 7.5: The IEEE 802.11ad ACK mechanisms in RoF system

in the transmission of data frames and corresponding ACK frames. More details about ACK schemes can be found in the IEEE 802.11ad [7]. In Fig. 7.5, **F** is the extra delay due to the fiber distribution network.

P_{suc}, T_{suc} and T_{fail} for *Dly-Ack* and *Blk-Ack* with burst size 'K' are given by the following equations respectively,

$$P_{suc-Dly-Ack} = (1 - p_{hdr})^{(KL_{hdr}+L_{Dly-Ack})} \times (1 - p_{data})^{KL_{data}}. \tag{7.6}$$

$$T_{suc-Dly} = K(T_{pre} + T_{hdr} + T_{data}) + T_{Dly-Ack} + (K-1)MIFS + 2SIFS + t_{prop}. \tag{7.7}$$

$$T_{fail-Dly} = K(T_{pre} + T_{hdr} + T_{data}) + RIFS + t_{prop}. \tag{7.8}$$

$$P_{suc-Blk-Ack} = (1 - p_{hdr})^{(L_{hdr}+L_{sub-hdr}+L_{Blk-Ack})} \times (1 - p_{data})^{KL_{data}}. \tag{7.9}$$

$$T_{suc-Blk} = T_{pre} + T_{hdr} + T_{sub-hdr} + KT_{data} + T_{Blk-Ack} + 2SIFS + t_{prop}. \tag{7.10}$$

$$T_{fail-Blk} = T_{pre} + T_{hdr} + T_{sub-hdr} + KT_{data} + RIFS + t_{prop}. \tag{7.11}$$

7.5.4. Performance evaluation

We used MATLAB to evaluate the impact of fiber length on the throughput of the CSMA/CA and the TDMA channel access assuming that devices in a room are uniformly distributed in a circular area of 10 m radius around the RAP. The values of PHY and MAC parameters are taken from the IEEE 802.11ad standard [7]. The signal conversion times from electrical to optical and optical-to-electrical domains are assumed to be negligible. For base header transmissions,

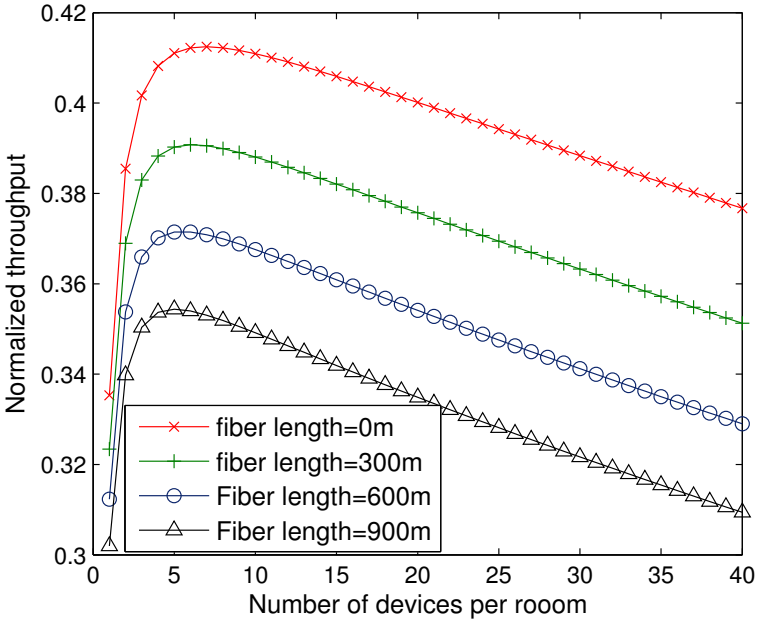

Figure 7.6: CBAP throughput vs number of devices for different fiber lengths.

the common mode signaling rate (PHY data rate = 27.5 Mbps) is used. The IEEE 802.11ad MCS12 having PHY data rate of 4 Gbps is used for data frames which uses 16-QAM modulation scheme with a code rate of 3/4. The data frame size for CBAPs is considered to be 1024 Bytes while it is 2.5 KB for the SPs.

Fig. 7.6 shows the CBAP throughput for various lengths of fiber (300, 600 and 900 m). Since collisions of the simultaneously transmitted packets is the main concern in CSMA/CA based channel access, we assumed perfect wireless and fiber-optic channels. From Fig. 7.6 we can observe that in the presence of fiber, CBAP throughput drops only by 2 to 3% when using a fiber of 300 m as compared to when no fiber used. Such a drop is insignificant. Further, 4 to 6% and 6 to 8% of decay in throughput is observed for fiber lengths of 600 m and 900 m, respectively. We have modified the values of DIFS, SIFS and ACK timeout to accommodate the delay introduced by the fiber length, which is necessary to ensure the the proper functioning of the CSMA/CA channel access. The decrease in channel utilization with the increasing number of devices conforms the channel contention observed in the CSMA/CA based access schemes. We can observe that the behavior of CSMA/CA channel access follows the similar trend for each of the different fiber length because IFs are modified according to the length of fiber. If the extra delay caused by the fiber distribution network is not accommodated, a high amount of packet collisions will result in unreliable transmissions and a poor channel utilization.

Fig. 7.7 shows the SP throughput for varying BERs for a fixed packet size of 20 Kb and fiber lengths of 0, 300, 600 and 900 m, respectively. Optical fiber is assumed to be an ideal channel which is a reasonable assumption when compared with a wireless channel. The data frame size during SP is considered to be 20 Kb. A large frame size is chosen as compared to the CBAP channel access because SP part is likely to be used for high data rate applications such as large file transfer or uncompressed/HD video streaming. We have considered the block of 8 frames for both the DlyAck and the BlkAck schemes. A continuous frame arrival is assumed for both the DlyAck and the BlkAck schemes. When the BER is between 10^{-4} and 10^{-2}, BlkAck out performs all the other ACK mechanisms. But, as soon as the BER reaches 10^{-2}, throughput performance for all the ACK mechanisms deteriorates very rapidly. This is because the error correction code cannot correct the corrupted bits any more. Another important observation is that the throughput curves of the BlkAck and DlyAck for different fiber lengths are very close while the throughput curves of the ImmAck are well separated

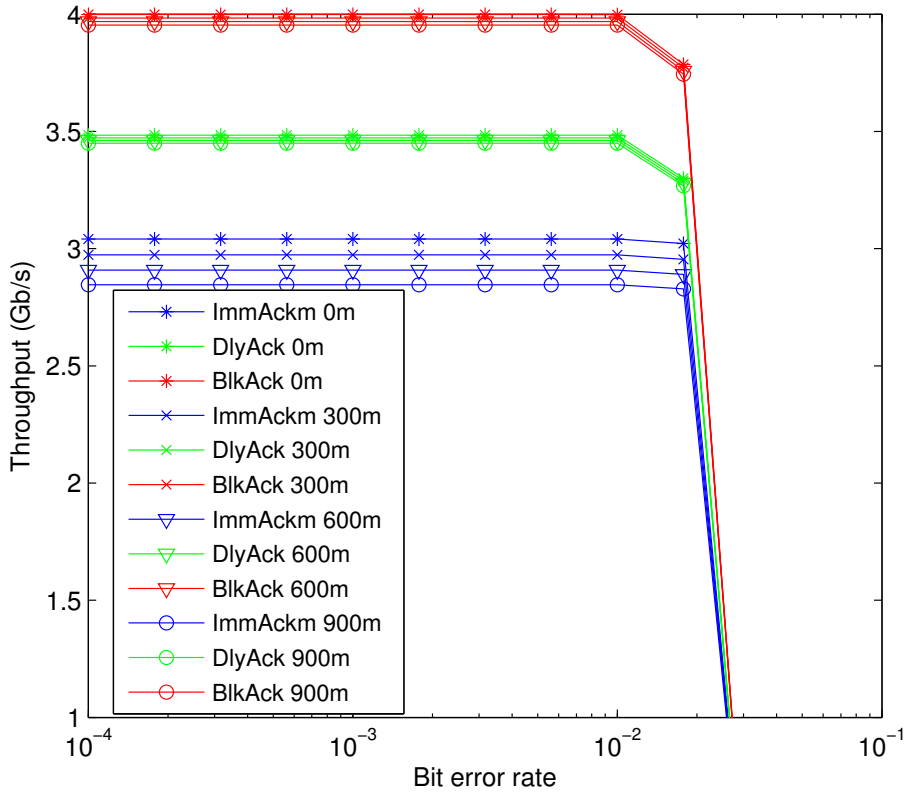

Figure 7.7: SPs throughput vs BER for different fiber lengths and ACK schemes.

from each other.

Fig. 7.8 shows the SPs throughput for a fixed BER=10^{-3}, varying fiber length from 0 to 600 m, and different ACK mechanisms. We consider BER=10^{-3} because according to Fig. 7.7, this value of BER falls in the region where stable performance is achieved, a further increase in the BER results in sudden throughput deterioration. For the fixed BER of 10^{-3}, BlkAck gives the best performance amongst all the ACK mechanisms. The ImmAck obtains the least throughput because for each frame using the ImmAck mechanism, an ACK frame is sent. The BlkAck and DlyAck throughputs are less affected as compared to the ImmAck when fiber length is increased because an ACk frame is sent only after K data frames.

From Fig. 7.7 and Fig. 7.8 we can see that the fiber length has more influence on the CSMA/CA based channel access as compared to the TDMA based channel access. This is because of the several inter-frame spaces (DIFS and SIFS) involved in the channel sensing and smaller packet size which results in a large amount of channel time wasted in idle listening. As the modifications in IFs are dependent on the fiber lengths, it is difficult to fix standard values for these. The large standard IFs may lead to under utilization of wireless channel if distance from HCC to RAP is small. On the other hand, if small IFs may lead to improper functioning of medium access mechanism. Hence tunable MAC protocols are required that can self-adjust the IFs based on the fiber length to ensure the high

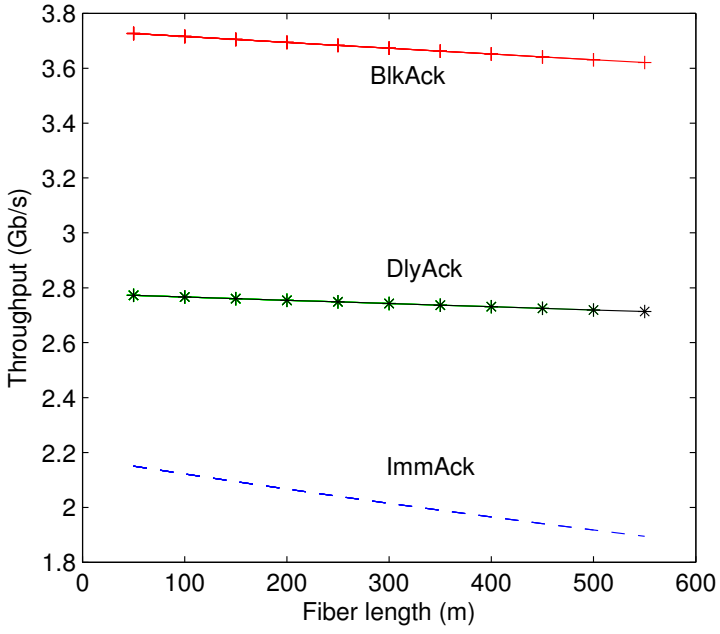

Figure 7.8: SPs throughput vs fiber length with BER = 10^{-3} and different ACK schemes.

channel utilization and proper functioning of the wireless MAC protocols in RoF systems.

7.6. Conclusions

For ultra-dense small cell deployments, the C-RAN architecture looks promising due to its ability to increase both the energy and the spectral efficiency. Since indoor mobile data traffic will overwhelmingly dominate the total data traffic in the 5G era, cost effective and easily managed indoor network architectures are needed. In this chapter, we proposed μC-RAN, an indoor network architecture for 5G communications which consists of 60 GHz wireless access and an RoF based centralized signal distribution network. Our main goal was to exploit the advantages of the C-RAN network architecture for indoor communications and provide a unified view of the RoF based implementation of the scaled-down version of the C-RAN architecture for the indoor communication infrastructure.

We discussed the various requirements of the proposed μC-RAN architecture and provided a unified perspective of physical layer, medium access control and network architectures rather than the standalone and isolated analysis of each layer. Complete system modules were defined and their functionalities and requirements were analysed. We proposed to utilize TTD-based beamforming for remotely steering the radio beams which simplifies the radio access points employing directional antennas. Finally, we evaluated the performance of the IEEE 802.11ad MAC protocol in the proposed network architecture. It was shown that by adopting some changes in the MAC protocol parameters, IEEE 802.11ad can be used in the proposed architecture. We believe that 60 GHz communication will play an important role in 5G networks where μC-RAN architecture addresses the challenges of short range multi-Gb/s connectivity in ultra-dense indoor/hotspot environments. Although RoF based network architecture enables smooth network management and flexible resource allocation, the use of wireless access protocols require adaptation of various protocol parameters that are highly dependent on the fiber lengths. We believe that the MAC protocols in which MAC parameters can be self-tuned to the fiber length without the interventions of operators are highly needed to enable the RoF based network architecture a reality.

8

Conclusions

The availability of enormous bandwidth in mmWave frequency band has the potential to support the unprecedented growth in mobile data traffic in the coming years. Recent developments in the semiconductor technology have made it possible to manufacture low cost, highly efficient, and low form factor transceivers for mmWave communications. Thus, the time has come to reap the benefits of the availability of large amounts of spectrum in this band. The necessary use of directional antennas and the susceptibility to line-of-sight blockage poses many challenges to the medium access control (MAC) and network layers. These challenges force a rethinking of the design choices for the MAC protocol and the network architecture. In this dissertation we specifically focused on these challenges in the 60 GHz band, and proposed solutions for them. We evaluated the performance of our proposed solutions using the IEEE 802.11ad standard MAC and Physical Layer specifications. Though we specifically used the 60 GHz frequency band, since we abstracted the physical properties – antenna gain, beamwidth and the wavelength-dependent path loss – the proposed solutions can be easily extended to other mmWave bands such as the 28–30, 38–42, and 78—80 GHz bands. Let us first recapitulate our journey so far picking up the pebbles of our contributions followed by vistas for future.

8.1. Recapitulation

We started with the analysis of the IEEE 802.11ad MAC protocol and investigated the impact of beamwidth on the throughput and packet delay of the contention based access mechanisms. We have shown that the beamwidth of access points (AP) can effectively control the collisions in the contention-based medium-access. Further, we investigated the trade-offs arising due to the high gain of narrow beamwidth antennas and the corresponding beam alignment and beam searching overheads. We showed that how a judicious selection of the beamwidth can optimize the link capacity. We have also proposed a simple but

very effective beam searching mechanism that results in a massive decrease in the beam searching overhead. Further, we delved into the network architecture aspects and proposed a hybrid network architecture consisting of 2.4 or 5 GHz control plane and a 60 GHz data plane for indoor hotspot environments. The proposed architecture aims to complement the enormous capacity in the 60 GHz band with the excellent coverage provide by the 2.4/5 GHz signals. We have also investigated the performance of the IEEE 802.11ad MAC protocol in 60 GHz radio-over-fiber (RoF) networks. To circumvent the frequent link outages due the misalignment between transmit and receive antennas, caused by movement of users, we envisage to exploit the motion sensors that are part of the most of the mobile devices. We show that by predicting the next location of a mobile device, proactive beam switching can be performed to maintain the beam alignment and avoid loss of performance. We now proceed to summarize the key contributions of this thesis.

8.2. Contributions

8.2.1. Optimizing design parameters of MAC

In the existing wireless access technologies such as WiFi and LTE, all the devices that are registered with a particular access point (AP) or base station (BS) can instantly compete for the channel resources due to the omni-directional transmission and reception. However, this is not likely to be the case in mmWave wireless systems due to the use of directional antennas. To ensure a successful transmission, it is necessary that the transmit and receive antenna beams pointing in the desired directions. In infrastructure mode, this leads to the sectorization of the area served by an AP/BS such that devices in a particular sector communicate with the AP/BS at a predefined time, resulting in complex medium access procedures. This is also evident from the hybrid MAC protocols specified in the standards, IEEE 802.11ad and IEEE 802.15.3c, that rely on both random access (CSMA/CA) as well as fixed access (TDMA) mechanisms. This makes the performance evaluation of the MAC protocol difficult and requires new analytical models that can accommodate these features. We considered the IEEE 802.11ad MAC protocol and proposed a thorough framework for performance evaluation, which considers all the provisions.

We used a three dimensional Markov chain based model that takes into account both the contention and the fixed access periods used in the hybrid MAC mechanism. We have shown that directional antennas bring an extra degree of freedom in terms of beamwidth, in optimizing the throughput and delay performance of the CSMA/CA based channel access. We showed that the appropriate selection of sector-beamwidth can contain packet collisions in the CSMA/CA-based channel access resulting in a significant improvement in throughput and delay performance. Our proposed adaptive beamwidth-selection scheme maintains a stable throughput performance when the number of users increases by taking advantage of this extra degree of freedom.

8.2.2. Trade-offs in mmWave directional links

The gain of a directional antenna is inversely proportional to its beamwidth. This leads to a common assumption that the quality of a link using narrow beamwidth transmit (Tx) and receive (Rx) antennas would always outperform that of a wider beamwidth. However, narrow beamwidth directional links require a strict alignment of Tx and Rx beam directions. A small misalignment of Tx and Rx antenna can result in link outage. Further, if very narrow beamwidth antennas are employed, the beam searching mechanism consumes a significant amount of channel time. Therefore, the beam -misalignment and -searching overheads limit the actual data transmission capacity in highly directional mmWave links. We provided a novel capacity model that considers tradeoffs in highly directional mmWave links considering Tx-Rx beamwidths, beam searching overhead, antenna misalignment and allocated slot duration.

Our analysis provided important insights into the behaviour of directional mmWave links. We have shown that the beam searching overhead and antenna misalignment can reduce the link capacity by an order of magnitude if extremely narrow Tx-Rx beamwidths (1° to 5°) are used. We therefore concluded that using narrow beamwidth not always results in a better link quality and that the Tx-Rx beamwidths must be carefully chosen to exploit the full potential of mmWave communications. We also used commodity IEEE 802.11ad hardware to measure the re-beamforming time when link alignment is disturbed. Our measurements have shown that it takes considerable time (100 ms–300 ms) for an IEEE 802.11ad link to regain its alignment once it is disturbed. Hence, efficient beamforming is needed to realize mmWave-based mobile networks in 5G communications. In our analytical framework, we have only considered the performance of a single link. In case of multiple links operating simultaneously, a misaligned link could become a source of interference to others and thus can have an adverse effect on the spatial reuse in mmWave communication.

8.2.3. Fast beam setup and beam switching

Before establishing a multi-Gbps wireless link using narrow beams, the beam setup procedure needs to be accomplished to determine the best transmit and receive directions. The beam setup procedure involving exhaustive search over the beam search space causes significant overhead. This is further exacerbated, in case of mobile devices, by the beam misalignment caused by user movements requiring frequent re-beamforming. Hence, it is important to have beam searching protocols that minimize the searching overhead. We proposed a beam searching protocol employing a decrease-and-conquer approach. This protocol outperforms the 60 GHz IEEE 802.11ad beam searching protocol in terms of the required number of training packets to find the best transmit and receive beam directions. Compared to the IEEE 802.11ad, the number of required training packets is reduced by 60% for a 20° beamwidth and 85-88% for a 2°-5° beamwidth. We have shown that the proposed mechanism is equally effective in reducing the beamsearching overheads in both 2-D and 3-D beamforming systems. The frequent re-beamforming not only results in high overhead but it may also lead to

poor quality of experience (QoE). Hence, maintaining the Tx-Rx alignment is not only important from the throughput perspective, but also from the perspective of the QoE. We took the first step to incorporate motion sensor data to improve the performance of directional mmWave links. We showed that by using commonly available motion sensors in mobile devices (accelerometer, gyroscope and magnetometer), it is possible to predict the next beam sector required by the device and perform proactive beam switching without disrupting the data transmission.

8.2.4. Network architecture

Many challenges need to be addressed from the network architecture perspective due to the mandatory use of directional antennas and high attenuation caused by obstacles in 60 GHz bands. Some of them are, fast network discovery and seamless handovers among closely spaced AP/BSs. Providing guaranteed connectivity in a dynamic environment would not only require new approaches for intelligent path or relay selection in the mmWave bands, but also the support for fallback to sub-6 GHz bands, given their excellent coverage compared to mmWave bands. We have proposed a hybrid network architecture *CogCell* for indoor or hotspot environments consisting of a 2.4/5 GHz control plane and a 60 GHz data plane. The provision of a data plane fallback to the 2.4/5 GHz band, when the 60 GHz link becomes unavailable, has also been proposed. The *CogCell* architecture promises easier network management, a more robust user experience and better spectrum utilization by switching between the 2.4/5 GHz and the 60 GHz bands. It results in a faster device discovery, leading to a speedy network association and reduced latency in the medium access. We have also explored radio over fiber (RoF) network architecture for indoor communications with a 60 GHz radio interface. In mmwave communications, each indoor space requires a 60 GHz AP, since communication across the wall is not possible due to the blockage. The centralized baseband processing and network management capabilities offered by RoF network architecture are well suited for 60 GHz communications. We have investigated the performance of the IEEE 802.11ad MAC protocol for a 60 GHz RoF network architecture and pointed out the crucial constraints on MAC parameters such as inter-frame spaces and acknowledgment time-outs.

8.3. Future research directions

This thesis investigated the impact of narrow beamwidth antennas on the behavior of mmWave links. We provided solutions for efficient medium access, beamwidth adaptation, fast beam searching and robust network architectures for mmWave communications focusing on the 60 GHz band. The first generation of mmWave communication standards such as IEEE 802.11ad and IEEE 802.15.3c targeted WLAN/WPAN applications in the 60 GHz band. However, recent studies have demonstrated the applicability of mmWave for cellular and wireless back- and front-haul communications [8, 103, 104]. It has become clear that mmWave communications will be an integral part of the future multi-radio access interface to deliver multi-Gbps wireless access. However, there are still many challenges

that need to be addressed. Let us briefly describe some of the important ones.

8.3.1. Joint optimization of mmWave wireless back/fronthaul and access network

Apart from the high data-rate access in small cells, the multi-Gbps wireless transmission capacity makes mmWave communications an excellent candidate for wireless backhaul and fronthaul connectivity [105, 9, 106, 107, 108]. In the upcoming 5G networks 27.5–29.5 GHz, 38.6–40 GHz, 57–66 GHz, 71–86 GHz and 81–86 GHz bands will be used for offering multi-Gbps wireless access both for backhaul and fronthaul connectivity [10, 109, 110, 111]. This will require joint optimization of last meter, backhaul and fronthaul for efficient spectrum utilization, load balancing and the fulfilment of the latency requirements.

8.3.2. Beamforming architecture

Beamforming is essential to combat the high pathloss at mmWave frequencies. It is easy to closely pack a large number of antenna elements to attain high antenna gains in mmWave communications. The high bandwidth of mmWave signals and a large number of antenna elements result in high power consumption, making digital beamforming an unattractive choice[112, 113]. Although the analog beamforming appears as a power efficient choice, it is not capable of providing the spatial multiplexing gain and flexibility offered by the digital beamforming. Recently, to exploit both the beamforming gain and the spatial multiplexing gain, hybrid beamforming – a combination of analog and digital beamforming – have been proposed [57, 58, 114]. The operating regime (bandwidth limited or power limited) and the spatial correlation between antenna elements plays an important role in deciding the splitting of antenna elements in hybrid beamforming [115]. Hence further investigations into splitting of the antenna elements, design of beamforming codebook and beam searching protocols are needed.

8.3.3. Reliable low latency high speed communications

Ultra-reliable and low-latency communication (U-RLLC) has emerged as an important 5G requirement, targeting communication and control in industrial manufacturing, intelligent transportation, remote surgery, etc. Currently, LTE-A is being investigated to support U-RLLC. However, some of these applications would also require very high data rate communication. mmWave communications is therefore likely to become a natural choice to support wireless access for high data rate U-RLLC [116]. Although mmWave can deliver very high data rates, support for ultra-reliability and low latency requires further research, in particular, to reduce MAC and beamforming delays and ensure coverage by an AP or BS when required.

8.3.4. Multi-connectivity and interworking of mmWave and sub-6 GHz access technologies

The 5G air-interface will consist of multiple wireless access technologies operating from sub-6 GHz to mmWave frequency bands [117, 118]. Both the sub-6 GHz and the mmWave bands have licensed as well as unlicensed frequency bands available. To exploit the full potential of the available spectrum, efficient interworking solutions are needed [119, 120, 121, 122, 123]. Interworking of air-interfaces can be mainly facilitated by two means: (i) offloading or fallback, and (ii) aggregation. Offloading is the procedure of vertical handover among different radio access technologies which is primarily aimed to de-congest the licensed frequency bands. Fallback is also a vertical handover but it is initiated when it is difficult to operate in a particular frequency band. This is particularly the case with mmWave bands, when the bad channel conditions arise due to blockages and support of a sub-6 GHz band is desired to maintain the connectivity. On the other hand, aggregation aims to combine all the available frequency bands to boost the data rate by providing simultaneous multi-band connectivity.

Currently, offloading in the sub-6 GHz band is facilitated between WiFi and 3G/4G access networks using the Access Network Query protocol(ANQP) provided by 3GPP and the Access Network Discovery Function (ANDSF) provided by the Hotspot Alliance [124, 125]. Both of these offloading solutions work at the core-networking (CN) and are referred to as loose coupling solutions as they are outside the operator's control and hence best suited for the best-effort traffic offloading to WiFi. Since handover decisions are taken at the CN level, a long handover delay is introduced. In particular, mmWave band APs or BSs would have a small coverage area resulting in frequent handovers. This requires a radio access network (RAN)-level coupling between different air-interfaces so that the handover process can be expedited [126]. Further, the use of directional antennas makes it difficult for a mmWave BS or AP to initiate the handovers. This would also require a split control and data plane at the access-network level, which will also facilitate efficient fallback when needed. Presently, LTE-A supports carrier aggregation by combining contiguous as well as non-contiguous frequency bands to boost the data rate. In the 5G multi-radio-access-technology environment, the strongly different propagation characteristics of sub-6 GHz and mmWave signals will require new solutions for efficient carrier aggregation.

References

[1] "5G PPP use cases and performance evaluation models," vol. Version: 1.0, 2016. [Online]. Available: https://5g-ppp.eu/wp-content/uploads/2014/02/5G-PPP-use-cases-and-performance-evaluation-modeling_v1.0.pdf

[2] NGMN Alliance, "5G White Paper," 2015. [Online]. Available: https://www.ngmn.org/uploads/media/NGMN5GWhitePaperV10.pdf

[3] ICT-671650-mmMAGIC/D1.1, "Use case characterization, kpis and preferred suitable frequency ranges for future 5g systems between 6 ghz and 100 ghz," vol. Deliverable D1.1, 2015. [Online]. Available: https://bscw.5g-mmmagic.eu/pub/bscw.cgi/d54427/mmMAGIC_D1.1.pdf

[4] A. Ghosh, T. A. Thomas, M. C. Cudak, R. Ratasuk, P. Moorut, F. W. Vook, T. S. Rappaport, G. R. MacCartney, S. Sun, and S. Nie, "Millimeter-wave enhanced local area systems: A high-data-rate approach for future wireless networks," *IEEE Journal on Selected Areas in Communications*, vol. 32, no. 6, pp. 1152–1163, 2014.

[5] "IEEE Standard for Information Technology — Telecommunications and Information Exchange between Systems — Local and Metropolitan Area Networks — Specific Requirements. Part 15.3: Wireless Medium Access Control (MAC) and Physical Layer (PHY) Specifications for High Rate Wireless Personal Area Networks (WPANs) Amendment 2: Millimeter-Wave-Based Alternative Physical Layer Extension," *Report*, pp. 1–187, Apr. 2009.

[6] "High rate 60 GHz PHY, MAC and HDMI PALs," *Standard ECMA-387*, Dec 2010.

[7] "Draft standard- part 11:Wireless LAN medium access control (MAC) and physical layer (PHY)specifications - Amendment 4: Enhancements for very high throughput in the 60GHz band," *IEEE P802.11adTM/D9.0*, July 2012.

[8] T. Rappaport, S. Sun, R. Mayzus, H. Zhao, Y. Azar, K. Wang, G. Wong, J. Schulz, M. Samimi, and F. Gutierrez, "Millimeter Wave Mobile Communications for 5G Cellular: It Will Work!" *Access, IEEE*, vol. 1, pp. 335–349, 2013.

[9] C. Dehos, J. Gonzalez, A. De Domenico, D. Ktenas, and L. Dussopt, "Millimeter-wave access and backhauling: the solution to the exponential

data traffic increase in 5g mobile communications systems?" *Communications Magazine, IEEE*, vol. 52, no. 9, pp. 88–95, September 2014.

[10] M. Tercero, P. von Wrycza, A. Amah, J. Widmer, M. Fresia, V. Frascolla, J. Lorca, T. Svensson, M.-H. Hamon, S. Destouet Roblot *et al.*, "5g systems: The mmmagic project perspective on use cases and challenges between 6-100 ghz," 2016.

[11] "Flex5Gware (Flexible and efficient hardware/software platforms for 5G network elements and devices)," 2015. [Online]. Available: http://www.flex5gware.eu/

[12] A. Osseiran, F. Boccardi, V. Braun, K. Kusume, P. Marsch, M. Maternia, O. Queseth, M. Schellmann, H. Schotten, H. Taoka, H. Tullberg, M. A. Uusitalo, B. Timus, and M. Fallgren, "Scenarios for 5g mobile and wireless communications: the vision of the metis project," *IEEE Communications Magazine*, vol. 52, no. 5, pp. 26–35, May 2014.

[13] P. Smulders, "Exploiting the 60 ghz band for local wireless multimedia access: prospects and future directions," *Communications Magazine, IEEE*, vol. 40, no. 1, pp. 140–147, 2002.

[14] W. Roh, J.-Y. Seol, J. Park, B. Lee, J. Lee, Y. Kim, J. Cho, K. Cheun, and F. Aryanfar, "Millimeter-wave beamforming as an enabling technology for 5G cellular communications: theoretical feasibility and prototype results," *Communications Magazine, IEEE*, vol. 52, no. 2, pp. 106–113, February 2014.

[15] M. Jacob, S. Priebe, R. Dickhoff, T. Kleine-Ostmann, T. Schrader, and T. Kurner, "Diffraction in mm and sub-mm wave indoor propagation channels," *Microwave Theory and Techniques, IEEE Transactions on*, vol. 60, no. 3, pp. 833–844, 2012.

[16] H. Shokri-Ghadikolaei, C. Fischione, G. Fodor, P. Popovski, and M. Zorzi, "Millimeter wave cellular networks: A mac layer perspective," *Communications, IEEE Transactions on*, vol. PP, no. 99, pp. 1–1, 2015.

[17] H. Shokri-Ghadikolaei and et al., "Millimeter wave cellular networks: A MAC layer perspective," *IEEE Trans. on Commun.*, vol. 63, no. 10, pp. 3437–3458, 2015.

[18] G. Bianchi, "Performance analysis of the IEEE 802.11 distributed coordination function," *IEEE J. Sel. Areas Commun.*, vol. 18, pp. 535–547, March 2000.

[19] P. Chatzimisios, A. Boucouvalas, and V. Vitsas, "IEEE 802.11 packet delay-a finite retry limit analysis," in *Global Telecommunications Conference, 2003. GLOBECOM '03. IEEE*, vol. 2, dec. 2003, pp. 950 – 954 Vol.2.

[20] E. Ziouva and T. Antonakopoulos, "Csma/ca performance under high traffic conditions: Throughput and delay analysis," *Comput. Commun.*, vol. 25, no. 3, pp. 313–321, Feb. 2002. [Online]. Available: http://dx.doi.org/10.1016/S0140-3664(01)00369-3

[21] Z. ning Kong, D. H. K. Tsang, B. Bensaou, and D. Gao, "Performance analysis of ieee 802.11e contention-based channel access," *IEEE J. Sel. Areas Commun.*, vol. 22, no. 10, pp. 2095–2106, Dec 2004.

[22] J. Wang, Z. Lan, C. woo Pyo, T. Baykas, C.-S. Sum, M. Rahman, J. Gao, R. Funada, F. Kojima, H. Harada, and S. Kato, "Beam codebook based beamforming protocol for multi-gbps millimeter-wave wpan systems," *IEEE JSAC*, vol. 27, no. 8, pp. 1390–1399, October 2009.

[23] Y. M. Tsang, A. S. Poon, and S. Addepalli, "Coding the beams: Improving beamforming training in mmwave communication system," in *Global Telecommunications Conference (GLOBECOM 2011), 2011 IEEE*. IEEE, 2011, pp. 1–6.

[24] J. Kim and A. Molisch, "Fast millimeter-wave beam training with receive beamforming," *Communications and Networks, Journal of*, vol. 16, no. 5, pp. 512–522, Oct 2014.

[25] B. Li, Z. Zhou, W. Zou, X. Sun, and G. Du, "On the efficient beam-forming training for 60ghz wireless personal area networks," *Wireless Communications, IEEE Transactions on*, vol. 12, no. 2, pp. 504–515, February 2013.

[26] T. Nitsche, A. Flores, E. Knightly, and J. Widmer, "Steering with eyes closed: mm-wave beam steering without in-band measurement," in *in Proceedings of IEEE INFOCOM*, 2015.

[27] H. S. Ghadikolaei, L. Gkatzikis, and C. Fischione, "Beam-searching and transmission scheduling in millimeter wave communications," *IEEE ICC*, 2015. [Online]. Available: http://arxiv.org/abs/1501.02516

[28] J. Wildman, P. Nardelli, M. Latva-Aho, and S. Weber, "On the joint impact of beamwidth and orientation error on throughput in directional wireless poisson networks," *Wireless Communications, IEEE Transactions on*, vol. 13, no. 12, pp. 7072–7085, Dec 2014.

[29] A. Thornburg and R. W. Heath, "Ergodic capacity in mmwave ad hoc network with imperfect beam alignment," in *Military Communications Conference, MILCOM 2015 - 2015 IEEE*, Oct 2015, pp. 1479–1484.

[30] S. Singh, F. Ziliotto, and U. Madhow, "Blockage and directivity in 60 GHz wireless personal area networks: From cross layer model to multi-hop mac design," *IEEE J. Sel. Areas Commun., Special Issue on Realizing Gbps Wireless Personal Area Networks*, vol. 27, pp. 1400–1413, Oct. 2009.

[31] X. An, C.-S. Sum, R. Prasad, J. Wang, Z. Lan, J. Wang, R. Hekmat, H. Harada, and I. Niemegeers, "Beam switching support to resolve link-blockage problem in 60 ghz wpans," in *Personal, Indoor and Mobile Radio Communications, 2009 IEEE 20th International Symposium on*, 2009, pp. 390–394.

[32] M. Park and H. K. Pan, "A spatial diversity technique for ieee 802.11ad wlan in 60 ghz band," *Communications Letters, IEEE*, vol. 16, no. 8, pp. 1260–1262, 2012.

[33] Z. Genc, G. Olcer, E. Onur, and I. Niemegeers, "Improving 60 ghz indoor connectivity with relaying," in *ICC, IEEE*, 2010, pp. 1–6.

[34] X. Zhu, A. Doufexi, and T. Kocak, "Throughput and coverage performance for ieee 802.11ad millimeter-wave wpans," in *Vehicular Technology Conference (VTC Spring), 2011 IEEE 73rd*, May 2011, pp. 1–5.

[35] C. Zhang, Z. Xiao, H. Wu, L. Zeng, and D. Jin, "Performance analysis on the ofdm phy of ieee 802.11ad standard," in *Computational Problem-Solving (ICCP), 2011 International Conference on*, Oct 2011, pp. 708–713.

[36] Q. Chen, J. Tang, D. Wong, X. Peng, and Y. Zhang, "Directional cooperative mac protocol design and performance analysis for ieee 802.11ad wlans," *Vehicular Technology, IEEE Trans. on*, vol. 62, no. 6, pp. 2667–2677, 2013.

[37] C. Hemanth and T. G. Venkatesh, "Performance analysis of contention-based access periods and service periods of 802.11ad hybrid medium access control," *IET Networks*, vol. 3, no. 3, pp. 193–203, September 2014.

[38] C. W. Pyo and H. Harada, "Throughput analysis and improvement of hybrid multiple access in ieee 802.15.3c mm-wave wpan," *Sel Areas Comm., IEEE Journal on*, vol. 27, no. 8, pp. 1414–1424, 2009.

[39] L. Goratti, T. Wysocki, M. Akhavan, J. Lei, H. Nakase, and S. Kato, "Optimal beamwidth for beacon and contention access periods in ieee 802.15.3c wpan," in *PIMRC, IEEE*, 2010, pp. 1395–1400.

[40] J. Wang, Z. Lan, C. woo Pyo, T. Baykas, C.-S. Sum, M. Rahman, J. Gao, R. Funada, F. Kojima, H. Harada, and S. Kato, "Beam codebook based beamforming protocol for multi-gbps millimeter-wave wpan systems," *Sel. Areas Comm., IEEE Journal on*, vol. 27, no. 8, pp. 1390–1399, 2009.

[41] A. Miura, M. Ohira, S. Kitazawa, and M. Ueba, "60-ghz-band switched-beam eight-sector antenna with sp8t switch for 180 azimuth scan," *IEICE Transactions*, vol. 93-B, no. 3, pp. 551–559, 2010.

[42] S. F. A. Shah, S. Srirangarajan, and A. Tewfik, "Implementation of a directional beacon-based position location algorithm in a signal processing framework," *Wireless Comm., IEEE Trans. on*, vol. 9, no. 3, pp. 1044–1053, 2010.

[43] M. Di Renzo, "Stochastic geometry modeling and analysis of multi-tier millimeter wave cellular networks," *Wireless Communications, IEEE Transactions on*, vol. PP, no. 99, pp. 1–1, 2015.

[44] Y. Zhu, Z. Zhang, Z. Marzi, C. Nelson, U. Madhow, B. Y. Zhao, and H. Zheng, "Demystifying 60GHz outdoor picocells," in *The 20th Annual International Conference on Mobile Computing and Networking, MobiCom'14, Maui, HI, USA, September 7-11, 2014*, 2014, pp. 5–16.

[45] S. Sur, V. Venkateswaran, X. Zhang, and P. Ramanathan, "60 ghz indoor networking through flexible beams: A link-level profiling," *ACM SIGMETRICS*, 2015.

[46] S. K. Saha, L. Sun, and D. Koutsonikolas, "Improving connectivity, coverage, and capacity in 60 ghz indoor wlans using relays," in *Proceedings of the 2015 Workshop on Wireless of the Students, by the Students, & for the Students*, ser. S3 '15, 2015, pp. 35–37.

[47] S. K. Saha, V. V. Vira, A. Garg, and D. Koutsonikolas, "60 ghz multi-gigabit indoor wlans: Dream or reality?" *arXiv preprint arXiv:1509.04274*, 2015.

[48] J. Ansari, N. Perpinias, A. Nahring, P. Mahonen, and M. Petrova, "Empirical characterization of mm-wave communication links in realistic indoor scenarios," in *IEEE, WCNC*. IEEE, 2015, pp. 1799–1804.

[49] L. Cai, L. Cai, X. Shen, and J. W. Mark, "Rex: A randomized exclusive region based scheduling scheme for mmwave wpans with directional antenna," *Wireless Communications, IEEE Transactions on*, vol. 9, no. 1, pp. 113–121, January 2010.

[50] I. K. Son, S. Mao, M. Gong, and Y. Li, "On frame-based scheduling for directional mmwave wpans," in *INFOCOM, 2012 Proceedings IEEE*, March 2012, pp. 2149–2157.

[51] H. Shokri-Ghadikolaei, Y. Xu, L. Gkatzikis, and C. Fischione, "User association and the alignment-throughput tradeoff in millimeter wave networks," in *RTSI, 2015 IEEE 1st International Forum on*, Sept 2015, pp. 100–105.

[52] H. Li, Y.-D. Yao, and J. Yu, "Outage probabilities of wireless systems with imperfect beamforming," *Vehicular Technology, IEEE Transactions on*, vol. 55, no. 5, pp. 1503–1515, Sept 2006.

[53] "The dell wireless docking station (wld15: Wigig capable)." [Online]. Available: http://www.dell.com/support/Article/us/en/04/SLN297279/EN

[54] "Intel® tri-band wireless-ac 17265." [Online]. Available: http://www.intel.com/content/www/us/en/support/network-and-i-o/

wireless-networking/intel-wi-fi-products/intel-wireless-17000-series/intel-tri-band-wireless-ac-17265.html

[55] F. Boccardi, R. Heath, A. Lozano, T. Marzetta, and P. Popovski, "Five disruptive technology directions for 5g," *Communications Magazine, IEEE*, vol. 52, no. 2, pp. 74–80, February 2014.

[56] G. Grimmett and D. Stirzaker, *Probability and random processes*. Oxford university press, 2001.

[57] A. Alkhateeb, O. El Ayach, G. Leus, and R. W. Heath, "Channel estimation and hybrid precoding for millimeter wave cellular systems," *IEEE Journal of Selected Topics in Signal Processing*, vol. 8, no. 5, pp. 831–846, 2014.

[58] T. E. Bogale, L. B. Le, and X. Wang, "Hybrid analog-digital channel estimation and beamforming: Training-throughput tradeoff," *IEEE Transactions on Communications*, vol. 63, no. 12, pp. 5235–5249, Dec 2015.

[59] J. Qiao, X. Shen, J. Mark, and Y. He, "Mac-layer concurrent beamforming protocol for indoor millimeter-wave networks," *Vehicular Technology, IEEE Transactions on*, vol. 64, no. 1, pp. 327–338, Jan 2015.

[60] Y. Tsang and A. Poon, "Detecting human blockage and device movement in mmwave communication system," in *Global Telecommunications Conference (GLOBECOM 2011), 2011 IEEE*, Dec 2011, pp. 1–6.

[61] M. Park and H. K. Pan, "Effect of device mobility and phased array antennas on 60 ghz wireless networks," in *Proceedings of the 2010 ACM International Workshop on mmWave Communications: From Circuits to Networks*, ser. mmCom '10. New York, NY, USA: ACM, 2010, pp. 51–56. [Online]. Available: http://doi.acm.org/10.1145/1859964.1859978

[62] D.-S. Shim, C.-K. Yang, J. H. Kim, J. P. Han, and Y. S. Cho, "Application of motion sensors for beam-tracking of mobile stations in mmwave communication systems," *Sensors*, vol. 14, no. 10, pp. 19 622–19 638, 2014. [Online]. Available: http://www.mdpi.com/1424-8220/14/10/19622

[63] J. H. Kim, J. H. Choi, and Y. S. Cho, "An efficient beam-tracking technique for mmwave communication systems," in *Information and Communication Technology Convergence (ICTC), 2014 International Conference on*, Oct 2014, pp. 845–846.

[64] L. E. Peterson, "K-nearest neighbor," vol. 4, no. 2, p. 1883, 2009, revision #136646.

[65] J. Deissne and et al, "RPS Radiowave Propagation Simulator User Manual-Version 5.4," *Actix GmbH*, 2008.

[66] Z. Genc, U. Rizvi, E. Onur, and I. Niemegeers, "Robust 60 ghz indoor connectivity: Is it possible with reflections?" in *Vehicular Technology Conference (VTC 2010-Spring), 2010 IEEE 71st*, May 2010, pp. 1–5.

[67] A. Maltsev and et. al., "Channel models for 60 ghz wlan systems," May 2010. [Online]. Available: https://mentor.ieee.org/802.11/dcn/09/11-09-0334-08-00ad-channel-models-for-60-ghz-wlan-systems.doc

[68] O. Banos, J.-M. Galvez, M. Damas, H. Pomares, and I. Rojas, "Window size impact in human activity recognition," *Sensors*, vol. 14, no. 4, pp. 6474–6499, 2014. [Online]. Available: http://www.mdpi.com/1424-8220/14/4/6474

[69] F. Boccardi, R. W. Heath Jr, A. Lozano, T. L. Marzetta, and P. Popovski, "Five disruptive technology directions for 5G," *arXiv preprint arXiv:1312.0229*, 2013.

[70] J. Andrews, S. Buzzi, W. Choi, S. Hanly, A. Lozano, A. Soong, and J. Zhang, "What 5G will be?" *Selected Areas in Communication, Journal of*, Sep 2014.

[71] T. Rappaport, J. Murdock, and F. Gutierrez, "State of the Art in 60-GHz Integrated Circuits and Systems for Wireless Communications," *Proceedings of the IEEE*, vol. 99, no. 8, pp. 1390–1436, Aug 2011.

[72] "Cisco Visual Networking Index: Global Mobile Data Traffic Forecast Update, 2012-2018," Feb. 2014.

[73] F. Rusek, D. Persson, B. K. Lau, E. G. Larsson, T. L. Marzetta, O. Edfors, and F. Tufvesson, "Scaling up MIMO: Opportunities and Challenges with Very Large Arrays," *CoRR*, vol. abs/1201.3210, 2012.

[74] Y. Kishiyama, A. Benjebbour, T. Nakamura, and H. Ishii, "Future steps of LTE-A: evolution toward integration of local area and wide area systems," *Wireless Communications, IEEE*, vol. 20, no. 1, pp. 12–18, 2013.

[75] J. Deissne and et al, "RPS Radiowave Propagation Simulator User Manual-Version 5.4," *Actix GmbH*, 2008.

[76] [Online]. Available: http://newsroom.intel.com/community/intel_newsroom/blog/2015/03/02/intel-launches-new-mobile-socs-lte-solution

[77] M. Kotaru, K. Joshi, D. Bharadia, and S. Katti, "Spotfi: Decimeter level localization using wifi," *SIGCOMM Comput. Commun. Rev.*, vol. 45, no. 4, pp. 269–282, Aug. 2015. [Online]. Available: http://doi.acm.org/10.1145/2829988.2787487

[78] E. M. Mohamed, H. Kusano, K. Sakaguchi, and S. Sampei, "Wifi assisted multi-wigig AP coordination for future multi-gbps wlans," *CoRR*, vol. abs/1506.05857, 2015. [Online]. Available: http://arxiv.org/abs/1506.05857

[79] X. An, R. Venkatesha Prasad, and I. Niemegeers, "Impact of antenna pattern and link model on directional neighbor discovery in 60 ghz networks," *Wireless Communications, IEEE Transactions on*, vol. 10, no. 5, pp. 1435–1447, May 2011.

[80] M. Peng, Y. Sun, X. Li, Z. Mao, and C. Wang, "Recent advances in cloud radio access networks: System architectures, key techniques, and open issues," *IEEE Communications Surveys Tutorials*, vol. 18, no. 3, pp. 2282–2308, thirdquarter 2016.

[81] P. Chanclou, A. Pizzinat, F. L. Clech, T. L. Reedeker, Y. Lagadec, F. Saliou, B. L. Guyader, L. Guillo, Q. Deniel, S. Gosselin, S. D. Le, T. Diallo, R. Brenot, F. Lelarge, L. Marazzi, P. Parolari, M. Martinelli, S. O'Dull, S. A. Gebrewold, D. Hillerkuss, J. Leuthold, G. Gavioli, and P. Galli, "Optical fiber solution for mobile fronthaul to achieve cloud radio access network," in *Future Network and Mobile Summit (FutureNetwork-Summit), 2013*, July 2013, pp. 1–11.

[82] S. Park, C. B. Chae, and S. Bahk, "Large-scale antenna operation in heterogeneous cloud radio access networks: a partial centralization approach," *IEEE Wireless Communications*, vol. 22, no. 3, pp. 32–40, June 2015.

[83] N. Ghazisaidi, M. Maier, and C. M. Assi, "Fiber-wireless (fiwi) access networks: A survey," *IEEE Communications Magazine*, vol. 47, no. 2, pp. 160–167, 2009.

[84] N. Ghazisaidi and M. Maier, "Fiber-wireless (fiwi) access networks: Challenges and opportunities," *IEEE network*, vol. 25, no. 1, pp. 36–42, 2011.

[85] A. Checko, H. Holm, and H. Christiansen, "Optimizing small cell deployment by the use of c-rans," in *European Wireless 2014; 20th European Wireless Conference; Proceedings of*. VDE, 2014, pp. 1–6.

[86] Z. Jia, J. Yu, G. Ellinas, and G.-K. Chang, "Key enabling technologies for optical-wireless networks: Optical millimeter-wave generation, wavelength reuse, and architecture," *Lightwave Technology, Journal of*, vol. 25, no. 11, pp. 3452–3471, Nov 2007.

[87] N. Pleros, K. Vyrsokinos, K. Tsagkaris, and N. D. Tselikas, "A 60 ghz radio-over-fiber network architecture for seamless communication with high mobility," *J. Lightwave Technol.*, vol. 27, no. 12, pp. 1957–1967, Jun 2009.

[88] G. Smith, D. Novak, and C. Lim, "A millimeter-wave full-duplex fiber-radio star-tree architecture incorporating wdm and scm," *Photonics Technology Letters, IEEE*, vol. 10, no. 11, pp. 1650–1652, Nov 1998.

[89] M. Huchard, M. Weiss, A. Pizzinat, S. Meyer, P. Guignard, and B. Charbonnier, "Ultra-broadband wireless home network based on 60-ghz wpan cells interconnected via rof," *Lightwave Technology, Journal of*, vol. 26, no. 15, pp. 2364–2372, 2008.

[90] A. Das, M. Mjeku, A. Nkansah, and N. Gomes, "Effects on ieee 802.11 mac throughput in wireless lan over fiber systems," *Lightwave Technology, Journal of*, vol. 25, no. 11, pp. 3321–3328, 2007.

[91] B. L. Dang, R. V. Prasad, I. G. Niemegeers, M. G. Larrode, and A. M. J. Koonen, "Toward a seamless communication architecture for in-building networks at the 60 ghz band," in *LCN'06*, 2006, pp. 300–307.

[92] B. L. Dang, R. V. Prasad, and I. Niemegeers, "On the MAC protocols for radio over fiber indoor networks," *First Int. Conf. Communications and Electronics ICCE '06*, pp. 112–117, Oct. 2006.

[93] Z. Cao, J. Yu, W. Wang, Q. Tang, and L. Chen, "Low-cost 60-ghz radio-over-fiber architecture compatible with wavelength-division-multiplexing passive optical networks by employing directly modulated laser and frequency quadruple techniques," *Optical Engineering*, vol. 49, no. 6, pp. 065 005–065 005, 2010.

[94] Z. Cao, N. Tessema, S. Latkowski, X. Zhao, Z. Chen, V. Moskalenko, K. A. Williams, H. P. A. van der Boom, E. Tangdiongga, and A. M. J. Koonen, "Integrated remotely tunable optical delay line for millimeter-wave beam steering fabricated in an inp generic foundry," *Opt. Lett.*, vol. 40, no. 17, pp. 3930–3933, Sep 2015. [Online]. Available: http://ol.osa.org/abstract.cfm?URI=ol-40-17-3930

[95] K. Lee, J. H. Park, and H. Jung, "Comparison of digitized and analog radio-over-fiber systems over wdm-pon networks," in *2013 International Conference on ICT Convergence (ICTC)*. IEEE, 2013, pp. 705–706.

[96] F. Gross, *Smart Antennas for Wireless Communications with MATLAB*. Communications Engineering book from C.H.I.P.S., 2005.

[97] B. Razavi, *RF microelectronics*. Prentice Hall, Nov., 1997.

[98] Optically beam-formed antennas for adaptive broadband fixed and mobile wireless access networks -project in the 6th framework programme of the european commission. [Online]. Available: homepage:http://ist-obanet.upv.es

[99] L. G. Madsen C.K., "Optical all-pass filters for phase response design with applications for dispersion compensation," vol. 10, no. 7, pp. 994–996, Jul 1998.

[100] B. Vidal, D. Madrid, J. Coffal, and J. Marti, "Novel photonic true-time-delay beamformer based on the free-spectral-range periodicity of arrayed waveguide gratings and fiber dispersion," *Photonics Technology Letters, IEEE*, vol. 14, no. 11, pp. 1614–1616, Nov 2002.

[101] P. Ritoša, B. Batagelj, and M. Vidmar, "Optically steerable antenna array for radio over fibre transmission," *Electronics Letters*, vol. 41, no. 16, pp. 917–918, 2005.

[102] X. An, Z. Lan, R. V. Prasad, R. Hekmat, H. Harada, and I. G. Niemegeers, "Performance analysis of the frame aggregation mechanisms in IEEE 802.15.3c," in *PIMRC*, 2009, pp. 2095–2100.

[103] Z. Pi and F. Khan, "An introduction to millimeter-wave mobile broadband systems," *IEEE Communications Magazine*, vol. 49, no. 6, 2011.

[104] Y. Kim, H.-Y. Lee, P. Hwang, R. K. Patro, J. Lee, W. Roh, and K. Cheun, "Feasibility of mobile cellular communications at millimeter wave frequency," *IEEE Journal of Selected Topics in Signal Processing*, vol. 10, no. 3, pp. 589–599, 2016.

[105] A. De La Oliva, X. C. Pérez, A. Azcorra, A. Di Giglio, F. Cavaliere, D. Tiegelbekkers, J. Lessmann, T. Haustein, A. Mourad, and P. Iovanna, "Xhaul: toward an integrated fronthaul/backhaul architecture in 5g networks," *IEEE Wireless Communications*, vol. 22, no. 5, pp. 32–40, 2015.

[106] X. Ge, H. Cheng, M. Guizani, and T. Han, "5g wireless backhaul networks: challenges and research advances," *IEEE Network*, vol. 28, no. 6, pp. 6–11, 2014.

[107] Z. Pi, J. Choi, and R. Heath, "Millimeter-wave gigabit broadband evolution toward 5g: fixed access and backhaul," *IEEE Communications Magazine*, vol. 54, no. 4, pp. 138–144, 2016.

[108] A. I. Sulyman, A. Alwarafy, G. R. MacCartney, T. S. Rappaport, and A. Alsanie, "Directional radio propagation path loss models for millimeter-wave wireless networks in the 28-, 60-, and 73-ghz bands," *IEEE Transactions on Wireless Communications*, vol. 15, no. 10, pp. 6939–6947, 2016.

[109] S. Jaeckel, M. Peter, K. Sakaguchi, W. Keusgen, and J. Medbo, "5g channel models in mm-wave frequency bands," in *European Wireless 2016; 22th European Wireless Conference; Proceedings of.* VDE, 2016, pp. 1–6.

[110] K. Chandra, Z. Cao, T. Bruintjes, R. V. Prasad, G. Karagiannis, E. Tangdiongga, H. van den Boom, and A. Kokkeler, "mcran: A radio access network architecture for 5g indoor communications," in *In IEEE ICC 2015 - Workshop on Fiber-Wireless Integrated Technologies, Systems and Networks (ICC'15 - Workshops 09).*, 2015.

[111] K. Chandra, R. V. Prasad, and I. Niemegeers, "An architectural framework for 5g indoor communications," in *2015 International Wireless Communications and Mobile Computing Conference (IWCMC)*. IEEE, 2015, pp. 1144–1149.

[112] R. W. Heath, N. Gonzalez-Prelcic, S. Rangan, W. Roh, and A. M. Sayeed, "An overview of signal processing techniques for millimeter wave mimo systems," *IEEE journal of selected topics in signal processing*, vol. 10, no. 3, pp. 436–453, 2016.

[113] Y. Wang, Z. Shi, K. Zeng, and P. Zhu, "Two layers of beam alignment for millimeter-wave communications," in *Digital Information Processing, Data Mining, and Wireless Communications (DIPDMWC), 2016 Third International Conference on*. IEEE, 2016, pp. 262–267.

[114] W. B. Abbas and M. Zorzi, "Towards an appropriate receiver beamforming scheme for millimeter wave communication: A power consumption based comparison," in *European Wireless 2016; 22th European Wireless Conference; Proceedings of*. VDE, 2016, pp. 1–6.

[115] W. b. Abbas, F. Gomez-Cuba, and M. Zorzi, "Millimeter wave receiver efficiency: A comprehensive comparison of beamforming schemes with low resolution adcs," *arXiv preprint arXiv:1607.03725*, 2016.

[116] R. Ford, M. Zhang, M. Mezzavilla, S. Dutta, S. Rangan, and M. Zorzi, "Achieving ultra-low latency in 5g millimeter wave cellular networks," *arXiv preprint arXiv:1602.06925*, 2016.

[117] A. Ravanshid, P. Rost, D. S. Michalopoulos, V. V. Phan, H. Bakker, D. Aziz, S. Tayade, H. D. Schotten, S. Wong, and O. Holland, "Multi-connectivity functional architectures in 5g," in *Communications Workshops (ICC), 2016 IEEE International Conference on*. IEEE, 2016, pp. 187–192.

[118] J. G. Rois, B. Lorenzo, F. González-Castaño, and J. C. Burguillo, "Heterogeneous millimeter-wave/micro-wave architecture for 5g wireless access and backhauling," in *Networks and Communications (EuCNC), 2016 European Conference on*. IEEE, 2016, pp. 179–184.

[119] M. Giordani, M. Mezzavilla, S. Rangan, and M. Zorzi, "Multi-connectivity in 5g mmwave cellular networks," in *Ad Hoc Networking Workshop (Med-Hoc-Net), 2016 Mediterranean*. IEEE, 2016, pp. 1–7.

[120] K. Chandra, A. Doff, Z. Cao, R. V. Prasad, and I. Niemegeers, "60 ghz mac standardization: Progress and way forward," in *2015 12th Annual IEEE Consumer Communications and Networking Conference (CCNC)*. IEEE, 2015, pp. 182–187.

[121] K. Chandra, R. V. Prasad, B. Quang, and I. Niemegeers, "Cogcell:cognitive interplay between 60ghz picocells and 2.4/5ghz hotspots in the 5g era,"

IEEE Communications Magazine, Special issue on Emerging Applications, Services and Engineering for Cognitive Cellular Systems (EASE4CCS),, 2015.

[122] K. Chandra and R. V. Prasad, "Directional mac protocols for 60 ghz millimeter wave wlans," in *Wireless Network Performance Enhancement via Directional Antennas: Models, Protocols, and Systems*. CRC Press, 2015, pp. 169–187.

[123] K. Chandra, R. V. Prasad, I. G. Niemegeers, and A. R. Biswas, "Adaptive beamwidth selection for contention based access periods in millimeter wave wlans," in *2014 IEEE 11th Consumer Communications and Networking Conference (CCNC)*. IEEE, 2014, pp. 458–464.

[124] Q. Chen, G. Yu, H. Shan, A. Maaref, G. Y. Li, and A. Huang, "Cellular meets wifi: Traffic offloading or resource sharing?" *IEEE Transactions on Wireless Communications*, vol. 15, no. 5, pp. 3354–3367, 2016.

[125] J. Ling, S. Kanugovi, S. Vasudevan, and A. K. Pramod, "Enhanced capacity and coverage by wi-fi lte integration," *IEEE Communications Magazine*, vol. 53, no. 3, pp. 165–171, 2015.

[126] E. M. Mohamed, K. Sakaguchi, and S. Sampei, "Wi-fi/wigig coordination for optimal wigig concurrent transmissions in random access scenarios," in *Vehicular Technology Conference (VTC Spring), 2016 IEEE 83rd*. IEEE, 2016, pp. 1–5.

Propositions

accompanying the thesis

Towards Realizing 5G: Efficient Medium Access and Beamwidth Adaptation in 60 GHz Communications

by

Kishor Chandra

1. Directional antennas provide an important degree-of-freedom, i.e., beamwidth, which can be used to control almost everything in the directional networks [Chapter 2].
2. 60 GHz links using narrow beamwidths do not always result in the best link capacity. It is important to consider the misalignment and searching overheads [Chapter 3].
3. mmWave networks cannot stand alone, interactions with sub-6 GHz is a must [Chapter 6].
4. 5G will end up as an urban communication system, aggravating the digital divide.
5. A few vague ideas make a researcher, too many of them destroy him/her.
6. One of the biggest challenges for a PhD student is not-to-become a copy of his/her advisor.
7. People who seek saints end-up being led by thugs.
8. Learning the art of *accepting rejections* and *rejecting acceptances* is essential for a successful academic career.
9. Hypocrisy is best covered by morality.

These propositions are regarded as opposable and defendable, and have been approved as such by the promoter prof. dr. ir. I. G. M. M. Niemegeers.

List of Publications

Here, I present the comprehensive list of my publications (published and under revision/preparation) during the PhD.

Journals, Letters and Magazine Papers

(J.1) K. Chandra, R. V. Prasad and I. Niemegeers, "Performance Analysis of IEEE 802.11ad MAC Protocol," *Accepted for Publication in IEEE Communications Letters*.

(J.2) K. Chandra, R. V. Prasad, Q. Bien, Niemegeers, and I. Niemieegers,, "Cogcell: Cognitive Interplay between 60 GHz Picocells and 2.4/5 GHz Hotspots in the 5G Era," *IEEE Communications Magazine, Special issue on Emerging Applications, Services and Engineering for Cognitive Cellular Systems (EASE4CCS)*, July 2015.

(J.3) Z. Cao, H. P. van den Boom, E. Tangdiongga, K. Chandra, and A. Koonen, "Long reach Hybrid Fiber-Wireless System with Remote Up-conversion and Local Exchange," *IEEE Photonics Technology Letters*, vol. 25, no. 8, 2013.

(J.4) Q. Bien, R. Prasad, K. Chandra, I. Niemieegers, and H. Nguyen, "Resource management in indoor hybrid fi-wi network," *Wiley's Transactions on Emerging Telecommunications Technologies*, 2014.

Book Chapters

(B.1) K. Chandra and R. V. Prasad, "Directional MAC Protocols for 60 GHz Millimeter Wave WLAN," in *Wireless Network Performance Enhancement via Directional Antennas: Models, Protocols, and Systems*. CRC Press, 2015,

Conference Papers

(C.1) K. Chandra, Z. Cao, T. Bruintjes, R. V. Prasad, G. Karagiannis, E. Tangdiongga, H. van den Boom, and A. Kokkeler, "mCRAN: A Radio Access Network Architecture for 5G Indoor Communications," in *In IEEE ICC 2015 - Workshop on Fiber-Wireless Integrated Technologies, Systems and Networks (ICC'15 - Workshops 09).*, 2015.

(C.2) K. Chandra, R. V. Prasad, and I. Niemegeers, "An Architectural Framework for 5G Indoor Communications," in *2015 International Wireless Communications and Mobile Computing Conference (IWCMC)*. IEEE, 2015.

(C.3) A. W. Doff, K. Chandra, and R. V. Prasad, "Sensor-Assisted Movement Identification and Prediction for Beamformed 60 GHz Links," in *2015 12th Annual IEEE Consumer Communications and Networking Conference (CCNC)*. IEEE, 2015.

(C.4) K. Chandra, A. Doff, Z. Cao, R. V. Prasad, and I. Niemegeers, "60 GHz MAC Standardization: Progress and Way Forward," in *2015 12th Annual IEEE Consumer Communications and Networking Conference (CCNC)*. IEEE, 2015.

(C.5) K. Chandra, R. V. Prasad, I. Niemegeers, and A. R. Biswas, "Adaptive Beamwidth Selection for Contention based Access Periods in Millimeter Wave WLANs," in *2014 IEEE 11th Consumer Communications and Networking Conference (CCNC)*. IEEE, 2014.

(C.6) K. Chandra, R. V. Prasad, B. Van Quang, I. Niemegeers, and A. R. Biswas, "Analysis of Fi-Wi Indoor Network Architecture based on IEEE 802.15.3c," in *2014 IEEE 11th Consumer Communications and Networking Conference (CCNC)*. IEEE, 2014.

(C.7) R. V. Prasad, B. Van Quang, K. Chandra,X. An, N. Huong and I. Niemegeers, "Analysing IEEE 802.15. 3c protocol in Fi-Wi hybrid networks," in *2014 IEEE 10th Consumer Communications and Networking Conference (CCNC)*. IEEE, 2013.

Under Revision/Preparation

(J.5) K. Chandra, R. V. Prasad and I. Niemegeers, "A *Decrease-and-Conquer* based Beam Searching Protocol for mmWave Communications," *Submitted to IEEE Wireless Communications Letters*.

(J.6) K. Chandra, S. Niknam, R. V. Prasad, B. Natarajan and I. Niemegeers, "Trade-offs in narrow beamwidth mmWave Links," *To be Submitted to IEEE Transactions on Wireless Communications*.

(J.7) K. Chandra, R. Hersyandika and R. V. Prasad, "Handovers in 60 GHz picocells: An experimental study using IEEE 802.11ad COTS devices," *To be Submitted to IEEE Transactions on Mobile Computing*.